Wetting Stability of Aged Limestone in the presence of HPAM polymer

- An experimental study

Department of Physics and Technology

A Master Thesis in Reservoir Physics

By Martine Folgerø Sandnes

UNIVERSITY OF BERGEN

May 2020

Abstract

The Norwegian Petroleum Directorate required that a polymer field pilot should be performed in the Johan Sverdrup field in the second phase of the field development to confirm potential enhanced recovery potential at the field and collect valuable data. Polymer increases the viscosity of the aqueous phase, which gives a more favourable mobility ratio and improved volumetric sweep efficiency during production of high viscous oil or production in heterogeneous reservoirs. Although polymer injection is an established enhanced oil recovery method, it is still not established if injection of a hydrophilic polymer (HPAM) alter the wettability preference of oil-wet rock towards water-wet. This is important to answer because wettability largely dictates important flow functions.

This experimental thesis evaluates change in wetting preferences during polymer injection using heterogeneous limestone rock core samples. A previously verified rock/brine/oil system was utilized to produce oil-wet rock surfaces, and systematic core scale tests have been used to describe important properties including: wetting preference stability in brine/oil systems, and the influence of hydrophilic polymers on wettability. Multiple Amott-Harvey cycles were used to determine wettability preferences and alterations in 29 core plugs. In-situ visualization by MRI, high-resolution CT and PET-CT assisted in the interpretation.

Amott-Harvey cycles were first performed to determine wetting preference stability in brine/oil systems, where the core plugs were aged to slightly oil-wet conditions. Spontaneous imbibition of oil was recorded during the first three Amott-Harvey cycles and the wettability remained stable. Previous studies have not been performed beyond three cycles, but in this study two additional cycles were performed. During the 4^{th} and 5^{th} cycle, spontaneous imbibition of oil stopped, and small volumes of water imbibed spontaneously into some core plugs. Hence; the wettability changed from slightly oil-wet towards neutral or slightly water-wet conditions during completion of five subsequent Amott-Harvey cycles.

When polymer was introduced to slightly oil-wet core plugs, oil imbibition ceased in the second Amott-Harvey cycle and polymer imbibition started in the third, i.e. polymer initiated a quicker change in wettability, and yielded stronger water-wet conditions than brine. Relative permeabilities of water and oil decreased when polymer was present in the pore volume. A

larger decrease in relative permeability of water than the relative permeability of oil was observed both in water-wet and oil-wet cores.

PET-imaging showed that oil and water displacement fronts propagated faster through a core plug when polymer was present in the pore volume, which indicated that the pore volume available for flow had been reduced by polymer injection. Blocking of narrow pores and pore throats by polymer, and adsorption of polymer layers on the pore walls was proposed as viable explanations for the observed behavior.

Acknowledgements

First of all, I would like to express my gratitude to my main supervisor Dr. Bergit Brattekås and co-supervisor Professor Martin Fernø at the Department of Physics and Technology at the University of Bergen, for the opportunity to work on an interesting research project. Thank you Bergit for motivation and support, and for excellent guidance. In addition, I would like to thank Professor Arne Graue and Associate Professor Geir Ersland for their contributions to the reservoir physics group.

A special thanks to my lab partner, PhD candidate Jaquelin Cobos Mora from Aalborg University, for good teamwork. Thank you for always staying positive, even after endless hours in the lab. I would also like to thank Dr. Marianne Steinsbø for help and guidance in the lab. Thanks to Dr. Stian Almenningen for help with the MRI-experiment, and to PhD candidate Benyamine Benali for technical support. Thanks to Heidi Espedal for help during the PET-experiment, and to Eivind Wilhelm Nagel Støren and Jan Magne Cederstrøm for helping with CT-imaging of my cores.

I would also like to express my gratitude to my fellow students during these five years at the University of Bergen for making these years memorable. Thank you for many interesting discussions, daily lunch breaks and social events. I wish you all the best in the future!

Finally, I would like to thank my family and friends for support and motivation.

Bergen, May 2020

Martine F. Sandnes

Table of Contents

Nomenclature

Abbreviations

AFO	All Faces Open
A-H	Amott-Harvey
BT	Break through
CT	Computed Tomography
DPR	Disproportionate Permeability Reduction
EOR	Enhanced Oil Recovery
FW	Fractionally wet
HPAM	Hydrolysed Polyacrylamide
IFT	Interfacial tension
MRI	Magnetic Resonance Imaging
MWL	Mixes-wet large
MWS	Mixed-wet small
NMR	Nuclear Magnetic Resonance
NWP	Non-wetting phase
PET	Positron Emission Tomography
PV	Pore volume
SI	Spontaneous imbibition

Nomenclature

Symbol	**Description**
θ_{ow}	Oil/water wetting angle
λ_D	Displacing fluid mobility
λ_d	Displaced fluid mobility
λ_i	Mobility of a fluid *i*
μ	Dynamic viscosity
μ_{gm}	The geometric mean of the water and oil viscosities
μ_i	Dynamic viscosity of a fluid *i*
ϕ_{tot}	Total porosity
ϕ_{eff}	Effective porosity
ρ_i	Density of a fluid *i*
σ	Interfacial tension

τ	Shear stress
A	Core plug cross sectional area
d_S	Diameter of a core plug
$\mathrm{I_{AH}}$	Amott-Harvey wettability index
$\mathrm{I_o}$	Wettability index of oil
$\mathrm{I_w}$	Wettability index of water
K	Absolute permeability
$\mathrm{k_{ie}}$	Effective permeability of fluid *i*
$\mathrm{k_{ri}}$	Relative permeability of fluid *i*
$k_{ro,iw}$	End-point relative permeability of oil
$k_{rw,or}$	End-point relative permeability of aqueous phase
L	Length of core plug
M_{Dd}	Mobility ratio between displacing fluid *D* and displaced fluid *d*
M_{ow}	Mobility ratio between oil and aqueous phase
M_{wo}	Mobility ratio between aqueous phase and oil
m_{dry}	Mass of dry core plug
m_{wet}	Mass of wet core plug
$\mathrm{P_c}$	Capillary pressure
$\mathrm{P_{nw}}$	Non-wetting phase pressure
$\mathrm{P_w}$	Wetting phase pressure
Q	Volumetric flow rate
R_1, R_2	Principal radii of the interface curvature
r	Core plug radius / radius of capillary tube
$\Delta\mathrm{S_{ws}}$	Change in water saturation during spontaneous imbibition
$\Delta\mathrm{S_{wt}}$	Total change in water saturation during spontaneous imbibition and forced injection
$\Delta\mathrm{S_{os}}$	Change in oil saturation during spontaneous imbibition
$\Delta\mathrm{S_{ot}}$	Total change in oil saturation during spontaneous imbibition and forced injection
S	Surface area
S_i	Saturation of a fluid *i*
s_f	standard deviation of the function *f*
t_D	Dimensionless time
T_2	Transversal relaxation time

V_b	Bulk Volume
V_i	Volume of a fluid *i* present in a core plug
V_m	Matrix Volume
V_p	Pore Volume
$V_{p,eff}$	Effective Pore Volume
x_{Ai}	The distance from the imbibition face to the no-flow boundary

1 Introduction

The population and the energy demand in the world are steadily increasing. In the 20th century, the population quadrupled, and the world energy demand went up 16 times. Currently, about 13 terawatts (TW) of energy is needed to sustain the lifestyle of 6.5 billion people worldwide. By the year 2050, an additional 10 TW of clean energy is needed to maintain the current lifestyle (Kamat, 2007). Figure 1.1 represents the global electricity demand by region from 2000-2040 in the stated policies scenario, where global electricity demand grows at 2.1% per year to 2040 (IEA, 2019c).

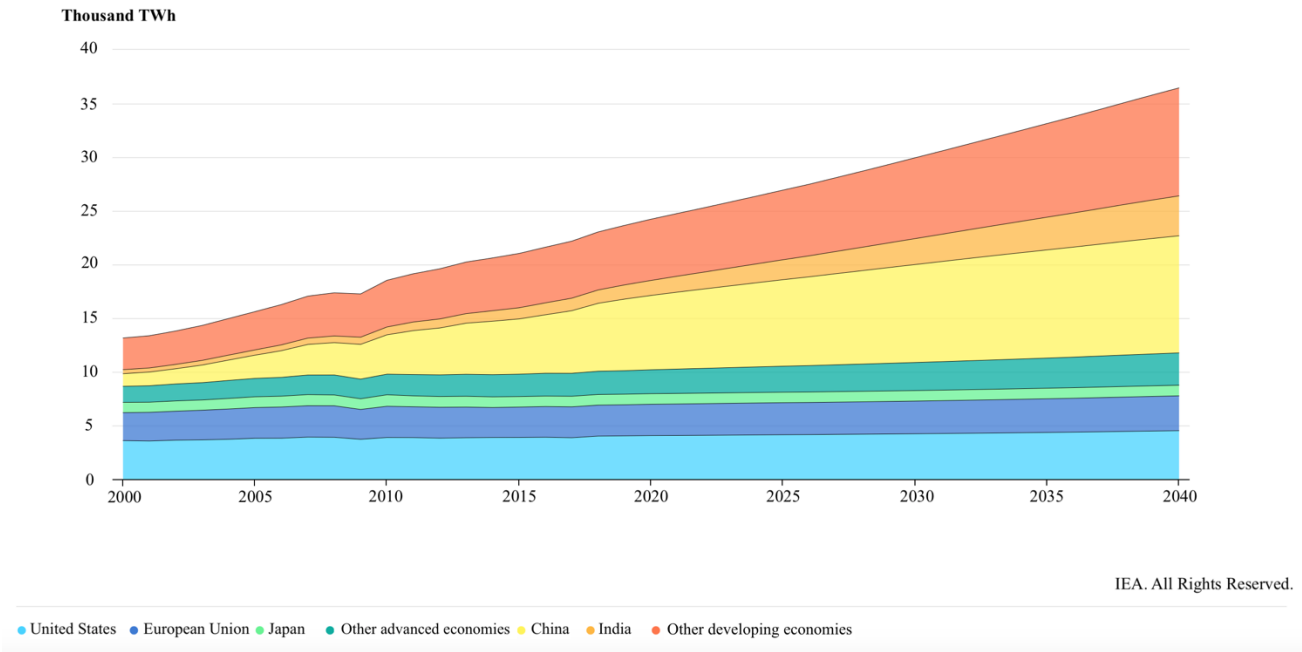

Figure 1.1: The global electricity demand by region in the period 2000-2040. (Modified from IEA (2019a)).

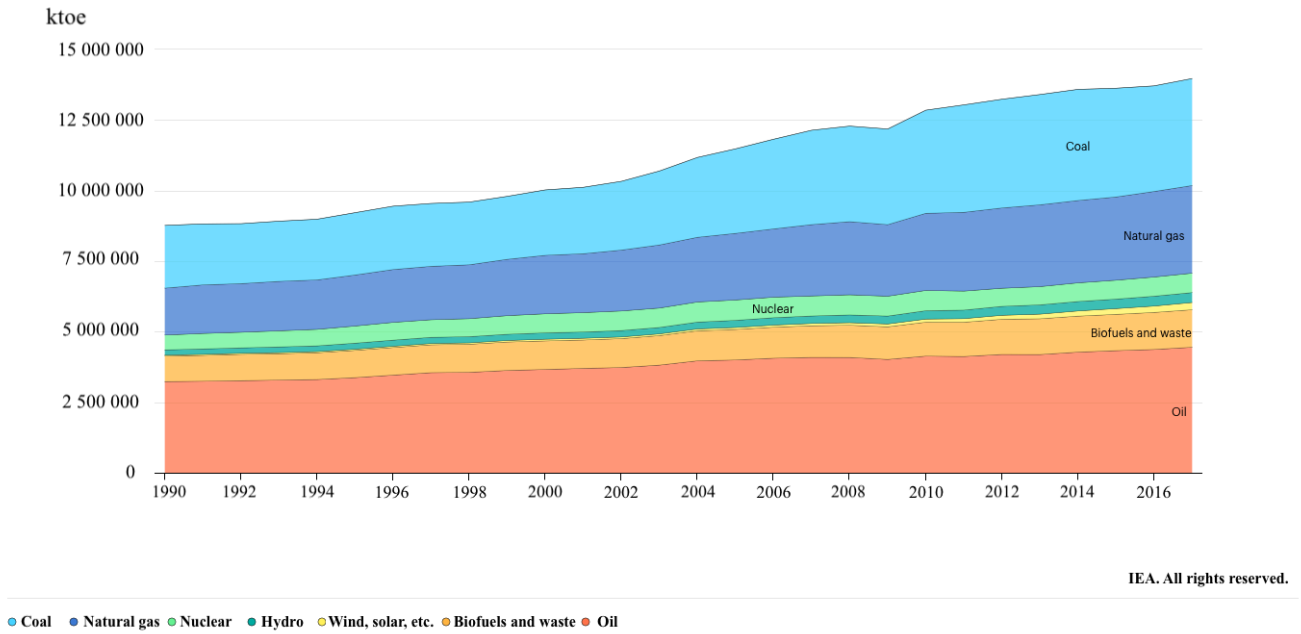

Figure 1.2: Total primary energy supply by source in the world from 1990-2017. (Modified from IEA (2019b)).

Oil is currently the main supplying energy source in the world (Figure 1.2). In 2017, 3% of the world electricity generation came from oil (IEA, 2019c). Only 20-50% of oil originally in place (OIIP) is possible to produce from a reservoir by primary and secondary recovery (Ali and Thomas, 1996). Huge volumes of oil are left behind; and are important resources to produce in order to meet the future energy needs. Polymer injection is a well-known and field-proven method to enhance oil recovery. Polymers increase the viscosity of the aqueous phase and reduce its relative permeability, which gives a more favourable mobility ratio and improved volumetric sweep efficiency during production of high viscous oil or production in heterogeneous reservoirs. Several authors report that polymer flooding has been more efficient than expected, which propose that other mechanisms are in play apart from increased aqueous viscosity (Zaitoun and Kohler, 1988, Liang et al., 1995, Nilsson et al., 1998, Al-Sharji et al., 1999, Willhite et al., 2002). Proposed mechanisms for this behaviour include shrinking/swelling, preferred pathways, wall effects and wettability effects. This thesis emphasized the effect of wettability, through systematic experimental work on the core scale. The influence of hydrophilic polymer (HPAM) on core plug wettability preference was investigated. The core material was Edwards Yellow Limestone from West Texas. Limestone is a carbonate rock, and according to Bjorlykke (2010), carbonate reservoir rocks contain almost 40% of the oil reserves in the world. Carbonate reservoirs are characterized by extremely heterogeneous porosity and permeability, caused by the wide spectrum of depositional

environments and by the susceptibility of the rocks to diagenetic alteration. 29 different core plugs with a diameter of 1.5” and lengths between 6.4cm and 7.6cm have been used for experiments. A total of 20 core plugs were aged towards oil-wet conditions by crude oil using two different aging methods: static aging and dynamic aging. The resulting wetting preference, and stability of the altered wettability, was investigated through several full Amott-Harvey cycles. Up to five Amott-Harvey cycles were performed, where wetting stability was assessed with and without the presence of polymers in the aqueous phase. Ekofisk brine, polymer solution or glycerol solution constituted the aqueous phase during spontaneous imbibition and forced displacement, while mineral oil (Decane) constituted the oil phase. Pore scale assessment of fluid distribution was performed by Magnetic Resonance Imaging (MRI) in one dynamically aged core plug. *In*-situ imaging by PET/CT was applied to visualize the displacement fronts before and after polymer injection in one of the core plugs. CT-images of two core plugs were used to assess the heterogeneity of the core material.*

** Due to the circumstances around the covid-19 pandemic, some experimental work was not completed. This includes some MRI measurements and quantitative analysis of PET/CT data. This is further described in the subsections of this thesis.*

2 Theory

In this chapter, theory describing the core material used, wettability, methods for wettability measurement, wettability alteration and wettability alteration by polymers will be presented. Fundamental concepts in core analysis, i.e. porosity, permeability, saturation, and capillary pressure, are further described in Appendix A-C. These concepts are important in order to understand the mechanism behind wettability and wettability alteration.

2.1 Basics of core analysis and the core material

Core plugs are small pieces of rock that are drilled out from geologic reservoirs or outcrops and further used for laboratory experiments. Core analysis is an important source of information, both when it comes to petrophysical and geological properties of reservoir rocks, and in regard to fluid flow through representative porous media. Recovery mechanisms and rock/fluid interactions may be investigated in detail on smaller scales, and upscaled to yield useful information about e.g. reservoir production. Outcrop limestone core plugs were used in this thesis, acquired from the Edwards formation in West-Texas. Edwards limestone is heterogeneous with a trimodal pore size distribution with both microporosity and vugs. Outcrop rock is expected to be water-wet.

Tipura (2008) presented a linear porosity-permeability relationship for Edwards limestone used in her work (Figure 2.1). The porosity was in range 16.9-26.9% and the permeability in range 4.4-28.5mD. The same core material was used in this work, but from a new supplier, so the core properties were expected to be in the same range.

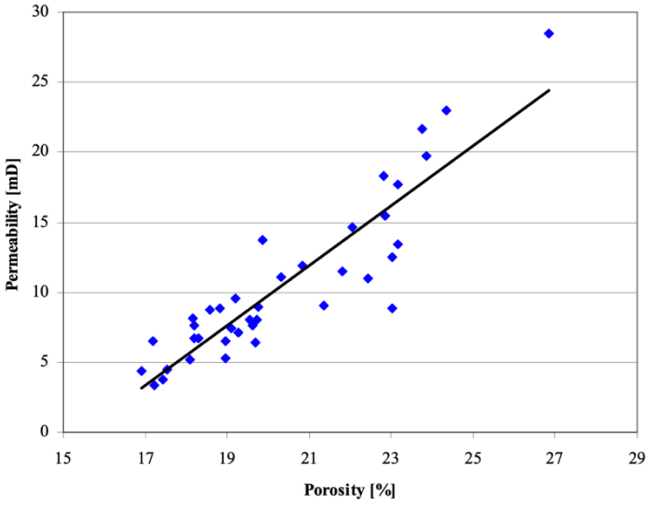

Figure 2.1: Linear porosity-permeability relationship for Edwards limestone (Tipura, 2008).

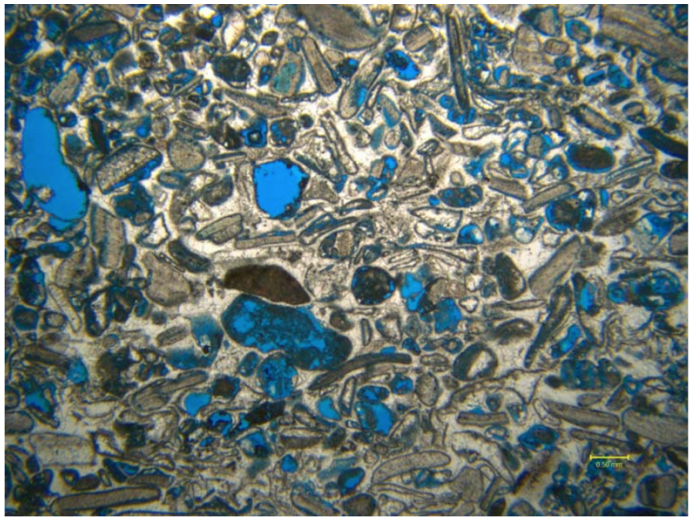

Figure 2.2: Thin section of Edwards limestone from Tipura (2008). A scale of 0.5 mm is displayed in the bottom corner.

Tipura (2008) presented a brief analysis of a thin section of Edwards limestone. The thin section is shown in Figure 2.2. Special blue epoxy was used to saturate the pores, while rock minerals and fragmental organic remains were represented by black and grey tone colours. The rock is clearly heterogeneous, with a variety of pore sizes (in the range 2mm to a few microns) randomly distributed in the rock. Two types of porosity were recognized in the thin section: primary porosity filled with sparry calcite cement and secondary porosity, which was dominant. No vugs were present in the rock. Pore size distributions of three Edwards limestone core plugs were also presented by Tipura (2008). The pore size distributions were obtained by mercury injection at certain pressure where volume of mercury was recorded. The intrusion pressures were transformed into pore throat radii with the Young-Laplace equation assuming cylindrical pore neck shapes (equation (C.3)). dV/dlogP, which is a measure of intensity/frequency for the given pore throat size, was plotted as a function of pore throat size (Figure 2.3). The largest pore throat radius for all core plugs was ~90 microns, while the lowest was between 0.1 and 0.01 microns.

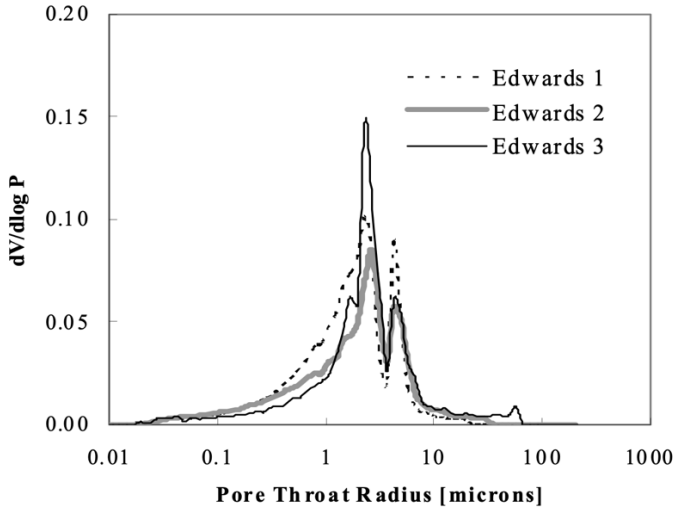

Figure 2.3: Pore throat distribution of three Edwards limestone samples from Tipura (2008).

2.2 Definition of wettability

Wettability can be defined as "the tendency of one fluid to spread on or adhere to a solid surface in the presence of other immiscible fluids" (Craig, 1971). When water preferentially spreads on the rock surface, the rock is said to be water-wet, while a surface is oil-wet when oil preferentially spreads on it. Figure 2.4 illustrates contact angles for different types of wettability. The contact angle may be measured through the water phase on a simplified mineral surface, but is here used to illustrate different types of wettability.

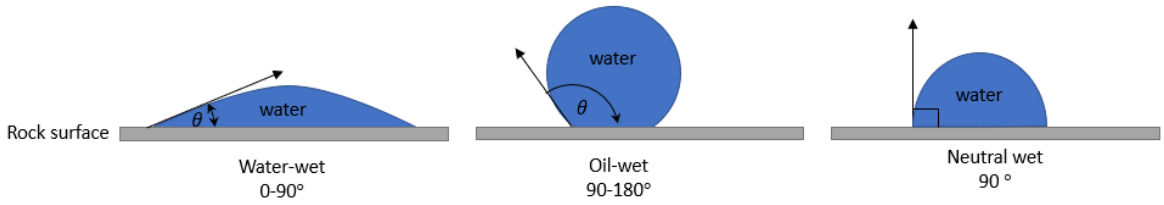

Figure 2.4: Contact angles representative of different wettabilities.

Wettability strongly influence capillary pressure, relative permeability and water flood behaviour (Anderson, 1986b). According to Bobek et al. (1958), core analysis also frequently show oil recoveries from preferentially water-wet systems to be significant higher than from preferentially oil-wet systems. In order to understand oil recovery on field scale, recovery on smaller scales (e.g. core scale) has to be understood. This thesis investigates whether polymer injection can alter the wettability preference of an aged core plug towards water-wet.

2.3 Wettability measurement

Many different methods for wettability measurements on the core scale are proposed, both quantitative and qualitative. Quantitative methods used in this thesis are the Amott-Harvey index, which is based on spontaneous imbibition and forced displacement, and magnetic resonance imaging (MRI). Scaled spontaneous imbibition curves and end-point relative permeabilities of oil and water are qualitative methods that may be used to indicate wettability or wettability changes. The different methods will be described in detail below.

2.3.1 Amott-Harvey Wettability Index

Amott (1959) devised a method to quantify the average wetting state of a porous medium. One full Amott-Harvey cycle consists of the following four steps (illustrated in Figure 2.5):

(1) spontaneous imbibition of water, (2) forced water injection, (3) spontaneous imbibition of oil, (4) forced oil injection, and is based on the fact that the wetting fluid will generally imbibe spontaneously into the core, displacing the nonwetting fluid (Anderson, 1986a). The Amott-Harvey wettability index, I_{AH}, is given by:

$$I_{AH} = I_w - I_o \tag{2.1}$$

where I_w is the wettability index of water and I_o is the wettability index of oil.

The wettability indices of water and oil are quantified by measuring the increase in water and oil saturation during spontaneous imbibition (ΔS_{ws} and ΔS_{os}) and the overall increase in water and oil saturation (ΔS_{wt} and ΔS_{ot}) after forced displacement.

The wettability index for water and oil, respectively, are given by:

$$I_w = \frac{\Delta S_{ws}}{\Delta S_{wt}} \tag{2.2}$$

$$I_o = \frac{\Delta S_{os}}{\Delta S_{ot}} \tag{2.3}$$

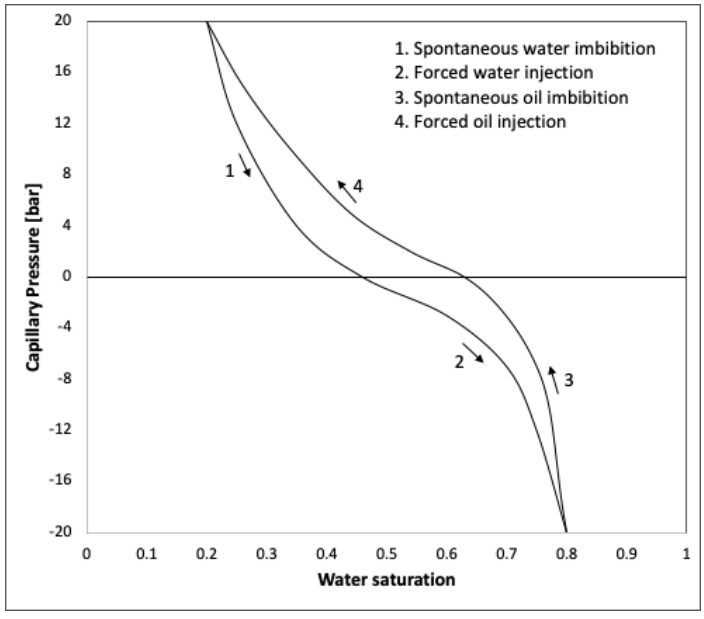

Figure 2.5: The four steps of one full Amott-Harvey cycle: Spontaneous water imbibition, forced water injection, spontaneous oil imbibition, and forced oil injection.

Table 2.1: Approximate relationship between wettability and the Amott-Harvey wettability Index.

	Amott-Harvey Index
Water-Wet	$0.3 \leq I_{AH} \leq 1.0$
Neutrally Wet	$-0.3 \leq I_{AH} \leq 0.3$
Oil-Wet	$-1.0 \leq I_{AH} \leq -0.3$

Table 2.1 gives approximate values of the Amott-Harvey index for water-wet, naturally wet and oil-wet cores. The Amott-Harvey method is insensitive near neutral wettability. This is because the volume of fluids spontaneously imbibed is much lower than for strongly wetted systems. The method is therefore more accurate on strongly water-wet or strongly oil-wet core plugs, where the volume imbibed is higher. The Amott-Harvey index is therefore not an ideal measure of the wettability of all aged core plugs in this work. The Amott-Harvey method still provides valuable information in core analysis of weakly wetted systems: the method is cheap and reproducible, it is possible to repeat it for many cycles, thereby indicating a change of wettability within a given core, and it is possible to do wettability measurements in many core plugs simultaneously to provide statistics. Complementary imaging by magnetic resonance imaging (MRI) provides spatial information concerning the wettability distribution within core plugs, although the method is both expensive and time-consuming. The wettability distribution of one dynamically aged core plug was performed using MRI, described further in section 3.9.1.

2.3.2 Spontaneous imbibition

Capillary pressure (defined in Appendix C) is the driving force for spontaneous imbibition. The wettability of a core plug affects the rate and amount of spontaneous imbibition of water or oil by affecting the capillary pressure.

The recovery efficiency is also affected by the capillary pressure. The rate of spontaneous imbibition and the capillary pressure curve versus water saturation can be used to determine the wettability of a core plug. Spontaneous imbibition of water from irreducible water saturation may increase the water saturation to the residual oil saturation in a strongly water-wet system (Donaldson, 2008). Lower imbibition rates and smaller volumes imbibed indicate more weakly wetted systems. If no water is imbibed, the core is either oil-wet or neutrally wet (Anderson, 1986a). According to Viksund et al. (1998), the relative rate of imbibition will increase with increase in initial water saturation.

2.3.2.1 Scaling of spontaneous imbibition

Scaling of spontaneous imbibition is important to be able to predict recovery behaviour on field scale from laboratory imbibition on the core scale. Recovery curves normalized by a reference volume are usually plotted versus a scaling time group in scaling practices (Mirzaei-Paiaman and Masihi, 2013). How to scale the non-wetting phase (NWP) recovery by counter-current spontaneous imbibition is therefore an important challenge that has been a focus of research for decades.

The scaling equations do not consider variations in wettability but provides a useful method to compare experiments with varying wetting phase viscosity and correct for small variations in core plug dimensions. According to Fischer and Morrow (2006), the correlation of imbibition data is obtained by compensating the geometric mean of the viscosities for an overall systematic increase in dimensionless time for recovery. The scaling equation developed by Ma et al. (1999) accounts for the effect of differences in viscosity ratio. It was found that imbibition rate depends on the square root of the oil/water viscosity. This is necessary to consider during spontaneous imbibition of high viscous polymer -and glycerol solutions, which is performed in this work. t_D is dimensionless time, and is given by:

$$t_D = t\sqrt{\frac{K}{\varphi}}\frac{\sigma}{\mu_{gm}}\frac{1}{L_C^2} \tag{2.4}$$

where K is the absolute permeability of the core plug, φ is the porosity, σ is the interfacial tension between the wetting and the non-wetting phase and t is the time. μ_{gm} is the geometric mean of the water and oil viscosities (μ_w, μ_o):

$$\mu_{gm} = \sqrt{\mu_w \mu_o} \tag{2.5}$$

L_c is the characteristic length, compensating for different boundary conditions. The general equation is (Ma et al., 1999):

$$L_c = \sqrt{\frac{V_b}{\sum_{i=1}^{i=n}\frac{A_i}{x_{Ai}}}} \tag{2.6}$$

where x_{Ai} is the distance from the imbibition face to the no-flow boundary. In this work all faces open (AFO) boundary condition were used during spontaneous imbibition in most

experiments. The characteristic length for this boundary condition was derived by Zhang et al. (1996) and is given by:

$$L_c = \frac{L_S d_S}{2\sqrt{d_S^2 + 2L_S^2}} \tag{2.7}$$

where L_S is the length of the core plug and d_S is the diameter of the core plug.

Interfacial tension

Interfacial tension (IFT) is a property of the interface between two immiscible phases (e.g. oil/water) and is one of the parameters in the scaling equation for spontaneous imbibition. Interfacial tension between the aqueous phase and the oil phase was not measured in this work, but measurements of IFT between brine/decane, 5000ppm HPAM/decane and 69wt% glycerol/decane were performed by Reite (2019). The interfacial tension measurements for all combinations of oleic and aqueous phases are presented in Figure 2.6. An average of the measured IFTs for each fluid combination was used for calculations in this thesis.

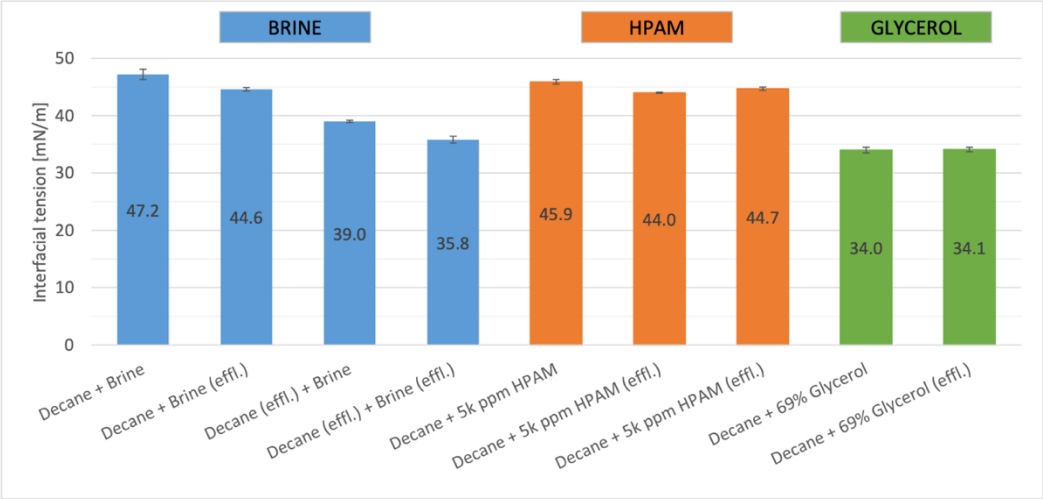

Figure 2.6: Interfacial tension measurements with error bars. IFT for each combination of fluids were measured 10 times. The deviation is equal to one standard deviation. (effl.) means effluent (Reite, 2019).

Viscosity

Viscosity is a parameter defining the internal resistance of a fluid to shear and is also a parameter in the scaling equation. The resistance occurs due to interaction between the molecules of the flowing fluid. Generally, the viscosity increases with molecular weight and decreases rapidly with increase in temperature (McCabe, 2005). The Newton model, quantifies

viscosity, μ, as the proportionality constant between the applied shear stress, τ, and the shear rate du/dy of a linear flow:

$$\tau = \mu \frac{du}{dy} \tag{2.8}$$

Most gases and liquids follow this relation and are called Newtonian fluids. Some fluids have rheological behaviour different from Newtonian fluids. These fluids, which are called non-Newtonian fluids, do not have a linear relationship between shear stress and shear rate (Metzner and Otto, 1957). Viscosity is an important aspect in this thesis because polymer solutions are used in spontaneous imbibition and forced displacement core scale experiments. Polymer solutions are non-Newtonian and have higher viscosities than e.g. oil or water (Newtonian fluids). Partially hydrolysed polyacrylamide (HPAM) polymer and glycerol were used to increase brine viscosity by a factor of 20-40 in this thesis (see chapter 3.1.1 and 4.5.1).

Waterflood in a hydrocarbon reservoir is highly affected by the oil/water viscosity ratio μ_o/μ_w. The mobility of a fluid *i*, λ_i, decreases with an increase in viscosity. Mobility is defined as:

$$\lambda_i = \frac{k_{ri}}{\mu_i} \tag{2.9}$$

where k_{ri} is the relative permeability of the given fluid and μ_i is its viscosity.

The mobility ratio is defined as the ratio of the displacing fluid mobility, λ_D, to the displaced fluid mobility, λ_d:

$$M = \frac{\lambda_D}{\lambda_d} = \frac{k_{rD}}{\mu_D}\frac{\mu_d}{k_{rd}} \tag{2.10}$$

where k_{rD} and μ_D are the relative permeability and viscosity of the displacing fluid, and k_{rd} and μ_d are the relative permeability and viscosity of the displaced fluid. The mobility ratio influences two-phase flow processes, e.g. the time of water break-through and duration of transient period (period of two-phase production).

2.3.3 End-point relative permeability

Relative permeability curves can give an indication of the wettability of a core plug, especially by considering the end-point relative permeability at irreducible wetting and non-wetting phase

saturation (permeability is defined in Appendix A). In a uniformly and strongly water-wet core plug, water will be located as a thin film in the larger pores, and fully saturating the smaller pores. The non-wetting fluid (e.g. oil) is located in the middle of the larger pores. The end-point relative permeability of the non-wetting fluid is generally higher than the end-point relative permeability of the wetting fluid. This occurs because the non-wetting fluid will easily flow in the larger pores, while the wetting fluid will flow through films and in the smaller pores (Anderson, 1987). Craig (1971) stated rules of thumb to attribute differences in the relative permeability curves to different wettabilities, Figure 2.7.

Craig's rules of thumb

	Water-Wet	Oil-Wet
Connate water saturation	$S_w > 0.2 - 0.25$	$S_w < 0.15$
Saturation at which oil and water relative permeabilities are equal	$S_w > 0.5$	$S_w < 0.5$
End point relative permeability of water	$k_{rw,or} < 0.3$	$k_{rw,or} = 0.5 - 1.0$

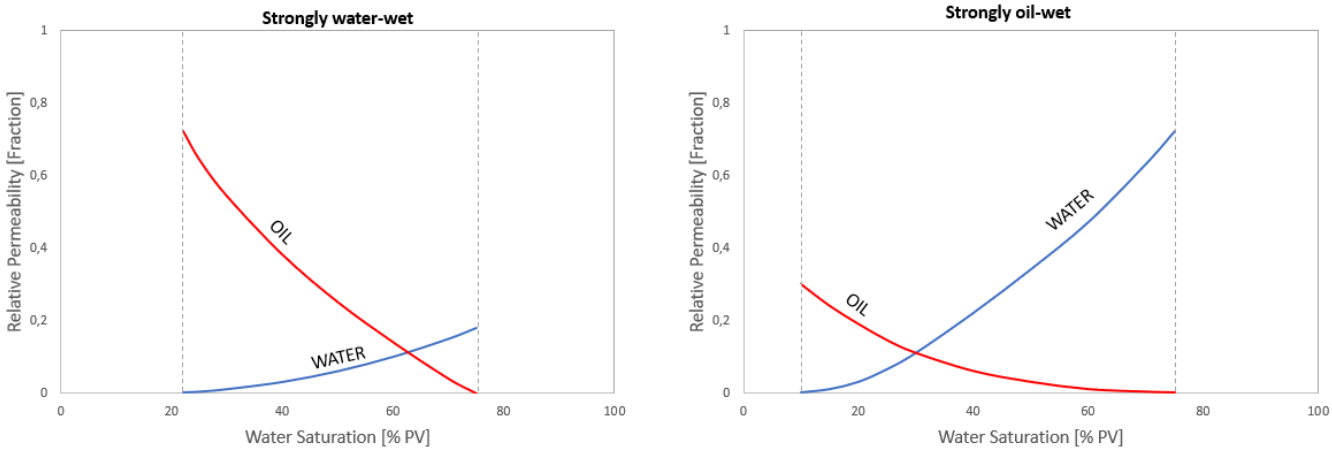

Figure 2.7: Craig's rules of thumb, and typical water-oil relative permeability curves of strongly water-wet rock to the left and strongly oil-wet rock to the right.

2.3.4 In-situ imaging

Three different imaging techniques used in petroleum engineering research are presented below: Magnetic Resonance Imaging (MRI), Computed Tomography (CT), and Positron Emission Tomography (PET). MRI is a quantitative method that can be used to quantify spatial wettability distribution in a core plug, while CT-imaging and PET-imaging are qualitative methods that can be used to describe wettability by quantifying fluid flow in the core.

2.3.4.1 Magnetic Resonance Imaging (MRI)

Magnetic Resonance Imaging (MRI) is a medical imaging technique that uses the principles of nuclear magnetic resonance (NMR), to record the stimulated absorption and emission of energy from nuclei placed within a magnetic field, thereby forming images representing the anatomy and/or the physiological processes of the body. MRI has also been used for studying the properties of water and/or oil saturated rocks since the early 1950´s. MRI provides information on the saturating fluid in the rock, and also yield information about pore size distribution, rock type and rock properties (Dunn, 2002). Tipura (2008) used MRI to study displacement mechanism in Edwards limestone as a function of wettability. A linear relationship between the MRI intensities and Decane saturation was found in the core samples. In addition, T_2 relaxation properties of oil- and water-saturated limestone were measured at various wettabilities and various fluid saturations in order to characterize wettability. The T_2 relaxation time for the oil phase at irreducible water saturation, S_{wi}, decreased almost linearly for stronger oil-wet conditions. In this thesis, MRI was used to evaluate the spatial wettability distribution in one core plug: first at strongly water-wet conditions, thereafter at oil-wet conditions after dynamic aging. Due to the circumstances surrounding the covid-19 pandemic it was not possible to complete the measurements on the aged core plug. The performed and planned experiments will be presented in section 3.9.1 and 4.2.1.

2.3.4.2 Computed Tomography (CT)

CT-imaging, which also is an imaging technique developed for clinical use, is based on an X-ray source that illuminates an object (e.g. a core plug) and projects the transmitted X-ray intensity onto an imaging device. Many X-ray measurements from different orientations are taken to create cross-sectional images of the object (Heindel, 2011). CT-imaging is also widely used as a qualitative and quantitative tool in petroleum engineering research (Akin and Kovscek, 2003). Withjack (1988) used CT-scanning to determine average porosities of Berea sandstone and dolomite core plugs. Close agreement (± 1 porosity %) was reported between the CT-derived porosities and those determined by conventional methods. CT-imaging has also been used to estimate permeability distribution by measuring in-situ flood-front velocities by CT-scanning (Withjack et al., 1991), or by measuring in-situ tracer concentrations by CT-scanning (Mohanty and Johnson, 1993, Johns et al., 1993), to visualize miscible and immiscible fluid displacements in core plugs (Fransham and Jelen, 1987, Peters and Hardham, 1990), and to characterize the nature of (homogeneous or heterogeneous) porous media (Bergosh and Lord, 1987, Peters and Afzal, 1992, Karacan and Okandan, 1999). In this thesis, CT-imaging was

used to assess and visualize the heterogeneity of the Edwards limestone core material. The results are presented in section 4.2.2.

2.3.4.3 Positron Emission Tomography (PET)

Positron Emission Tomography (PET) imaging is another frequently used method for medical in-situ 3D-imaging, but is also a valuable tool for in-situ characterization of fluid transport in porous media at the laboratory scale (Zahasky et al., 2019).

The flowing phase is labelled by positron-emitting radiotracers. When two phases are present, only one of the phases (injected or displaced) needs to be labelled in order to quantify fluid flow. As a result of the radioactive decay, positrons will be emitted. The positron will lose energy and slow down as it travels through the surrounding material. When the energy is low enough, the positrons interact with surrounding electrons which results in a complete annihilation of both particles. Two 511 keV photons (gamma rays) will be emitted in opposite directions to conserve momentum. A detector array in the PET scanner register the photons with time and use tomographic reconstruction methods to create 3D images of annihilation events within the defined time frame. The PET resolution is primarily limited by the positron travel distance before annihilation, which can be estimated with an uncertainty of ~1mm.

Fernø et al. (2015) successfully implemented combined PET/CT imaging to visualize and quantify fluid flow in sedimentary rocks. It was found that this method provided more information than from each method separately, and that it can be applied to a larger range of rock types and displacement processes. Brattekås et al. (2016) used PET/CT imaging to quantify the behaviour and blocking capacity of Cr(III)-acetate hydrolysed polyacrylamide gel during chase waterflooding. In this thesis, PET/CT imaging was used to visualize displacement fronts in a core plug during water, oil and polymer injection, further detailed in section 3.9.3.

2.4 Groups of wetting

The wettability of a core plug can range from strongly water-wet to strongly oil-wet. When water preferentially spreads on a surface in presence of oil, it is characterized as water-wet, while the surface is oil wet when oil preferentially spreads on it in presence of water. If the core plug has no strong preference for either oil or water, it is neutral wet (Anderson, 1986b). In addition, three intermediate wetting states can be defined: fractional wet (FW), mixed-wet large (MWL) and mixed-wet small (MWS). A FW core plug has one fraction of water-wet pores and another fraction of oil-wet pores, and the wettability distribution is uncorrelated to pore size. In a core plug that has MWL wettability, the largest pores are oil-wet while the smallest pores are water-wet. This relation is opposite for a core plug of MWS wettability (Skauge et al., 2007).

2.5 Wettability alteration (aging)

Most reservoir minerals are strongly water-wet in their original state. The rock wettability can change towards oil-wet by adsorption of polar compounds and/or the deposition of organic matter originally in the crude oil (Anderson, 1986b). Oil composition is key to wettability changes, because any wettability-altering components are in the oil phase in a water/oil/rock system (Abdallah et al., 2007). The same core material can be affected differently by different crudes and the same crude oil can cause different wettability effects in various core material. In addition to the oil and mineral surface composition, wetting alteration is also dependent on pressure, temperature, mineral surface, and brine chemistry, including ionic composition and pH (Bobek et al., 1958, Anderson, 1986b).

Buckley et al. (1989) performed adhesion tests in a rectangular glass cell with a contact angle goniometer for observations of oil-drop/water/glass contacts. An oil drop was introduced to the system for varying amounts of time before the oil was slowly retracted back into a burette. Two types of behavior were observed: non-adhesion, where the oil separated cleanly from the plate, and adhesion, where a drop of oil was left on the glass surface. It was found that the adhesion of the crude oil only occurred below a critical value of pH and above a critical Na^+ concentration. Liu and Buckley (1999) performed wettability alteration experiments on muscovite mica instead of glass. Mica has different surface structure and surface roughness compared to the glass cell. Wettability alteration of mica surfaces were observed by exposure to crude oils, but the adhesive areas were smaller than the corresponding areas on glass.

Graue et al. (2002) described two methods of wettability alteration: dynamic and static aging. The dynamic aging was based on continuous crude oil flooding through Rørdal chalk core plugs at elevated temperature with low injection rate for a specified period of time. Static aging was performed by flooding the core with crude oil to initial water saturation and thereafter submerging the core in crude oil at elevated temperature for a specified period of time. Flooding the core with crude oil during the entire aging process (dynamic aging), and reversing the flow direction halfway through the process, produced the most uniform wettability condition. Aging was more efficient at lower initial water saturations, i.e. yielding lower I_{AH}.

Ferno et al. (2010) performed dynamic aging of Rørdal chalk core plugs using variable duration of aging (48, 96 and 192h) and flow rates (1, 3, and 5 cm^3/h). An increase in the duration of aging yielded decreased Amott-Harvey water index. When the duration of aging was kept constant and injection rates varied, different wetting preferences were established. The lowest flow rate (1 cm^3/h) provided the least change in wetting, with a measured water index of $I_w = 0.53$. The water index was reduced to I_w=0.31 when the flow rate was increased to 3 cm^3/h. A further increase in the injection rate to 5 cm^3/h increased the water index to $I_w = 0.44$. It was suggested that the crude oil injection rate influenced the bulk crude oil interactions active in the wettability alteration process and that an optimal crude oil injection rate between 1 and 5 cm^3/h exists. Static aging was less effective than dynamic aging in altering wettability. Aging durations of up to 12 days were tested (Ferno et al., 2010).

In this thesis dynamic aging was performed using an injection rate of 1.5 ml/h (corresponding to 3 cm^3/h for 2-inch diameter core plugs) and aging duration of 144h. Static aging was performed by crude oil injection until initial water saturation was reached, and thereafter storing the core in a beaker of crude oil for 1000h at 80°C. The experimental procedures are described in detail in chapter 3.5.

Most of the core plugs used in this thesis were aged towards oil-wet conditions, but some cores spontaneously imbibed both water and oil. Submerging a core in an Amott cell filled with either water or oil will therefore be described as spontaneous imbibition of water or oil, respectively.

2.6 Wettability alteration by polymers

2.6.1 Polymers

Polymers are large molecules composed of many repeated subunits (monomers), that can be added to water to increase its viscosity. Polymer flooding also reduces the relative permeability to the aqueous phase, which promotes more favourable mobility ratio. Improved volumetric sweep efficiency during production of high viscous oil or production in heterogeneous reservoirs (Ali and Thomas, 1996) may therefore be seen.

Two types of polymers are used for Enhanced Oil Recovery (EOR); hydrolysed or partly hydrolysed polyacrylamide (HPAM) and biopolymers (such as xanthan gum). HPAM costs less and exhibits significantly greater viscoelasticity, and is therefore, by far, most applied (Sheng et al., 2015), but has not been widely used on the Norwegian Continental Shelf due to PLONOR regulations: chemicals are divided into different categories based on their environmental properties (black, red, yellow and green). Green chemicals, which are listed on the PLONOR list, are considered to pose little or have no negative impact on the environment. Permission is needed to emit chemicals that are not listed on the PLONOR list, i.e. are not in the green category. HPAM is in the red category (Wennberg and Petersen, 2017).

Polyacrylamides can be manufactured by polymerization of the acrylamide monomer, to produce a polymer that resembles a flexible coil. Macromolecules with average molecular weights ranging from 0.5 million to 30 million are produced during polymerization. The polyacrylamide, which adsorbs strongly on mineral surfaces, is partially hydrolysed to reduce adsorption by reacting polyacrylamide with a base. Hydrolysis converts some of the amide groups (NH_2) to carboxyl groups (COO^-), as shown in Figure 2.8 (Green, 1998).

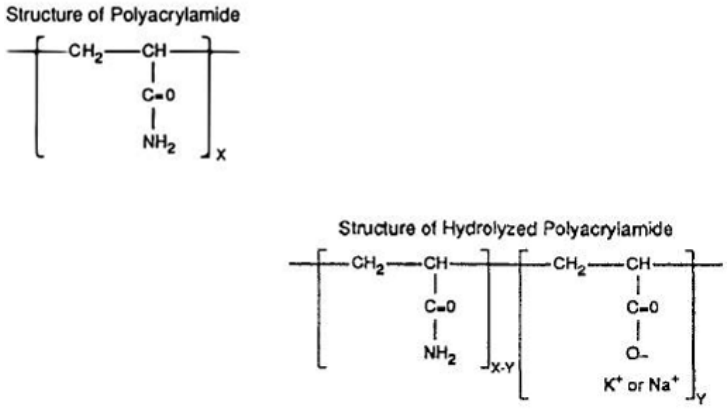

Figure 2.8: Molecular structure of high-molecular-weight polyacrylamides (Green, 1998).

Aqueous polymer solutions often exhibit non-Newtonian rheological behaviour, where the apparent viscosity decreases as shear rate increases. Fluids with this rheological characteristic are classified as shear thinning. Salinity content may also affect the rheological behaviour of polymer solutions, depending on the degree of hydrolysis. Hydrolysis of polyacrylamide introduces negative charges on the backbone of the polymer chain, which at low salinities can cause the polymer chain to stretch. Each polymer molecule occupies more space in solution, and the apparent viscosity of a dilute solution increases accordingly (Green, 1998).

Retention is a term used to cover all the mechanisms responsible for the reduction of mean velocity of polymer molecules during their propagation through porous media. Polymer retention varies with polymer type, polymer concentration, molecular weight, rock characteristics and composition, brine salinity hardness and pH, flow rate and temperature (Lake, 2014). All polymers experience retention in permeable media, predominantly by two mechanisms; adsorption of polymer molecules on the surface of large pores and mechanical entrapment in small pores (Huh et al., 1990). In addition, precipitation of polymer molecules can arise. These mechanisms are illustrated in Figure 2.9. The HPAM polymer solutions used in the experiments in this work were filtered before use to remove larger clusters of polymers and prevent unnecessary mechanical entrapment.

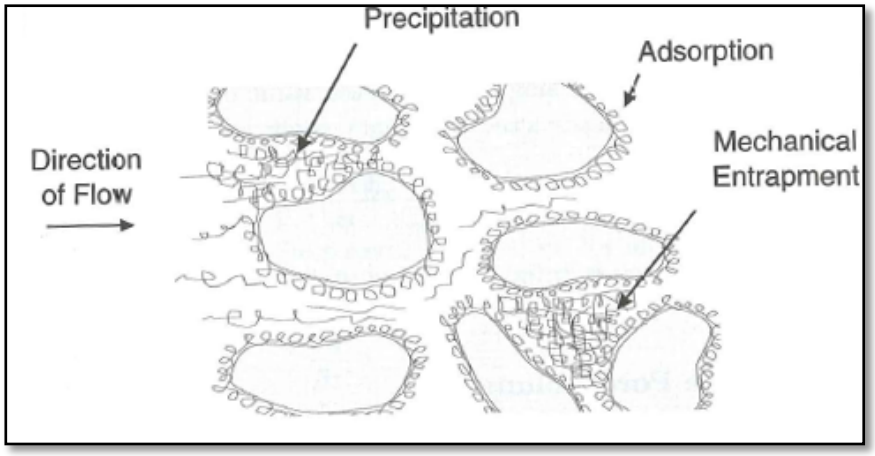

Figure 2.9: Types of Polymer Retention in Porous Media and Inaccessible Pore Volume, from Zolotuchin (2000).

In this thesis, partially hydrolysed polyacrylamide (HPAM) was used to investigate the effect of polymer injection on core plug wettability. Baseline experiments were performed using Glycerol as a viscosifying agent. Glycerol is a trihydric alcohol, of 1500 cP viscosity at 20℃. Glycerol is miscible with water and ethanol in all proportions, and immiscible with hydrocarbons. Viscosity decreases with increase in temperature and with addition of water, and increases with addition of electrolytes to its aqueous solutions (Monick, 1968, Takamura et al., 2012). Glycerol has previously been used as a viscosifying agent for aqueous solutions (Kyte and Rapoport, 1958, Rapoport and Leas, 1953, Fischer and Morrow, 2006, Reite, 2019, Saunes, 2018). Glycerol was used for spontaneous imbibition and forced injection in this thesis because the viscosity of a brine solution can be increased to the same level as with polymer, but without the presence of surface-active components that will potentially impact wettability.

2.6.1.1 Short summary of previous research

Elmkies et al. (2001) performed static crude oil aging at a temperature of 60 ℃ for 6 weeks on St-Maximin limestone and on Estaillades limestone. The crude oil aging was found to modify the wettability of the cores towards less water-wet and slightly oil-wet conditions. A nonionic polyacrylamide polymer was injected in the limestone cores and it was found that adsorption of the hydrophilic polymer in partially oil-wet cores, partly restored the initial water-wet wettability.

Barreau et al. (1997) flooded water-wet and oil-wet (silane-treated) sandstone core plugs with brine, mineral oil, and 2500ppm polymer solution made of a high-molecular-weight nonionic

polyacrylamide (PAM) and brine. Capillary pressure, relative permeability and end-point saturations were measured before and after polymer injection. There was a strong increase in irreducible water saturation after polymer adsorption both in the water-wet and the oil-wet cores (from 0.33 to 0.39 for water-wet cores and from 0.32 to 0.49 in oil wet cores). The residual oil saturation was almost unchanged after polymer injection in the water-wet core, while it decreased significantly (from 0.54 to 0.22) in the oil-wet core. The capillary pressure was strongly increased over the whole saturation range by the presence of adsorbed polymer in the water-wet core. The capillary pressure for the oil-wet core changed from negative to positive, with a higher maximum value, after polymer adsorption in the core. Because brine/oil and polymer-solution/oil IFTs are almost the same, this behaviour was explained by wettability improvements (stronger water-wet conditions) and pore-size reduction by the adsorbed polymer layer. For water-wet media, the increase in capillary pressure was suggested to be mainly the result of pore throat reduction, while for the oil-wet medium, a complete change of wettability was observed in addition to pore-size restriction. The relative permeability curves showed a greater reduction in relative permeability of water compared to relative permeability of oil, and the effect was stronger in the water-wet medium.

Juarez-Morejon et al. (2017) did spontaneous imbibition experiments in Bentheimer sandstone with intermediate wettability. Four types of experiments were performed: Amott tests in brine and in polymer solution (HPAM solution with a concentration of 2500ppm) to measure wettability index and determine the wettability of the cores, spontaneous imbibition using brine, polymer solution, and brine followed by polymer solution. Spontaneous imbibition in polymer solution showed a better efficiency in oil recovery than spontaneous imbibition in brine. The oil recovery was also enhanced when spontaneous polymer imbibition was performed after spontaneous brine imbibition. Amott-Harvey wettability indices were measured for two core plugs: one where brine constituted the aqueous phase and one where polymer constituted the aqueous phase. The measured brine wettability index was lower (I_{AH} =0.08) than the measured polymer wettability index (I_{AH} =0.81), indicating stronger water-wet conditions with polymer present in the pore network.

2.6.2 Disproportionate Permeability Reduction

Polymer injection influence the relative permeability of water more than oil; which must be understood in the interpretation of experiments. The end-point relative permeability of water is more reduced than the end-point relative permeability of oil when polymers or polymer gels saturate a porous medium. This phenomenon is usually referred to as disproportionate permeability reduction (DPR) (Zaitoun and Kohler, 1988, Liang et al., 1995, Nilsson et al., 1998, Al-Sharji et al., 1999, Willhite et al., 2002). DPR may be studied using pore-filling polymer gels, which will behave as polymer solutions during injection. After injection, the gelant solution (made by adding a crosslinker, e.g. chrome (Cr(III)) acetate, to the polymer solution) forms to gel. Polymer gels can be used to block high permeability zones in a reservoir, to reduce water cut and improve oil recovery. The mechanisms causing DPR are not well understood, and several possible mechanisms have been proposed, e.g. gravity effect and lubrication effects, gel shrinking and swelling, segregation of oil and water pathways and wettability effects.

Liang et al. (1995) flooded core plugs with Cr(III)-acetate/HPAM polymer gel, and suggested segregation of oil and water pathways within the porous medium to be the dominant mechanism for DPR. The aqueous gelant followed the water preferred pathways and blocked these when gel formed. Thus, many of the oil preferred pathways remained connected. Analogously, an oil-based gel would reduce the permeability of oil more than water. DPR was observed in systems of intermediate wettability as well as in strongly water-wet systems. The DPR was even more evident in a core of intermediate wettability than in a strongly water-wet core when a resorcinol/formaldehyde gel was used. The effect of wettability varied with the gel. Although the results showed that wettability effects could play a role in the DPR, but it was not suggested to be the main mechanism.

Nilsson et al. (1998) injected brine, white oil, HPAM based polymer with an added crosslinker, and biopolymer into water-wet, oil-wet and fractional wet sand packs. End-point relative permeabilities to oil and water were measured before and after polymer injection, and residual resistance factors (ratio of end-point relative permeability before and after gel treatment) of water and oil (RRF_w / RRF_o) were calculated. When HPAM gel was injected at 25% brine saturation in the oil-wet sand pack, a RRF_w of 810 was measured, while an RRF_o of 50 was measured. When the gel was placed at 40% brine saturation the core was completely blocked.

Complete blocking was also obtained when HPAM gel was placed at S_{or} in a water-wet system. HPAM gel was placed in two fractionally wet core plugs by simultaneously injecting gel and oil. The water end-point relative permeability was reduced by a factor of 50 in one of the cores, and by a factor of 3 in the other core. The oil end-point relative permeability was only reduced by factors of 4 and 1.1. It is important to preserve oil continuous channels after gel treatment, which was obtained in fractional wetted cores and oil-wet cores, but to a lesser extent in water-wet cores. The results supported segregated pathways for oil and water as the main mechanism causing DPR.

Flooding of sand packs and Berea sandstone cores using Cr(III)-acetate/HPAM gelant was performed by Willhite et al. (2002) and Nguyen et al. (2006). They discovered that new flow paths for brine and oil were created after injection of gelant and subsequent gelation. The new pathways were primarily caused by the dehydration of the gel by injection of oil. In this thesis gel was not used, but gel dehydration is anticipated to be analogous to polymer solution displaced by oil in my experiments. They suggested that the trapping of residual oil in this new pore space within gel, caused the decreased brine relative permeability as illustrated in Figure 2.10. Seright et al. (2004) and Seright et al. (2006) used X-ray computed microtomography to investigate DPR in small cores of water-wet Berea sandstone and oil-wet porous polyethylene after injection of Cr(III)-acetate/HPAM gel. When oil was injected after gel placement, the oil reduced the gel volume by 55% in the water-wet Berea core (insensitive to pore size), while it reduced the gel volume by only 16.3% in the oil-wet polyethylene core (mainly in the smaller pores). The resistance factor for water was 15 for the water-wet core after gel placement, while it was 24 for the oil-wet core. The results supported the gel dehydration (shrinking) as the main mechanism for DPR. S_{or} in the Berea core increased from 18.4% to 51% after gel placement, and it was assumed that the increase in trapped oil restricted the water flow, giving a resistance factor for water of 1220. In polyethylene, S_{or} was significantly lower after gel placement than before gel placement, although the resistance factor for water was 2130. Thus, oil trapping could not explain the large DPR seen in polyethylene, and gel rehydration was suggested as an explanation for this.

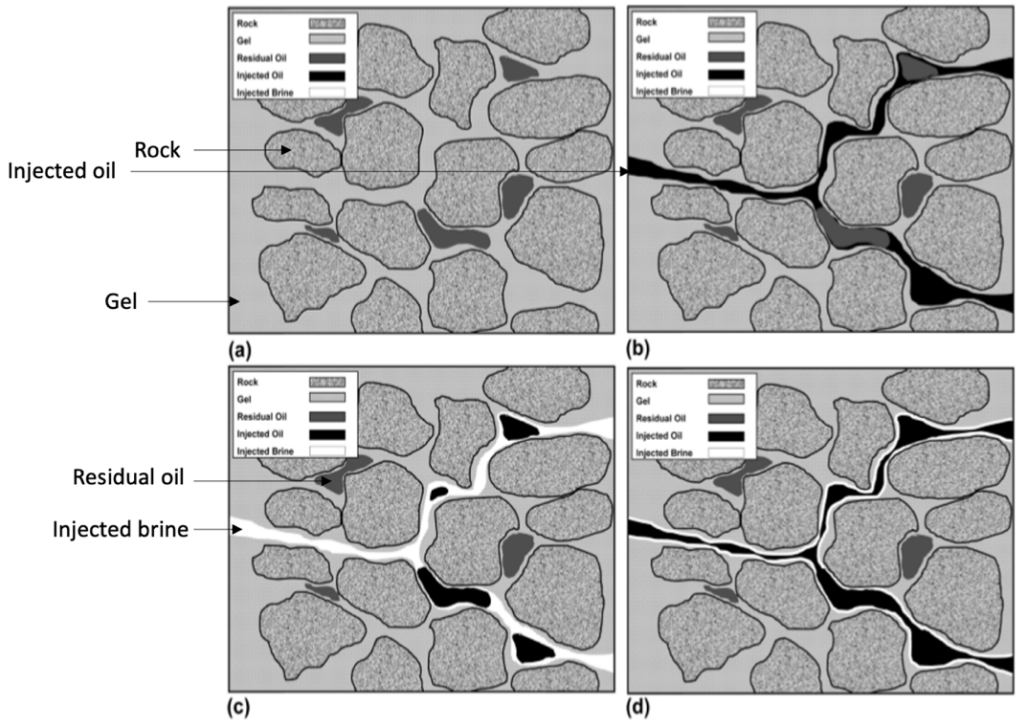

Figure 2.10: (a) Encapsulation of waterflood residual oil following in-situ gelation of chrome-acetate-polyacrylamide gelant; (b) generation of new pore space when gel is dehydrated by injection of oil; (c) trapping of residual oil in new pore space during brine flood, leading to disproportionate permeability reduction of brine; (d) flow paths of oil through new pore space, trapping low saturations of brine. Moderated from Willhite et al. (2002).

3 Experimental Procedures

A detailed description of how the different experiments were conducted is presented in this chapter. Procedures for fluid preparation and viscosity measurements are described in section 3.1 and 3.2. Section 3.3 and 3.4 describes core plug preparation, porosity measurement and permeability measurement. The two different aging procedures are described in section 3.5 and the procedure used to split core plugs is presented in section 3.6. Methods used for wettability measurements, spontaneous imbibition and end-point relative permeability, are explained in section 3.7 and 3.8. All these experiments were performed at the Department of Physics and Technology at the University of Bergen. In section 3.9 the in-situ imaging experiments (CT, PET and MRI) are described. In-situ PET-imaging was performed at the Molecular Imaging Centre at the Department of Biomedicine, CT-imaging was performed at the Department of Earth science, and MRI was performed at the MRI centre at Equinor, Sandsli.

3.1 Fluids

Properties of fluids used in this thesis are listed in Table 3.1. In section 3.1.1 and 3.1.2 the preparation of the fluids is described in detail.

Table 3.1: Fluid properties.

Fluids	Contents	Density 20°C $[g/cm^3]$	Density 80°C $[g/cm^3]$	Viscosity 20°C $[cP]$	Viscosity 80°C $[cP]$
Ekofisk brine	NaCl: 4 wt% $CaCl_2$: 3.4 wt% $MgCl_2$: 0.5 wt% 0.01 wt% NaN_3	1.05	-	1.09	-
n-Decane	Mineral oil, $C_{10}H_{22}$	0.73	0.68	0.92	0.40
Decahydro-naphtalene (Decalin)	Mineral oil, $C_{10}H_{18}$	-	0.90	-	0.85
North Sea Crude Oil	Acid Number: 0.09 mgKOH/g Base Number: 1.2 mgKOH/g Saturates: 53 wt% Aromates: 35 wt% Resins: 12 wt% Asphaltenes: 0.9 wt%	0.85	0.85	14.3	2.7

3.1.1 Aqueous fluids

Three different aqueous fluids were used for spontaneous imbibition and injection: Ekofisk brine, 5000ppm polymer solution, 61wt% glycerol and 69wt% glycerol.

Brine

Ekofisk brine was made by mixing 1000g of distilled water with 40g of NaCl, 34g of $CaCl_2$ and 5g of $MgCl_2$ using a magnetic stirrer until all salt was dissolved. 0.05 ml NaN_3 was added to the solution to prevent bacterial growth in the core plugs.

Polymer solution

Polymer solution was used as the aqueous phase in spontaneous imbibition and forced injection to investigate whether injection of a hydrophilic polymer (HPAM) could alter the wettability preference of an aged core plug towards water-wet. Alcoflood 935, which is a partially hydrolyzed polyacrylamide, was used in the experiments. This acrylamide polymer is commercially available and has a nominal molecular weight of 5×10^6 g/mol, and is hydrolyzed to a degree of 50-10 mole% (Sydansk et al., 2004). To make one liter of 5000 ppm HPAM solution, 5g of Alcoflood 935 powder was mixed with 1024.8g of pre-made Ekofisk brine. The powder was slowly added to the brine, in a vortex created by magnetic stirring, to prevent aggregation. When all the powder was dissolved in the brine, the speed of the magnetic stirrer was reduced to a minimum over night to ensure complete hydration. The polymer solution was filtered through a filter with a pore size of $5\mu m$ before use to remove microgels and other nonlinear, multimolecular structures (Foshee et al., 1977). The setup used for filtering is shown in Figure 3.1. The polymer solution was exposed to vacuum to promote flow of polymer solution through the filter. The polymer solutions were visually clearer and more transparent after filtration. Seven different polymer solutions were used in this thesis, all with the same polymer concentration.

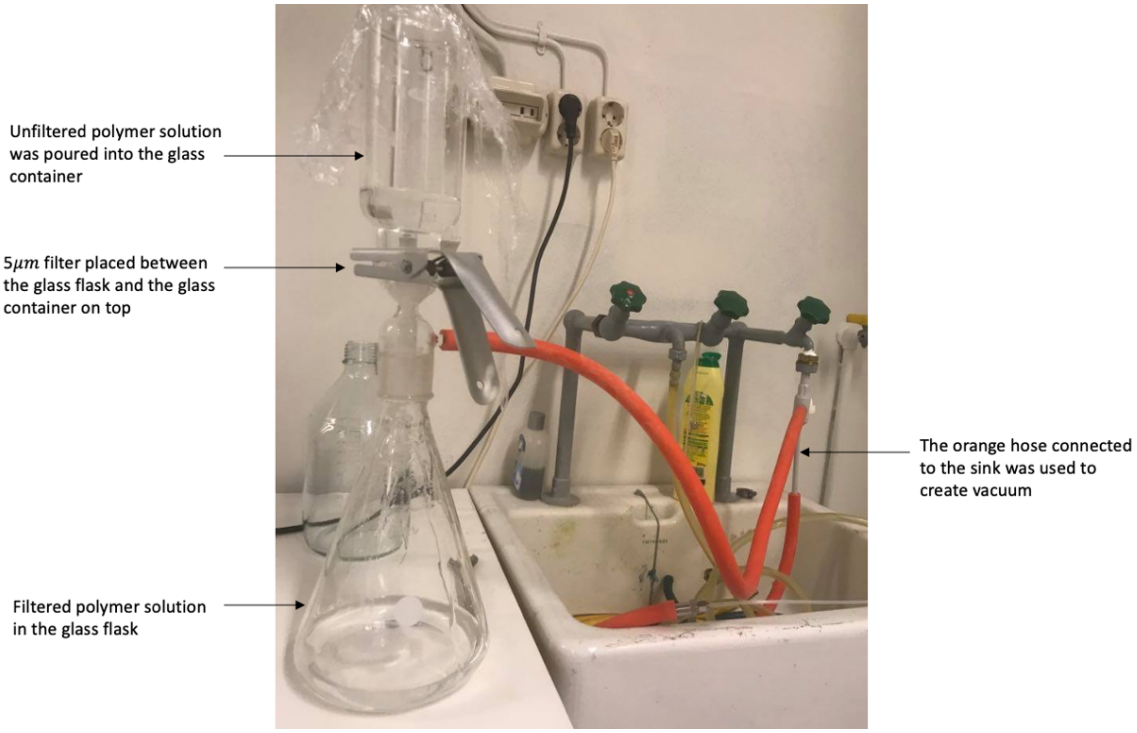

Figure 3.1: The setup used for filtration of the polymer solutions.

Glycerol

Glycerol was used as a viscosifying agent, because it can produce a solution with similar viscosity as a polymer solution but does not contain polar components that adsorb to mineral surfaces. The impact of glycerol imbibition and injection on aged core plugs therefore constituted a baseline to which polymer imbibition and injection could be compared. The glycerol solutions were made by mixing pre-made Ekofisk brine and a predetermined volume of glycerol. A magnetic stirrer was used to stir the solution until it appeared homogenous. The equations in Figure 3.2 were used to calculate which glycerol concentration was expected to yield viscosity similar to the polymer solutions. Four glycerol solutions were made, one containing 61wt% glycerol and three containing 69wt% glycerol, to produce a variation of viscosities (calculated range 13.6-24.9cP). The glycerol solutions were not filtered.

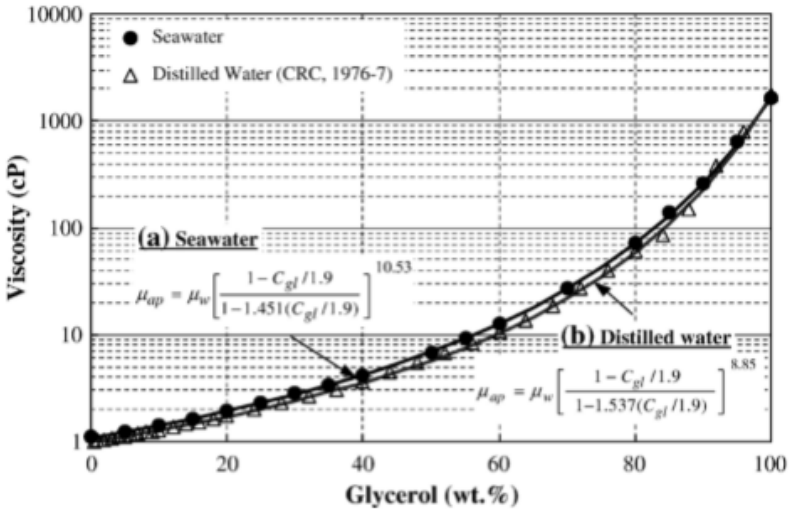

Figure 3.2: Aqueous phase viscosity of (a) glycerol/brine and (b) glycerol/distilled water, from (Fischer and Morrow, 2006).

3.1.2 Oleic fluids

Oleic fluids used in the experiments were North Sea Crude oil, n-Decane and Decaline. To remove surface active components, n-Decane was filtered through a column of glass wool, aluminum oxide, and silica gel, as suggested by Fernø et al. (2013). After filtering, the filtering components became discolored and the n-Decane was visually clearer. The setup for filtration of n-Decane is shown in Figure 3.3. Decaline was not filtered before use.

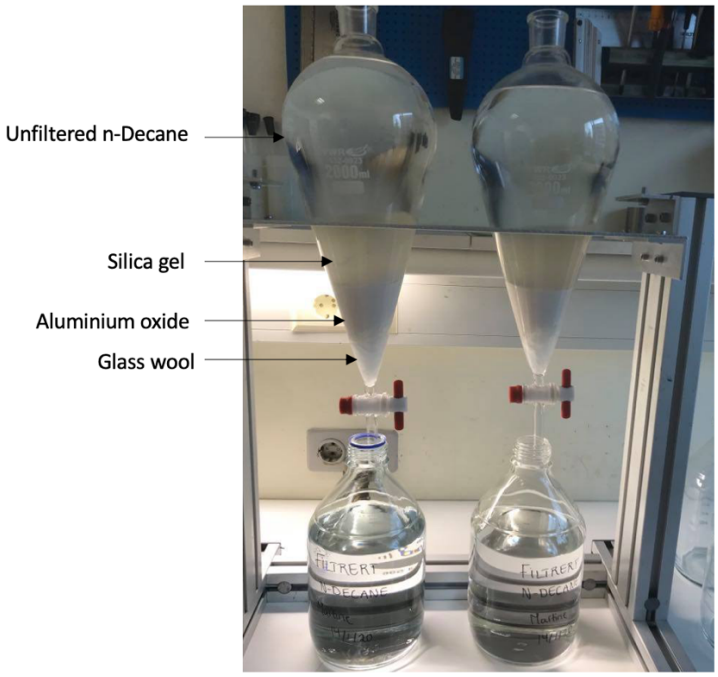

Figure 3.3: Column of glass wool, aluminium oxide, and silica gel for filtration of n-Decane.

3.2 Viscosity Measurements

To measure dynamic viscosities of polymer -and glycerol solutions, a Brookfield DV-II+Pro Viscometer (Model LVDV-II+Pro, cone part no. CPA-42Z) was used. The measurements were performed at ambient, constant temperature. 1 ml of fluid was placed in the middle of the sample cup. The cup was gently attached to the viscometer. Measurements were performed when the temperature stabilized at ambient conditions. Different rotation speeds were used for the measurements, and the viscosity, torque and temperature were recorded for each speed. The viscometer was cleaned between each viscosity measurement by spraying distilled water and Acetone in the sample cup and on the spindle until the devices were clean. In order to not destroy the apparatus, it could not be touched during cleaning. Viscosity of each polymer and glycerol solution was measured at least twice. In addition, viscosities of 20 production effluents were measured (only one measurement was done for each) to check if the viscosities were equal to the samples that had not been in contact with a core plug. Equations used to measure the shear stress the fluid samples were subjected to during viscosity measurements, and full-scale viscosity range for a given RPM are given in Appendix D.

3.3 Preparations

Porosity measurements

1.5" core plugs of Edward Limestone core material were drilled from an outcrop rock from West Texas. The core plugs were washed gently with tap water to remove loose particles and dried for two weeks in a heating cabinet holding 65℃. Core plug length, diameter and matrix weight were measured. The core plugs were thereafter placed in a glass cell for saturation. The experimental setup is illustrated in Figure 3.4. The glass cells containing core plugs and brine were first vacuum evacuated separately. Brine was thereafter introduced to the core plugs by opening the valve between the two glass cells until brine fully covered the core plugs. The core plugs were taken out of the container after 24 hours. The weight of each water saturated core plug was measured, and the effective pore volume, $V_{p,eff}$, and the effective porosity, ϕ_{eff}, (porosity is defined in Appendix A) were calculated from weight measurements using a gravimetric method, where the weight increase between a dry and saturated core plug were divided by the density of the saturating fluid, ρ_i (Jenkins, 1966) and equation (A.1):

$$\phi_{eff} = \frac{V_{p,eff}}{V_b} = \frac{\left(m_{wet} - m_{dry}\right)}{L \cdot \pi r^2 \cdot \rho_i} \tag{3.1}$$

where m_{dry} and m_{wet} are the weight of the core plug before and after it was saturated, respectively. Ekofisk brine was used as the saturating fluid for all core plugs.

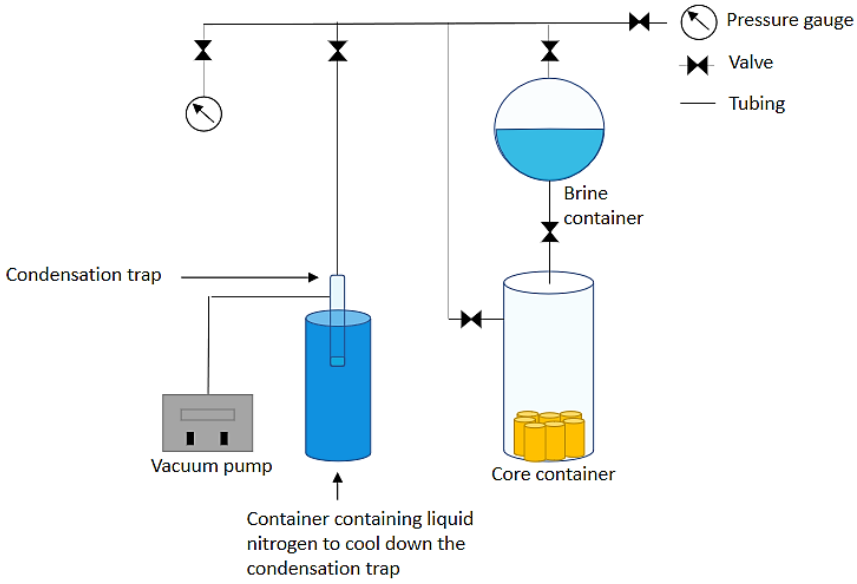

Figure 3.4: Schematic illustration of the setup used for vacuum evacuation and fluid saturation of core plugs.

3.4 Permeability measurements

The core plug was placed in a Hassler biaxial core holder with a confinement pressure for absolute permeability measurements (permeability is defined in Appendix A). Ekofisk brine was injected at a constant volumetric flow rate using a Quizix QX pump, and the pressure drop across the core plug was measured. The volumetric flow rate was increased consecutively, and the pressure drop recorded for each rate. The permeability was calculated using Darcy's law:

$$Q = \frac{KA}{\mu}\frac{dp}{dx} \tag{3.2}$$

where Q is the volumetric flow rate of a fluid with viscosity μ flowing through a porous medium with cross section area A. dp/dx is the differential pressure drop over a unit length of the porous medium.

The experimental setup is illustrated in Figure 3.5.

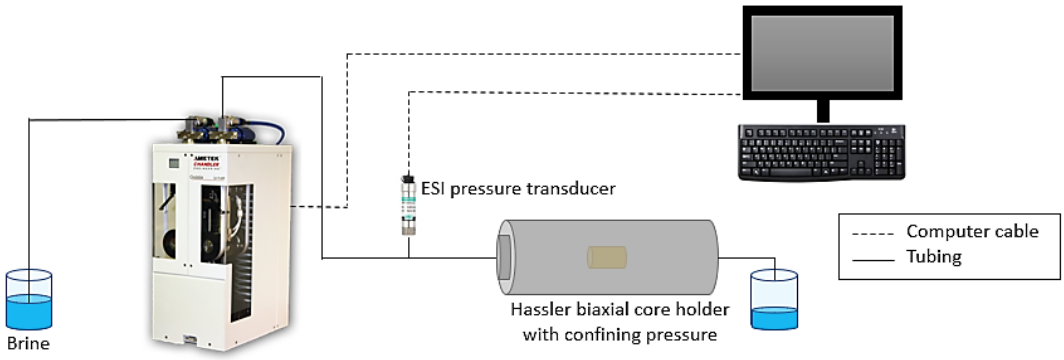

Figure 3.5: Experimental setup for absolute permeability measurements.

3.5 Wettability Alteration

In this section two different aging procedures will be described in detail: dynamic aging and static aging. In total 16 core plugs were dynamically aged, and four core plugs were statically aged. 10 of the core plugs (LS1-LS10) were aged in collaboration with Ph.D. student Jaquelin Cobos Mora. The experimental setup illustrated in Figure 3.6 was used for both dynamic and static aging.

3.5.1 Dynamic aging

Crude oil from the same barrel was used for aging all the core plugs. The barrel of North Sea crude oil was rotated to mix the crude oil before collecting it. The unfiltered crude oil was placed in an accumulator inside a heating cabinet and heated to 80°C. Thereafter, the crude oil was injected through a limestone filter at constant rate to remove impurities. After filtration, the crude oil was stored in closed containers at 80°C.

The dynamic aging setup is illustrated in Figure 3.6. The procedure of Fernø et al. (2010) was followed. A fully water-saturated core plug was placed in a Hassler biaxial core holder with a confinement pressure inside a heating cabinet holding 80°C. The core was oil-flooded, 2.5 pore volumes (PV) in both directions, by crude oil injection at high differential pressure (2 bar/cm) before the injection rate was reduced to 1.5 ml/h. Crude oil was continuously injected throughout the entire aging process, and the flow direction was reversed after 72h (midway in the process). The aging was completed after 144h (6 days). After aging, the core was flooded with 2.5 PV decahydronaphthalene (Decaline) in both directions to prevent crude oil and n-Decane mixing, which would likely cause asphaltene precipitation. 2.5 PV of n-Decane was

thereafter injected in both directions. The aged core plug was taken out of the core holder, placed in a container filled with n-Decane and cooled to ambient conditions. N-Decane was used as the oleic phase in all further experimental steps.

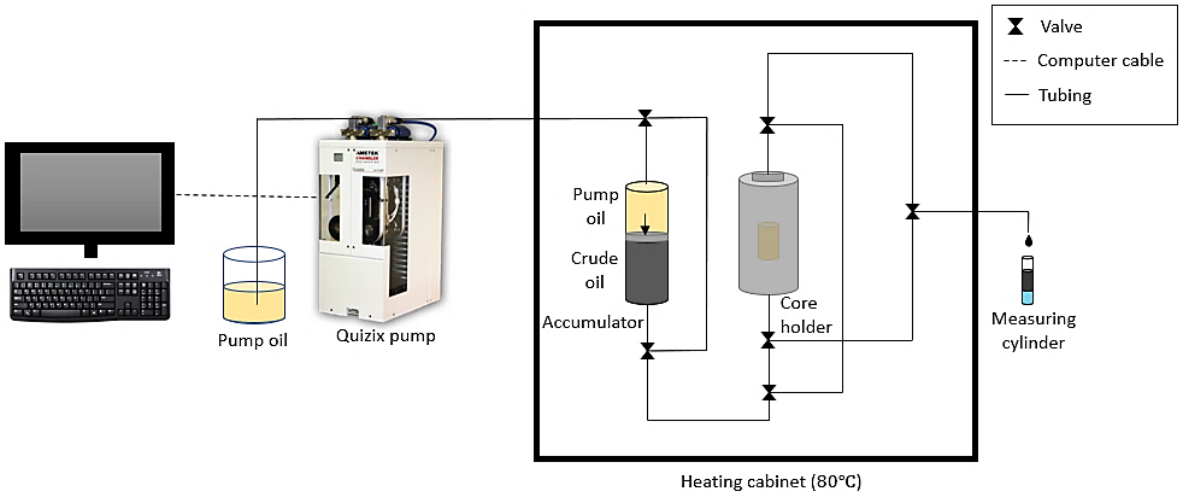

Figure 3.6: Experimental setup for the dynamic and static aging procedures.

3.5.2 Static Aging

A fully water-saturated core plug was placed in a Hassler biaxial core holder with a confinement pressure inside a heating cabinet holding 80℃. 2.5 PV of crude oil was injected in both directions through the core plug at a high differential pressure (2bar/cm), and the core plug was taken out of the core holder and placed in a beaker filled with filtered crude oil. The beaker was covered with aluminium foil and stored inside a heating cabinet at 80℃ for 1000h. Next, the core plug was placed back in the core holder and flooded with 2.5 PV of decahydronaphthalene (Decaline) in both directions, and thereafter 2.5 PV of n-Decane in both directions to avoid asphaltene precipitation. The core plug was taken out of the core holder and cooled to ambient conditions in a container filled with n-Decane.

3.6 Splitting Procedure

Some core plugs were split longitudinally to investigate wetting distribution and stability. The fracturing method was inspired by the Brazilian test described by Mellor and Hawkes (1971). The fracturing device was made up of two thick metal plates with indents to fit a circular core plug. The core plug was placed in the centre of the fracturing device, between the two sharp edges, and pressure from a hydraulic press was gradually applied onto the device until the core plug was fractured (Grøteide 2017). Rough fractures were made by this method. The fracturing device with a core plug placed inside and a core plug after splitting are shown in Figure 3.7.

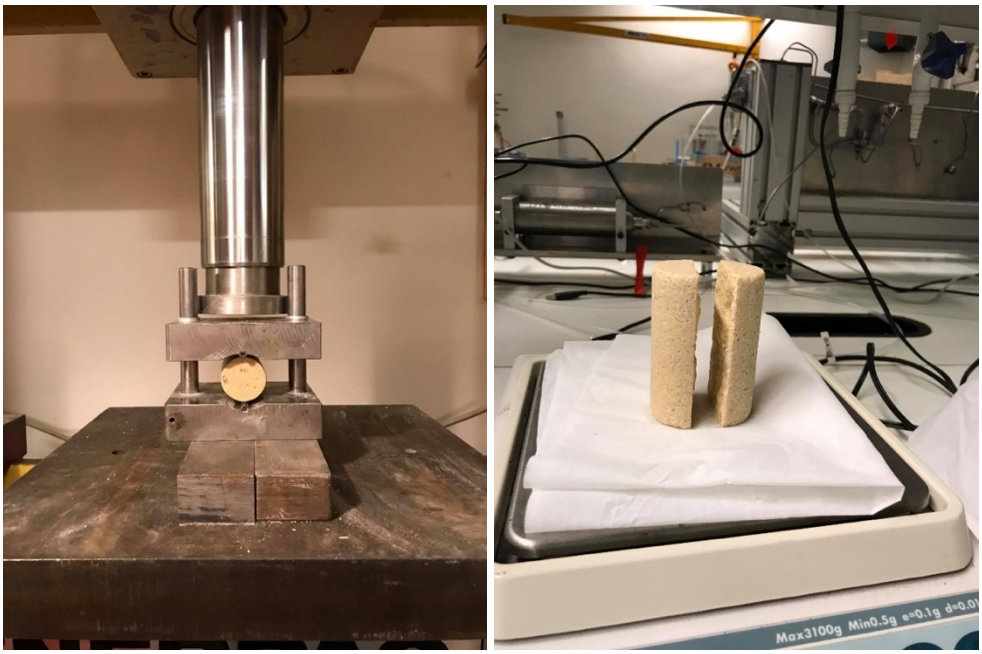

Figure 3.7: The fracturing device with a core plug inside to the left, and a split core plug to the right.

Wettability measurements

3.7 Spontaneous Imbibition (Amott-Harvey Index)

The boundary conditions during spontaneous imbibition (SI) were all faces open (AFO) for all experiments with whole core plugs, meaning the wetting fluid could invade the cylindrical core plug uninhibited through all faces, i.e. the core circumference and both end faces. SI was also performed on split core plugs where the inner part of the core plugs was exposed to the imbibing fluid as well. Core plugs at the irreducible water saturation (S_{iw}) were placed in Amott cells filled with the aqueous phase for at least 168 hours and oil production was measured as a function of time. Core plugs at the residual oil saturation (S_{or}) were placed in Amott cells filled with n-Decane (the oleic phase). Spontaneous imbibition of water or oil in Amott cells is illustrated in Figure 3.8. When no production was observed for several days, SI was assumed to have ended and the cores were taken out of the Amott cell. Because most core plugs used were not strongly wetted, saturation end points were not reached during SI. Forced injections were then performed to obtain end point saturations.

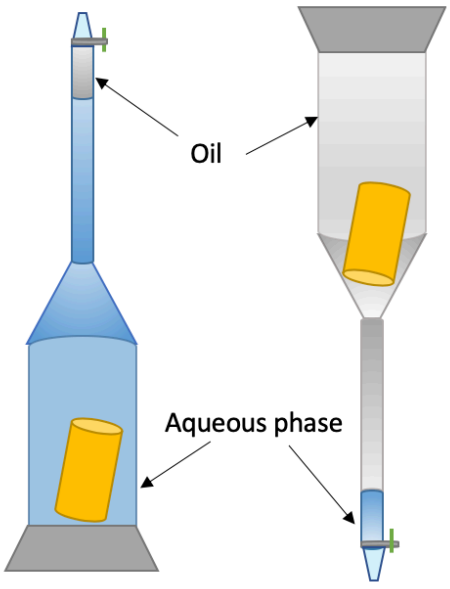

Figure 3.8: Core plugs placed in Amott cells for spontaneous imbibition. Spontaneous water imbibition to the left and spontaneous oil imbibition to the right.

Forced injections

To reach the irreducible fluid saturations, forced injections of the aqueous phase or n-Decane were performed. The experimental setup consisted of a Quizix QX pump connected to a Hassler biaxial core holder (see Figure 3.5). At least 2.5 PV of fluid was injected into the core plug in both directions with a differential pressure of 2 bar/cm. Effluent production was measured, and the saturation development monitored using material balance (described in Appendix B). A full Amott-Harvey cycle consisted of: spontaneous imbibition and forced injection of aqueous phase to measure the water index (I_w), calculated using equation (2.2), and spontaneous imbibition and forced injection of oil to measure the oil index (I_o). The oil index was calculated using equation (2.3). The water -and oil index was used to calculate the Amott-Harvey index (I_{AH}) using equation (2.1).

The setup was modified for injection of polymer/glycerol. An accumulator containing polymer or glycerol was connected between the Quizix pump and the core holder. At least 1.5 PV of polymer/glycerol was injected into the core plugs in both directions with a differential pressure of 2 bar/cm. Injection of polymer/glycerol was performed at much lower flow rates (between 5 and 20 ml/h) compared to injection of brine/oil (between 100 and 900 ml/h) due to rapid pressure build-up. In some of the cores brine injection was performed after polymer/glycerol injection to remove the polymer/glycerol from the pore network before spontaneous oil imbibition, and to assess the effect on spontaneous imbibition and end-point relative permeability. Table 3.2 gives an overview of injected fluids for each Amott-Harvey cycle in cores where polymer or glycerol was injected.

Table 3.2: Overview of injected fluids for each Amott-Harvey cycle in cores where polymer or glycerol was injected.

core	First cycle	Second cycle	Third cycle	Fourth cycle	Fifth cycle
LS11	Brine/oil	Polymer/oil	Polymer/oil	Polymer/oil	Polymer/oil
LS14	Brine/oil	Polymer/oil	Polymer+brine/oil	Polymer+brine/oil	Polymer+brine/oil
LS17	Brine/oil	Glycerol/oil	Glycerol/oil	Glycerol/oil	Glycerol/oil
LS18	Brine/oil	Glycerol/oil	Glycerol+brine/oil	Glycerol+brine/oil	Glycerol+brine/oil
LS20	Brine/oil	Brine/oil	Polymer/oil	Polymer/oil	-
LS21	Brine/oil	Brine/oil	Polymer/oil	Polymer+brine/oil	Brine/oil
LS22	Brine/oil	Brine/oil	Glycerol/oil	Glycerol/oil	Brine/oil

During forced injection of water or oil into the fractured cores, a piece of rubber was placed in the fracture volume to seal the fracture. Aluminium tape was wrapped around the core, consisting of two core halves with the rubber pieces in the middle, as illustrated in Figure 3.9. This made it possible to perform forced injections at elevated pressures, i.e. using constant differential pressures of at least 1.5 bar/cm.

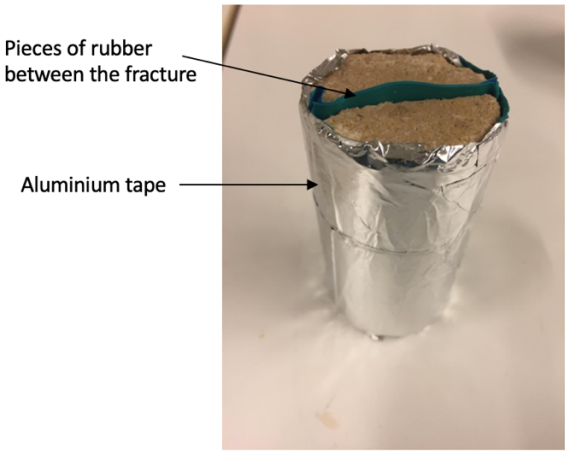

Figure 3.9: Fractured core plug with rubber pieces in the fracture, and aluminium tape wrapped around the core.

3.8 End-point relative permeability

End-point relative permeability was measured at the end of each forced injection, when the production of the displaced phase (now at irreducible saturation) had stopped. The pressure drop across the core plug was measured consecutively for at least three different volumetric flow rates, and the flowing phase relative permeability was calculated using equation (A.3) and (A.4). In cores where polymer or glycerol was injected, a longer period of time was needed to reach a stable differential pressure for a given flow rate (often one hour compared to 2-5 minutes in cores where water or oil were injected). Figure 3.10 shows the differential pressure development over time for different volumetric flow rates during water injection and polymer injection.

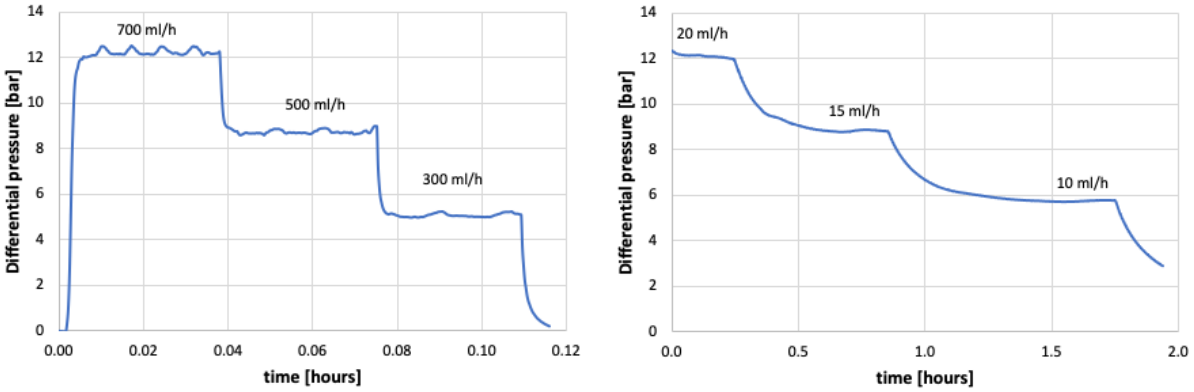

Figure 3.10: Differential pressure over time for different flow rates during water injection in LS19 to the left, and differential pressure over time for different flow rates during polymer injection in LS11 to the right.

3.9 In-situ imaging

3.9.1 MRI

An MRI-scanner (MRI centre, Equinor, Sandsli) was used to investigate the spatial wettability distribution in one Edwards limestone core plug, at strongly water-wet and dynamically aged to oil-wet conditions. The MRI-scanner was equipped with a superconductive magnet (BioSpec 47/40 USR, Bruker, Rheinstetten, Germany) with a magnetic field strength of 4.7 T (200MHz). The experimental setup is shown in Figure 3.11. One fully water saturated core plug, LS26, was placed inside a core holder made from polyether ether ketone and titanium materials. Confinement pressure was applied using nitrogen gas. The core holder was placed inside the MRI-scanner and Decane was injected at flow rates between 10 and 180 ml/h using a Quizix QX pump. Water production was measured with time, and the oil injection was stopped when residual oil saturation was reached. Static MRI-imaging and T_2 relaxation time measurements were performed before and after the injection (at $S_w = 1$ and at S_{wi}). The core plug was brought back to the Department of Physics and Technology at the University of Bergen for dynamic aging. The procedure in section 3.3.1 was followed, but the crude oil was injected with a maximum differential pressure of 3.5 bar (the maximum injection pressure reached during oil injection in the MRI-scanner) to avoid additional water production. After aging, one full Amott-Harvey cycle was performed to measure the wettability index.

MRI-imaging and T_2 relaxation time measurements should be performed before and after aging of the core plug, but due to the covid-19 pandemic it was not possible to complete the measurements: the aged core plug (at S_{wi}) should, according to the plan, be imaged using MRI during consecutive water and polymer injections. It was planned to perform static MRI-imaging and T_2 relaxation time measurements before and after each injection, in addition to dynamic measurements during both injections.

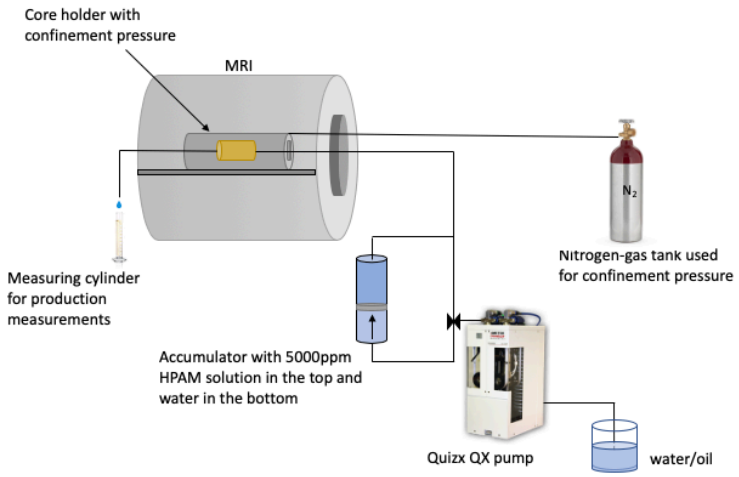

Figure 3.11: Experimental setup for fluid injections imaged by MRI at Equinor, Sandsli.

3.9.2 CT imaging

CT imaging of two core plugs was performed using a ProCon X-ray CT-ALPHA Computed Tomography (CT) scanner belonging to the Department of Earth Science at the University of Bergen, located at Realfagsbygget. The purpose of the CT-images was to visualize and quantify heterogeneities within the core plugs, which could influence displacement processes. The scanner is equipped with a 240kV micro-focus tube and 3000x3000 pixel detector scanning up to 150 cm long sediment cores with a diameter up to 125mm in a continuous helix motion, and is shown in Figure 3.12. Each core plug was placed inside a closed container filled with n-Decane, and attached to the top of a rotating device inside the CT shield cabinet.

Figure 3.12: A core plug placed inside the CT-scanner at the Department of Earth Science.

3.9.3 PET imaging

The nanoScan PET/CT belonging to the Department of Biomedicine at the University of Bergen, located at the Molecular Imaging Centre at Haukeland University hospital, was used to visualize displacement fronts before and after polymer injection in one dynamically aged Edwards limestone core plug. This PET/CT scanner is mainly for mice and rats but is also used by the reservoir physics group at the Department of Physics and Technology at the University of Bergen. The experimental setup is illustrated in Figure 3.13.

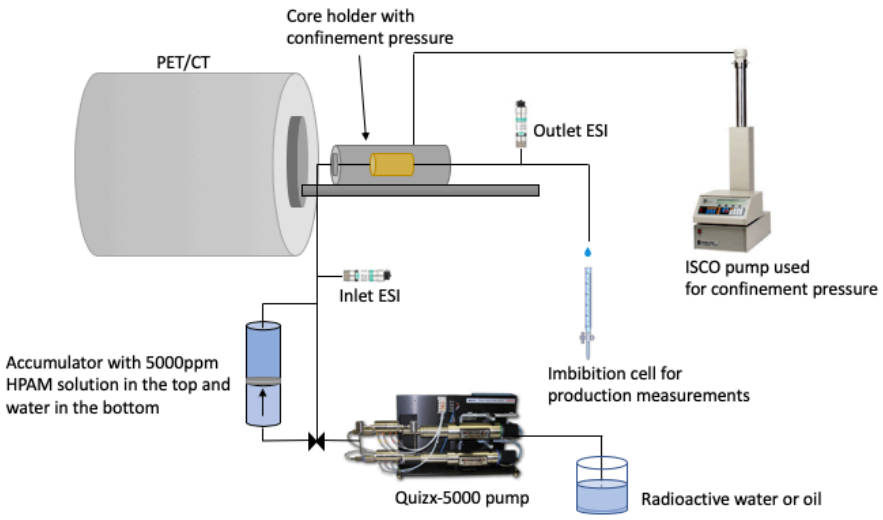

Figure 3.13: Experimental PET/CT set up at Haukeland University Hospital. The accumulator was used only for polymer injection.

The dynamically aged core plug was flooded with oil, polymer, and water in the PET-scanner. The order of injections is presented below:

- Injection of radioactive brine at S_{or}
- Oil injection
- Injection of radioactive 5000ppm polymer solution
- Second oil injection
- Second injection of radioactive brine
- Third oil injection

Table 3.3 gives an overview of radioactivity added to the injected brine/polymer.

Table 3.3: Overview of radioactivity added to the injected brine/polymer.

	Volume of fluid	Radioactivity [MBq]
First brine injection	200 ml brine	204.8
Polymer injection	185ml polymer solution + 20 ml brine	270.5
Second brine injection	175 ml brine	103.8

The core plug was placed inside a core holder, and a confinement pressure was applied using an ISCO pump filled with pump oil. Initial CT images were acquired to determine the position of the core plug. The core holder was thereafter moved into the PET scanner field of view. A Quizix-5000 pump was used for injection of fluids (brine, oil or polymer solution). The fluids were injected at low flow rates, between 10 and 30 ml/h, and produced effluents were monitored over time. Each injection was stopped when the average core saturation was stable. Inlet and outlet pressures were measured using two ESI pressure transducers.

4 Results and Discussion

This section presents results and discussions of the experimental work conducted in this thesis. A total of 29 Edwards limestone core plugs from the Edwards plateau in West Texas were prepared. 20 core plugs were aged using two different methods – static aging and dynamic aging. In total, four cores were statically aged, and 16 cores were dynamically aged. Multiple Amott-Harvey cycles were performed to estimate wettability, investigate the wetting stability resulting from each aging method and to assess whether polymer injection alters the wettability of the core plugs. Ekofisk brine, polymer solution or glycerol solution were used as the aqueous phase, and n-Decane constituted the oleic phase. One core plug was flooded with polymer, oil and water in a PET-scanner to visualize displacement fronts before and after polymer. CT-imaging was used to visualize the structure of the pore network and to create pore size distributions of two core plugs. MRI was used to describe the distribution of different pore sizes in one Edwards limestone core.

4.1 Core properties

Basic core properties were measured for 29 different limestone core plugs and are listed in Table 4.1. The core plug lengths ranged between 6.35cm and 7.59cm. Average porosity was 23.4% (measured range: 20.2 to 28.1%) and average permeability was 26.7mD (measured range: 14.1 to 52.6mD). A linear relationship between permeability and porosity was obtained, as shown in Figure 4.1. The linear trend is more obvious for lower porosity values but also more measurements are done in this specter than for cores with high porosity. The significant variations in permeability indicate heterogeneous core plugs.

Core properties of Edwards limestone core plugs were previously measured by other master students. Riskedal (2008) and Tipura (2008) used 34 different limestone core plugs with porosities between 16.9% and 26.9%, and permeabilities between 2.6mD and 28.5mD. Opdal (2014) measured porosity and permeability on 14 different core plugs, where the porosity was in range 21.3% to 25.5%, and permeability in range 12mD to 33mD. The 17 limestone core plugs used in the work of Skjelsvik (2018) had porosity values between 22.0 and 27.8%, and permeability values between 14mD and 68mD. The core plugs used in this work came from a new supplier but corresponded well with the previously measured ranges.

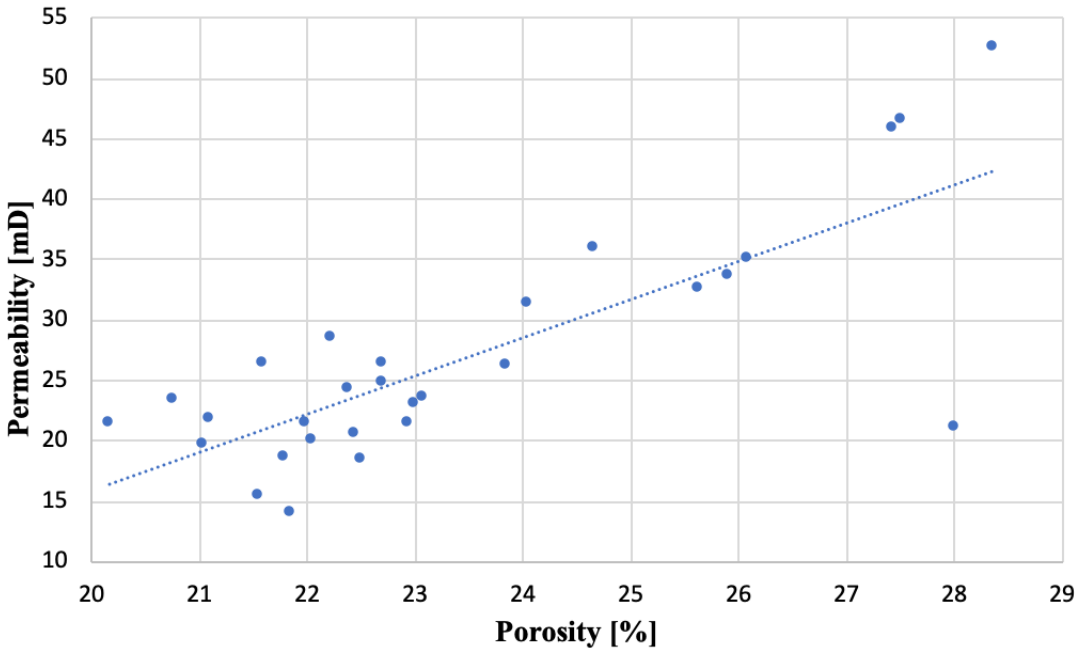

Figure 4.1: Linear porosity-permeability relationship for the Limestone cores.

Table 4.1: Basic core properties.

Core	Length ± 0.01[cm]	Diameter ± 0.01 [cm]	Pore Volume ± 0.01 [ml]	Porosity ± 0.06 [%]	Permeability ± 0.05 [mD]	Aging method	Aging time [h]
LS1	7.39	3.80	18.82	22.45	20.56	Static	1000
LS2	7.20	3.80	19.64	24.05	31.34	Dynamic	144
LS3	7.40	3.80	17.43	20.77	23.42	Dynamic	144
LS4	7.50	3.80	18.71	22.00	21.45	Static	1000
LS5	7.59	3.80	19.54	22.70	24.79	Dynamic	144
LS6	7.39	3.80	19.03	22.70	26.35	Dynamic	144
LS7	7.40	3.80	18.67	22.24	28.56	Dynamic	144
LS8	7.49	3.80	19.02	22.39	24.35	Dynamic	144
LS9	7.40	3.80	17.67	21.05	19.70	Static	1000
LS10	7.32	3.80	17.51	21.10	21.90	Static	1000
LS11	6.80	3.80	21.16	27.44	45.88	Dynamic	144
LS12	6.90	3.80	18.67	23.85	26.23	Dynamic	144
LS13	6.90	3.80	20.42	26.09	35.06	Dynamic	144
LS14	6.91	3.80	18.10	23.09	23.59	Dynamic	144
LS15	6.95	3.80	21.69	27.51	46.51	N/A	-
LS16	6.71	3.80	19.72	25.92	33.74	Dynamic	144
LS17	6.81	3.80	21.91	28.37	52.64	Dynamic	144
LS18	6.69	3.80	17.41	22.95	21.49	Dynamic	144
LS19	6.79	3.80	18.99	24.66	35.97	Dynamic	144
LS20	6.81	3.80	17.03	22.05	20.00	Not aged	-
LS21	6.35	3.80	18.47	25.64	32.63	Not aged	-
LS22	7.50	3.82	18.73	21.79	18.70	Not aged	-
LS23	7.15	3.80	16.35	20.17	21.39	Not aged	-
LS24	6.99	3.80	17.12	21.60	26.43	Not aged	-
LS25	7.00	3.80	17.12	21.57	15.46	Not aged	-
LS26	7.10	3.80	18.52	23.00	23.13	Dynamic	144
LS27	6.91	3.80	17.65	22.52	18.48	Dynamic	144
LS28	6.87	3.80	21.83	28.02	21.07	Not aged	-
LS29	6.93	3.80	17.18	21.86	14.09	Not aged	-
Average	7.07	3.80	18.76	23.43	26.72	N/A	-

4.2 Rock quantification with in-situ imaging

In this section MRI T_2 intensity curves and CT-imaging will be used for quantification of Edwards limestone properties. MRI T_2 intensity curves were used to describe the distribution of different pore sizes in one Edwards limestone core (LS26). CT-images of two limestone core plugs (LS17 and LS27) with different core properties were used to visualize the structure of the pore network and to create pore size distributions.

4.2.1 MRI T_2 intensity curves

The MRI-scanner at Equinor, Sandsli was used for T_2 relaxation time measurements of one limestone core plug (LS26) as described in section 3.9.1, and the results are presented in this section. MRI T_2 intensity curves of a fully water saturated Edward limestone core plug (LS26) were used to describe the distribution of different pore sizes. It was planned to compare measured T_2 relaxation time before and after aging of the core plug, and after polymer injection, to investigate the spatial wettability distribution in the core plug. Tipura (2008) and Riskedal (2008) used MRI to investigate the wettability distribution in Edwards limestone core plugs, and found that the T_2 relaxation time for the oil phase at irreducible water saturation decreased almost linearly for stronger oil-wet conditions. Only T_2 measurements before aging, at $S_w = 1$ and at S_{wi} (after oil injection), were completed in this work. The analysis of the wettability distribution in the core after aging must therefore be performed in future work.

The core plug was dynamically aged (as described in section 3.5.1), and one full Amott-Harvey cycle was performed. No water imbibed spontaneously into the core plug, but spontaneous imbibition of oil was recorded. The measured Amott-Harvey index was -0.12 (Table 4.2), which corresponds to weakly oil-wet conditions.

Table 4.2: Overview of water saturations and measured water index, oil index and Amott-Harvey index for one full Amott-Harvey cycle.

Core	S_{iw}	$S_{w,1}$	$S_{iw,1}$	I_w	I_o	I_{AH}
LS26	0.21	0.79	0.34	0	0.12	-0.12

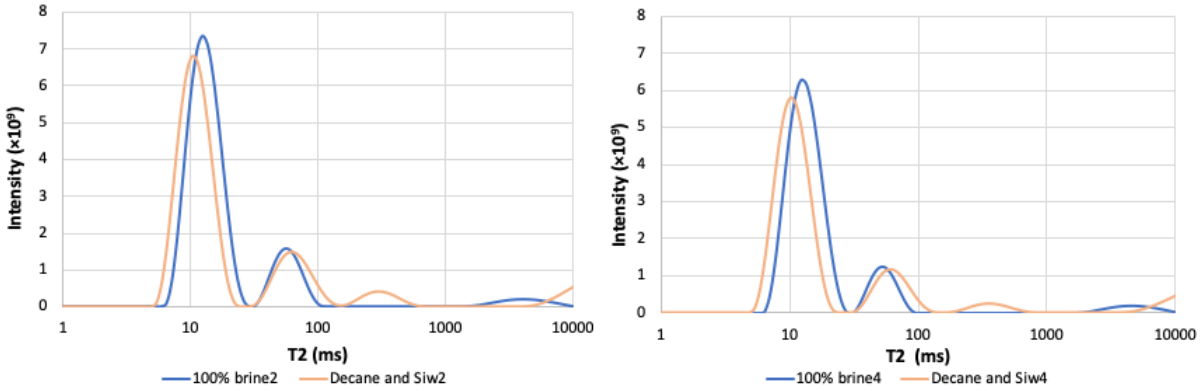

Figure 4.2: Intensity as a function of T_2 relaxation time in two different slices of the core before and after oil injection.

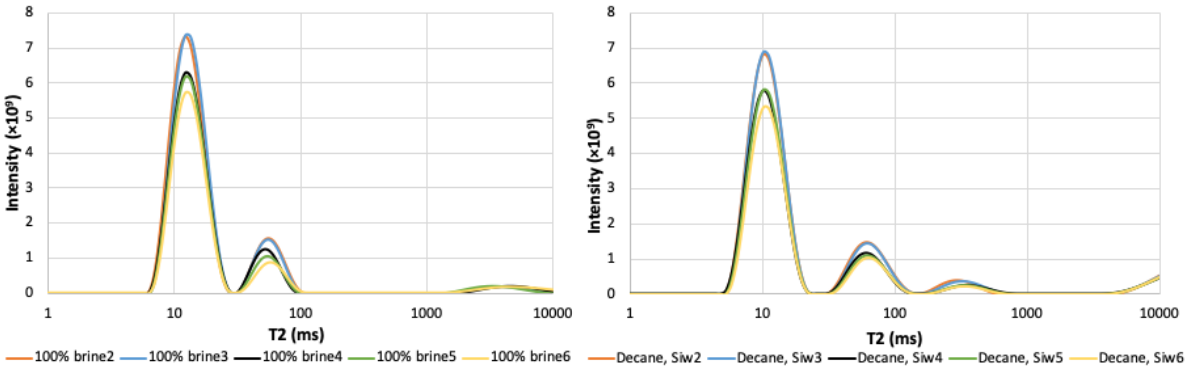

Figure 4.3: Intensity as a function of T_2 relaxation time in five slices of the core before oil injection (S_w = 1) to the left, and after oil injection (S_{wi}) to the right.

Figure 4.2 shows intensity as a function of T_2 relaxation time in two different slices of the core plug, 100% water saturated and at S_{wi} (after oil injection). Figure 4.3 shows intensity as a function of T_2 relaxation time in five slices of the core plug before and after oil injection. Pore size distribution of a core plug can be obtained from MRI T_2 distribution of a fully water saturated core plug, but it was not done in this experiment. Although, the T_2-curve for the fully water saturated core plug (Figure 4.3) provides information about the distribution of pore sizes: short T_2 relaxation times indicate smaller pore sizes, while longer T_2 relaxation times indicate larger pore sizes (Kenyon et al., 1989, Howard and Kenyon, 1992). A trimodal T_2 distribution was obtained for the fully water saturated core plug (LS26) in Figure 4.3. The fastest peak (shortest T_2), with highest intensity, represents the smallest pores in the core, the intermediate peak represents the intermediate pores and the slowest peak (highest T_2) represents the largest pores and vugs in the core. The intensity in the first peak is higher than the two other peaks, indicating a higher proportion of smaller pores in the core plug. The intensity peaks vary slightly for the different slices of the core. Heterogeneous pore network can explain this: some slices

may contain fewer small pores and more vugs, while other slices may contain more small pores. Tipura (2008) and Riskedal (2008) also performed MRI T_2 measurements in fully water saturated Edwards limestone core plugs, with permeabilities in range 3.4-13.7 mD. Unlike the core plug used in this thesis, the lowest intensities were measured at shortest T_2 relaxation times, while the highest intensities were measured at highest T_2 relaxation times, indicating a higher proportion of larger pores in the core plugs.

When the core was saturated by both oil and water (at S_{wi}), a shift in T_2 curves was observed. The first peak was shifted towards lower T_2 relaxation times, while the other peaks were shifted towards higher. The T_2 curves shifted due to different hydrogen content in water and oil. Water has a faster relaxation time than oil. Longer relaxation times were therefore obtained when the intermediate and large pores were filled with oil during oil injection. The fastest peak changed not much after oil was injected into the core because the smallest pores in the core were assumed to remain fully water saturated.

4.2.2 CT-imaging

The ProCon X-ray CT-ALPHA Computed Tomography (CT) scanner at the institute for geoscience was used for CT-imaging of two core plugs: LS17 with high permeability (52.6mD) and LS27 with low permeability (18.5mD). Spatial resolution of the CT-images was 25.3 μm. Pores smaller than the spatial resolution are not visible in the CT-images.

Figure 4.4 shows a CT-image of the whole length of core LS27, where the pores were segmented out. Vugs are marked in the image. Pores with a variety of sizes, included large vugs, can be seen in the image. The largest vug in the CT-image has a diameter of ~2mm. Tipura (2008) also observed pores as big as 2mm in a thin section of Edwards limestone presented in her work. Figure 4.5 shows CT-images of four different slices of core LS27 and Figure 4.6 shows CT-images of four different slices of core LS17. A diversity of pore sizes, included vugs, can also be seen in these CT-images. A greater proportion of small vugs were observed in the CT-images of core LS17 compared to LS27, which might explain the higher permeability in the core.

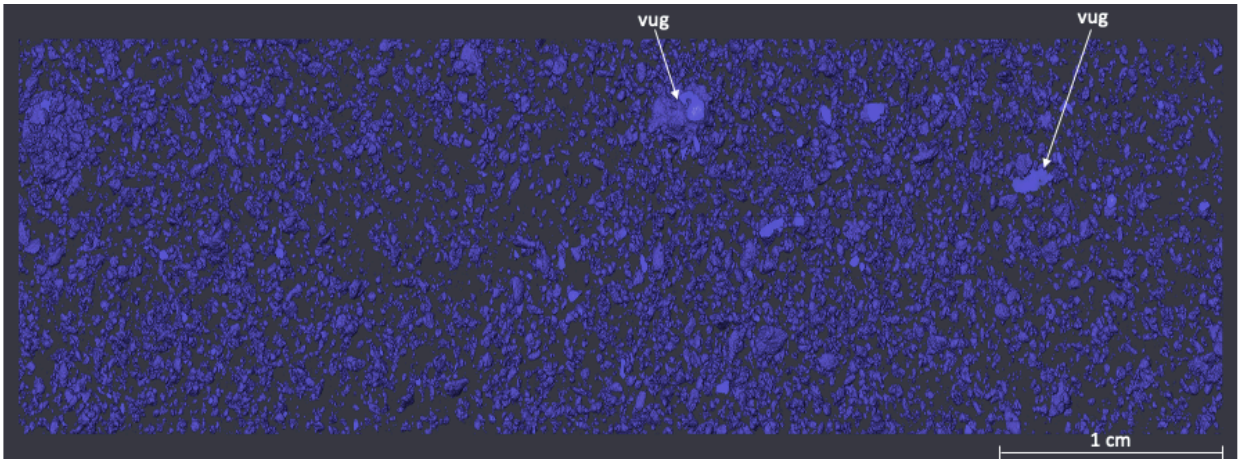

Figure 4.4: CT-image of LS27 with pores segmented out. The smallest pores are not represented in the image due to the spatial resolution of the CT-image. The scale in the lower corner is 1cm.

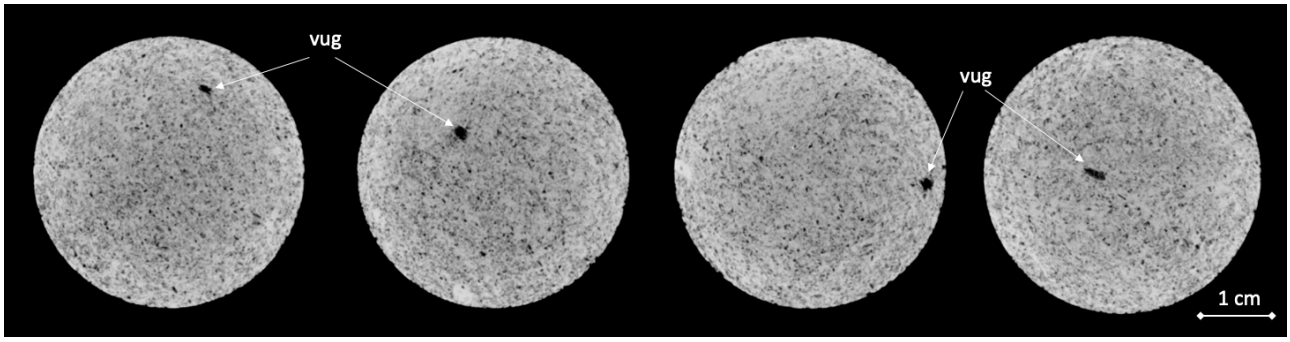

Figure 4.5: CT-images from four different slices of core LS27, where vugs are marked. The smallest pores are not represented in the image due to the spatial resolution of the CT-images. The scale in the lower corner is 1 cm.

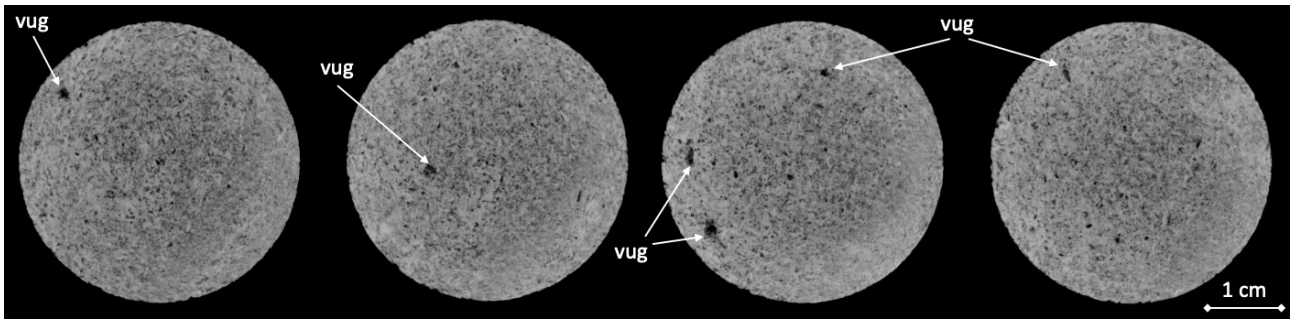

Figure 4.6: CT-images from four different slices of core LS17, where vugs are marked. The smallest pores are not represented in the image due to the spatial resolution of the CT-images. The scale in the lower corner is 1 cm.

Pore size distributions of cores LS17 and LS27 were obtained from the CT-images using ImageJ, which is an image processing software. Slices representing the whole cores were selected, approximately every hundred slices, and particle analysis was performed. The particle analysis involved thresholding the images using the default threshold in the software, which

converted the images into binary images. The area of each pore was calculated using the "analyse particles" function in the software. Figure 4.7 shows the pore size distributions of core LS17 and LS27, where the pore diameter is the diameter of the pore bodies. Each interval in the histograms is 10 μm. In core LS27, the largest proportion of pores visible in the CT-images (~70%) had diameters of 27 μm, while the largest proportion of pores in LS17 had diameters of 30 μm. A smaller proportion of the pores had diameters in the range 38-100 μm (LS27) and 40-110 μm (LS17). The large vugs in core LS27 had diameters in range 100-270 μm, while the diameters of the vugs ranged from 110-315 μm in LS17. Core LS17 had generally pores and vugs with larger pore body diameters than core LS27. In addition, a greater proportion of small vugs were observed in the CT-images of LS17, which explains the higher permeability in LS17.

A trimodal T_2 distribution was obtained for the core in the MRI-experiment presented in previous subsection, i.e. three different intervals of pore sizes. It is possible that the fastest peak in the T_2 distribution from the MRI represents the highest peak in the pore size distributions, but the peak might as well represent the smallest pores that are not visible in the CT-images. Tipura (2008) obtained pore size distributions of Edwards limestone from MRI T_2 distribution by scaling the T_2 value to the pore throat size measured by mercury injection. Pore body diameters in the range 1-70 μm were found. Larger pores and vugs in the Edwards limestone core material used in this work can explain the difference in permeability between the cores in this work and the Edwards limestone cores used by Tipura (2008).

The CT-images confirm the expected heterogeneous nature of the Edwards limestone core material, with a large range in pore sizes (27-300 μm) and presence of vugs. Pores smaller than the spatial resolution of the CT images (25.3 μm) were not captured.

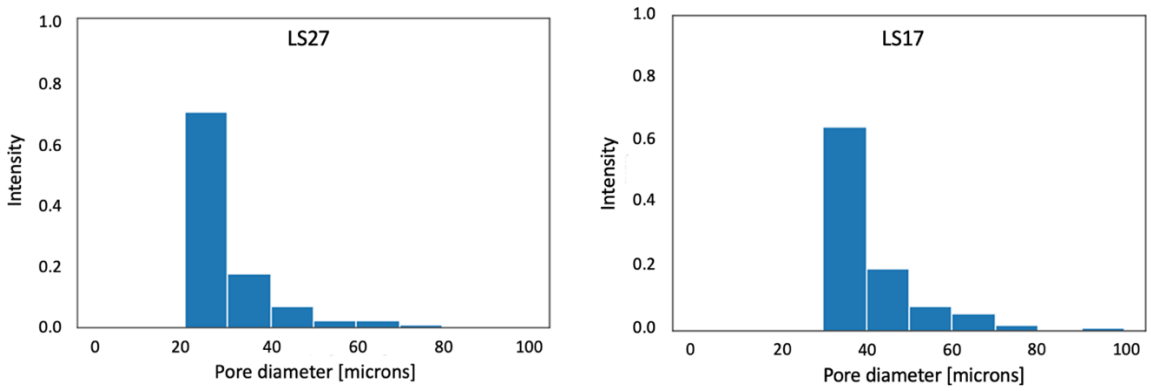

Figure 4.7: Pore size distribution obtained from the CT-images of LS27 and LS17, where the pore diameter is the diameter of the pore bodies. Each interval in the x-axis of the histograms is 10 µm. The smallest pores are not represented due to the spatial resolution of the CT-images.

4.3 Wettability alteration

This section presents results from 10 aged limestone core plugs, where brine constituted the aqueous phase and mineral oil (Decane) constituted the oil phase. The core plugs were used to investigate the wetting alteration produced by the given oil/brine/rock system by two different aging methods, and the results served as the baseline for further work in this thesis. The aging procedures were performed in collaboration with Ph.D. candidate Jacqueline Cobos Mora from Aalborg University. Four core plugs were statically aged (LS1, LS4, LS9, and LS10) and six were dynamically aged (LS2, LS3, LS5, LS6, LS7, and LS8). The two different aging methods are further described in section 3.5. After aging, full Amott-Harvey cycles were performed to measure wettability: spontaneous water imbibition, forced water injection, spontaneous oil imbibition, and forced oil injection. The Amott-Harvey index was thereafter calculated. Wettability alteration efficiency and stability were evaluated in whole and split core plugs. The results are summarized in Table 4.3. "Aging method" describes whether the cores were aged statically or dynamically, "core status" describes whether the cores were whole or split during the given Amott-Harvey cycle. I_w is the water index, I_o is the oil index and I_{AH} is the measured Amott-Harvey index, where the subscript indicates the cycle: 1 is the first cycle (measured for all cores), while 2 and 3 describe subsequent cycles, if performed.

Table 4.3: Overview of aging method used (static or dynamic), core status (whole or split) during the Amott-Harvey test, water indices, oil indices and Amott-Harvey indices for multiple cycles in baseline experiments.

Core	Aging method	Core status	$I_{w,1}$	$I_{o,1}$	$I_{AH,1}$	Core status	$I_{w,2}$	$I_{o,2}$	$I_{AH,2}$	Core status	$I_{w,3}$	$I_{o,3}$	$I_{AH,3}$
LS1	Static	Split	0	0.48	-0.48	-	-	-	-	-	-	-	-
LS2	Dynamic	Whole	0	0.06	-0.06	Whole	0	0.07	-0.07	Split	0	0.38	-0.38
LS3	Dynamic	Whole	0	0.01	-0.01	Whole	0	0.01	-0.01	-	-	-	-
LS4	Static	Split	0	0.46	-0.46	-	-	-	-	-	-	-	-
LS5	Dynamic	Whole	0	0.09	-0.09	Whole	0	0.07	-0.07	-	-	-	-
LS6	Dynamic	Whole	0	0.25	-0.25	Whole	0	0.17	-0.17	Split	0	0.55	-0.55
LS7	Dynamic	Split	0	0.51	-0.51	-	-	-	-	-	-	-	-
LS8	Dynamic	Split	0	0.58	-0.58	-	-	-	-	-	-	-	-
LS9	Static	Whole	0	0	0	Split	0	0.09	-0.09	-	-	-	-
LS10	Static	Whole	0	0	0	Split	0	0.07	-0.07	-	-	-	-

4.3.1 Comparison of whole cores

Wettability alteration by two different aging methods; static and dynamic, was compared. Wettability alteration efficiency and stability were first evaluated in six whole core plugs. Four of the core plugs were aged dynamically (LS2, LS3, LS5, and LS6) and two statically (LS9 and LS10). "Twin" core plugs with equal properties (approximately equal porosity and permeability) were aged under the same conditions to obtain optimum reproducibility. Examples of twin cores are LS2 and LS6, LS3 and LS5, and LS9 and LS10.

A full Amott-Harvey cycle was performed on all whole cores, where the Amott-Harvey index measured ($I_{AH,1}$) ranged from -0.01 to -0.25 for dynamically aged cores, indicating that the cores spontaneously imbibed oil. No water imbibition was recorded. Statically aged cores imbibed neither oil nor water, thus the measured Amott-Harvey indices were zero, corresponding to neutral wet conditions. Water imbibition was not observed during the second Amott-Harvey cycles either (dynamically aged cores only), but between 0.1 and 1.5 ml of water were produced during spontaneous oil imbibition. Good reproducibility was achieved during two full cycles for cores LS2, LS3, LS5, and LS6, with measured Amott-Harvey indices of $I_{AH,1}/I_{AH,2}$: -0.06/-0.07, -0.01/-0.01, -0.09/-0.07, and -0.25/-0.17, respectively. The measured Amott-Harvey indices correspond to nearly neutral wetting conditions, although spontaneous imbibition of oil suggests tendencies towards weakly oil-wet conditions. Figure 4.8 shows increase in oil saturation as a function of time during two cycles of spontaneous oil imbibition in cores LS2, LS3, LS5, and LS6.

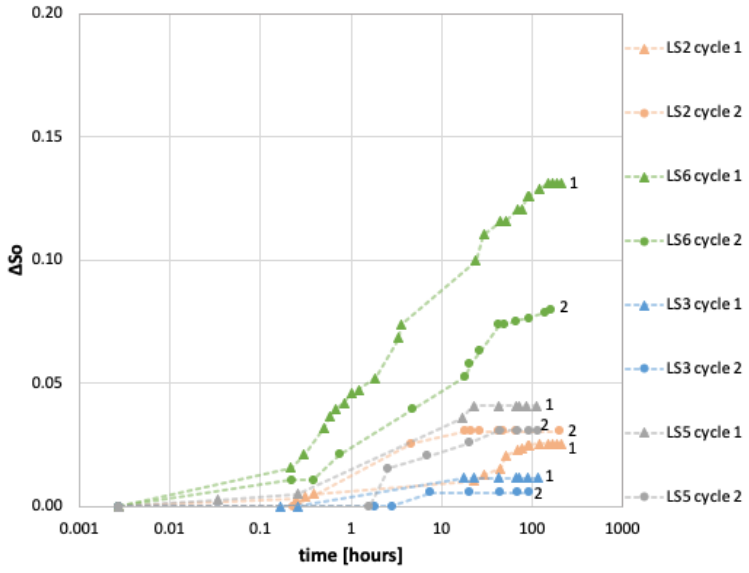

Figure 4.8: Increase in oil saturation (ΔS_o) as a function of time during two cycles of spontaneous oil imbibition in cores LS2, LS3, LS5, and LS6.

4.3.2 Comparison of split cores

Some of the cores were split longitudinally to investigate the wettability distribution within the core plugs. Higher recovery and imbibition rate were expected due to larger surface area in contact with the imbibing fluid. Water-wet baseline experiments in three limestone core plugs (LS23, LS24, and LS25) were performed to emphasize this. Four dynamically aged core plugs (LS2, LS6, LS9, and LS10) and four statically aged core plugs (LS1, LS4, LS7, and LS8) were split and Amott-Harvey cycles performed. LS2 and LS6 were split after completion of two Amott-Harvey cycles, while LS7 and LS8 were split after one full cycle. Cores LS1, LS4, LS9 and LS10 were split directly after aging. To obtain optimum reproducibility, "twin" core plugs with approximately equal porosity and permeability were aged under the same conditions. Sets of twin cores were LS2 and LS6, LS1 and LS4, LS7 and LS8 and, LS9 and LS10.

4.3.2.1 Water-wet baseline

Three water-wet limestone core plugs (LS23, LS24, and LS25) were used as baseline cores to assess the effect of core splitting on recovery and imbibition rate. The core properties were in range 15.5-26.4mD in permeability and 20.2-21.6% in porosity. Four subsequent Amott-Harvey cycles were first performed on whole core plugs. The cores were thereafter split and again placed in Amott cells for spontaneous water imbibition. LS25 was split after only three cycles of spontaneous imbibition. Figure 4.9 shows the increase in water saturation (ΔS_w) as a function of time. Figure 4.10 shows the water saturation, and Figure 4.11 shows imbibition rate as a function of time during spontaneous water imbibition for the three cores.

For all three cores the increase in water saturation (ΔS_w) varies slightly between each cycle of spontaneous imbibition in whole core plugs. After splitting, a greater increase in water saturation was observed for all cores. By comparing final values of ΔS_w after spontaneous water imbibition in the cycle before and after splitting, an increase of 2% for LS24 and 3% for LS23 and LS25 was obtained. By comparing the cycle with split cores and the cycle with lowest ΔS_w, an increase of 8% for LS23, 5% for LS24 and 6% for LS25 was achieved. In cores LS23 and LS25 slight increase in imbibition rate was observed as well. Heterogeneous pore network and capillary trapping can explain the variations in ΔS_w in the whole cores, but still there is a larger increase after splitting.

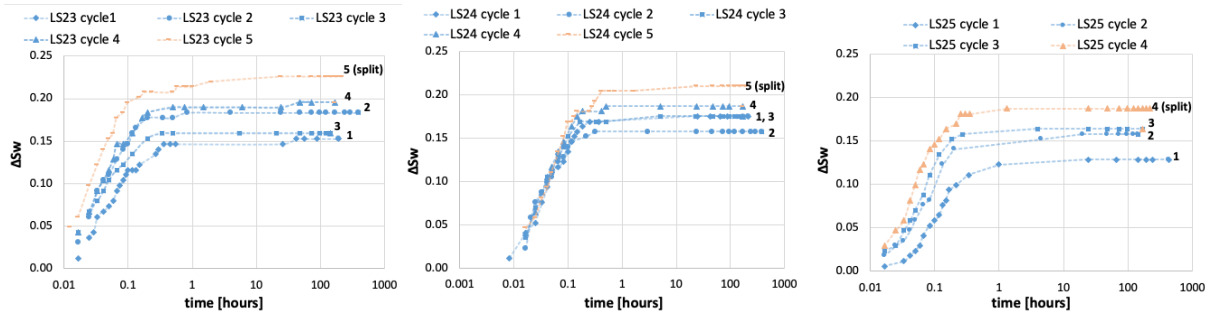

Figure 4.9: Increase in water saturation (ΔS_w) as a function of time during spontaneous water imbibition in LS23 to the left, LS24 in the middle and, LS25 to the right.

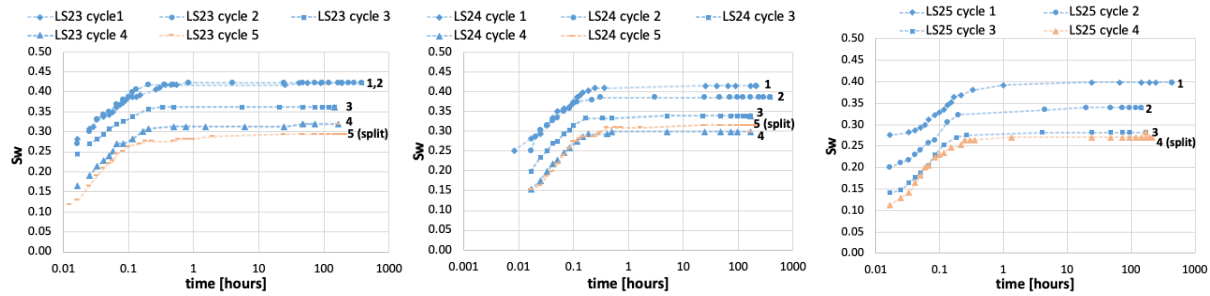

Figure 4.10: Water saturation as a function of time during spontaneous water imbibition in LS23 to the left, LS24 in the middle and, LS25 to the right.

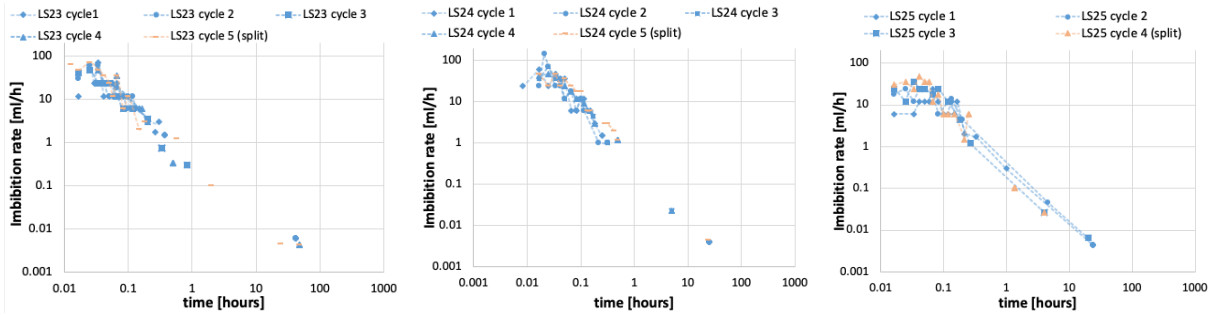

Figure 4.11: Imbibition rate as a function of time during spontaneous water imbibition in LS23 to the left, LS24 in the middle, and LS25 to the right.

4.3.2.2 Dynamically aged cores

Two of the dynamically aged core plugs, LS2 and LS6, were split after completion of two Amott-Harvey cycles and thereafter placed in Amott cells for imbibition to confirm uniform distribution of the altered wettability. Cores LS7 and LS8 were split directly after aging and placed in Amott cells.

Higher volumes of water, 3.0 ml (LS2) and 4.3 ml (LS6), were produced by spontaneous imbibition of oil when the inner part of the cores was exposed to oil compared to AFO boundary conditions (0.5 and 0.6 ml for LS2, 2.5 and 1.5 ml for LS6). Water imbibition was not recorded.

The measured I_{AH} were -0.38 for LS2 (compared to $-0.06/-0.07$ for AFO) and -0.55 (compared to $-0.25/-0.17$) for LS6, hence, the split cores exhibited stronger oil-wet conditions. The volume of water produced by spontaneous oil imbibition increased by 12% - 15% when the cores were split. Figure 4.12 shows the increase in oil saturation as a function of time during spontaneous oil imbibition in whole and split cores LS2 and LS6. Figure 4.13 shows imbibition rate as a function of time. Increase in imbibition rate was observed after splitting of the core plugs.

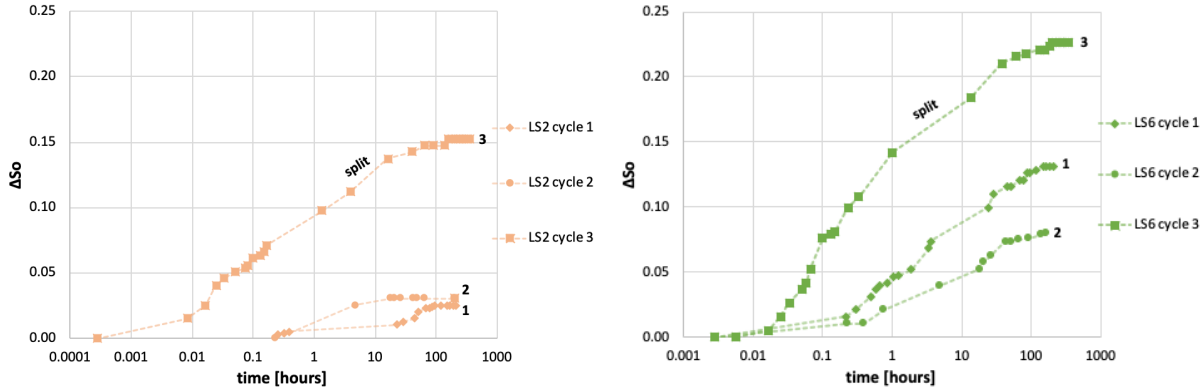

Figure 4.12: Increase in oil saturation (ΔS_o) as a function of time for three cycles of spontaneous oil imbibition in LS2 to the left and LS6 to the right.

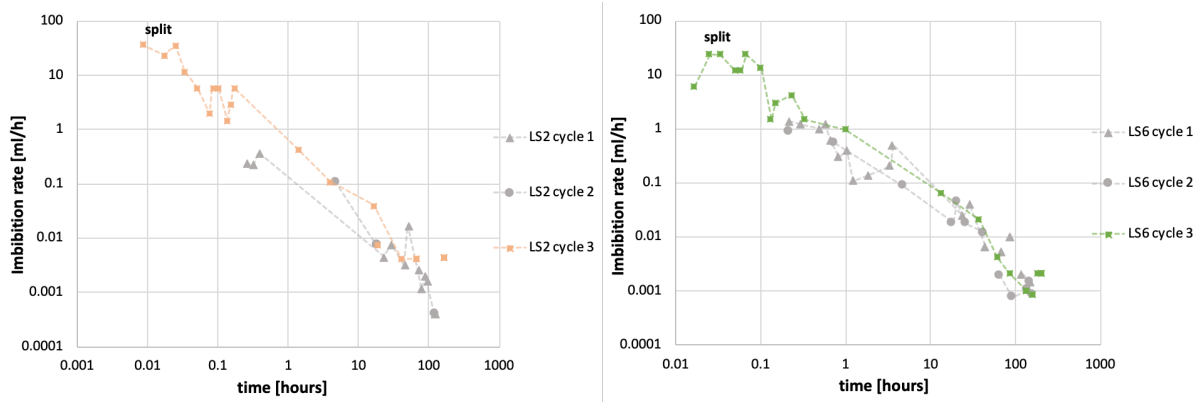

Figure 4.13: Imbibition rate as a function of time for three cycles of spontaneous oil imbibition in LS2 to the left and LS6 to the right.

Cores LS7 and LS8 were split directly after aging and subjected to spontaneous imbibition. Spontaneous water imbibition was not recorded in LS7 nor LS8, but oil imbibition occurred spontaneously. The measured Amott-Harvey indices were -0.51 and -0.58, respectively, corresponding to oil-wet conditions. Good reproducibility was obtained for the two cores both in Amott-Harvey indices and spontaneous imbibition curves. Figure 4.14 shows increase in oil

saturation and imbibition rate as a function of time during spontaneous oil imbibition for the two core plugs.

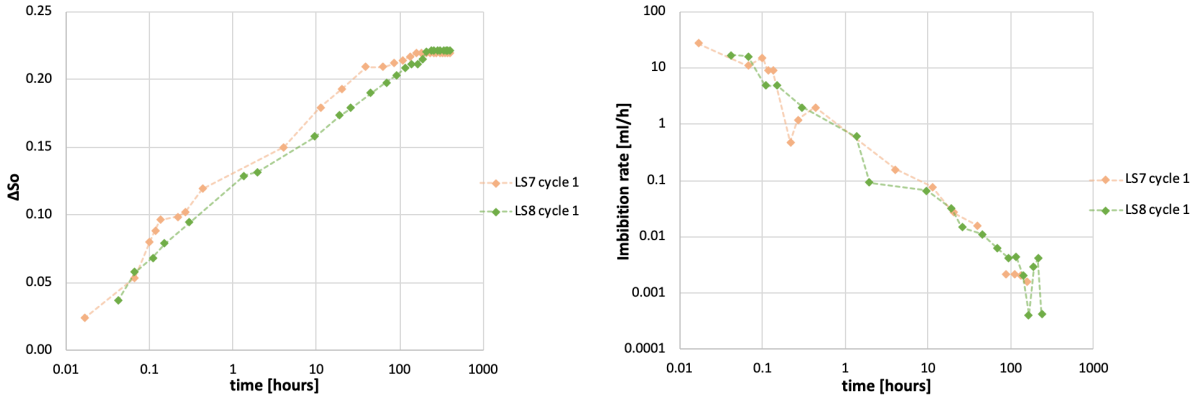

Figure 4.14: Increase in oil saturation (ΔS_o) as a function of time during spontaneous oil imbibition for split cores LS7 and LS8 to the left, and imbibition rate as a function of time to the right.

4.3.2.3 Statically aged cores

After completion of one full Amott-Harvey cycle, statically aged cores LS9 and LS10 were split and submitted to a second Amott-Harvey cycle. Statically aged LS1 and LS4 were split directly after aging and placed in Amott cells for spontaneous imbibition. None of the cores imbibed water after splitting, but oil imbibed spontaneously. An increase in water recovery and oil imbibition rate were observed by exposing the inner part of the core plugs to oil, as was also observed in dynamically aged core plugs.

LS9 and LS10 did not imbibe water or oil spontaneously before splitting (Table 4.3). After splitting, LS9 obtained an Amott-Harvey index of -0.09 and LS10 an index of -0.07, corresponding to near neutral wet conditions. Spontaneously imbibed oil increased the average oil saturation in the core plugs ΔS_o by 3-4 % after splitting as shown in Figure 4.15. Figure 4.16 shows imbibition rate as a function of time before and after splitting. An increase in imbibition rate was obtained after splitting.

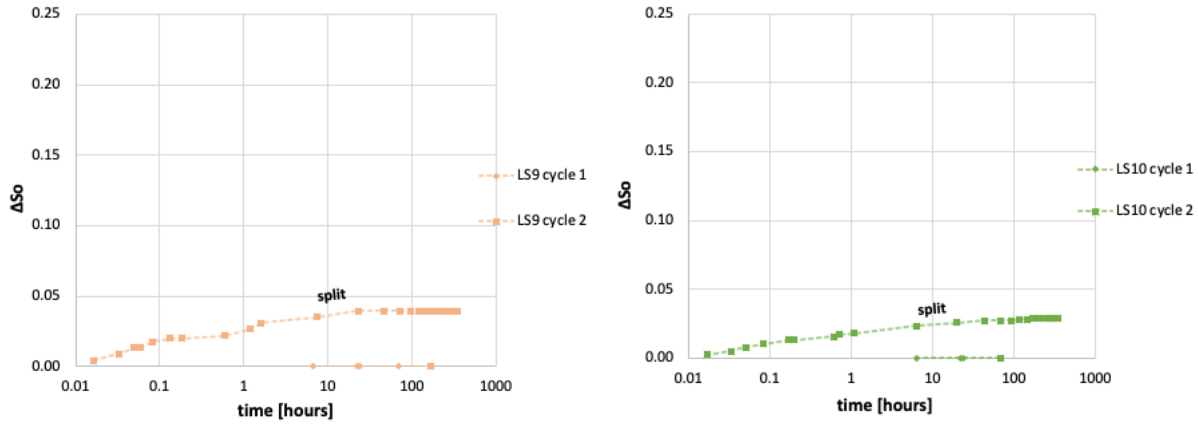

Figure 4.15: Increase in oil saturation as a function of time during spontaneous oil imbibition before and after splitting in LS9 to the left and LS10 to the right.

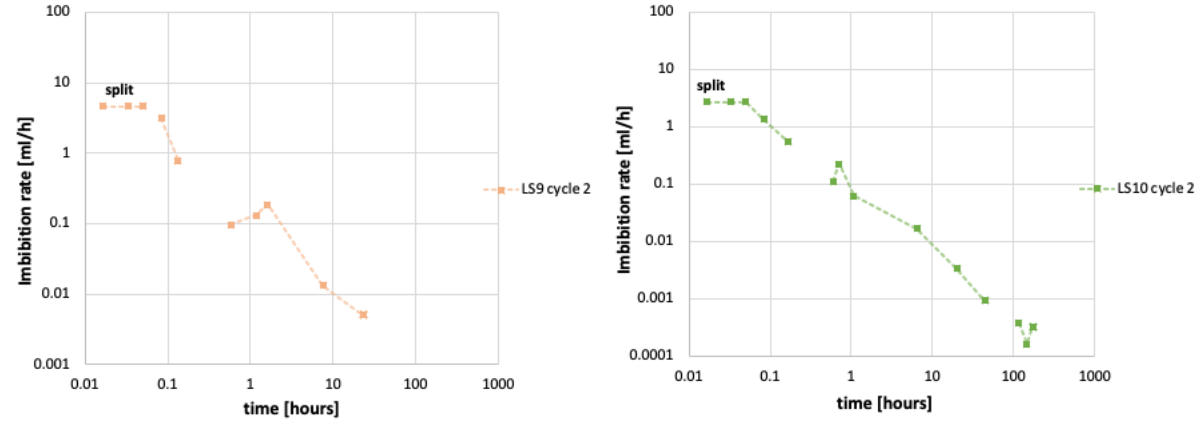

Figure 4.16: Imbibition rate as a function of time during spontaneous oil imbibition after splitting in LS9 to the left and LS10 to the right.

LS1 and LS4 were split directly after aging, and measured Amott-Harvey indices were -0.48 and -0.46, respectively, corresponding to oil-wet conditions. The imbibed volumes of oil in statically aged cores LS1 and LS4 were much higher than imbibed volumes in statically aged cores LS9 and LS10 after splitting. One possible explanation for this can be that the highly heterogenous pore geometry of the core plugs affected the aging and imbibition processes. The reproducibility in I_{AH} and spontaneous oil imbibition was good between these cores, as shown in Figure 4.17 where increase in oil saturation and imbibition rate during spontaneous oil imbibition is plotted as a function of time for the two cores.

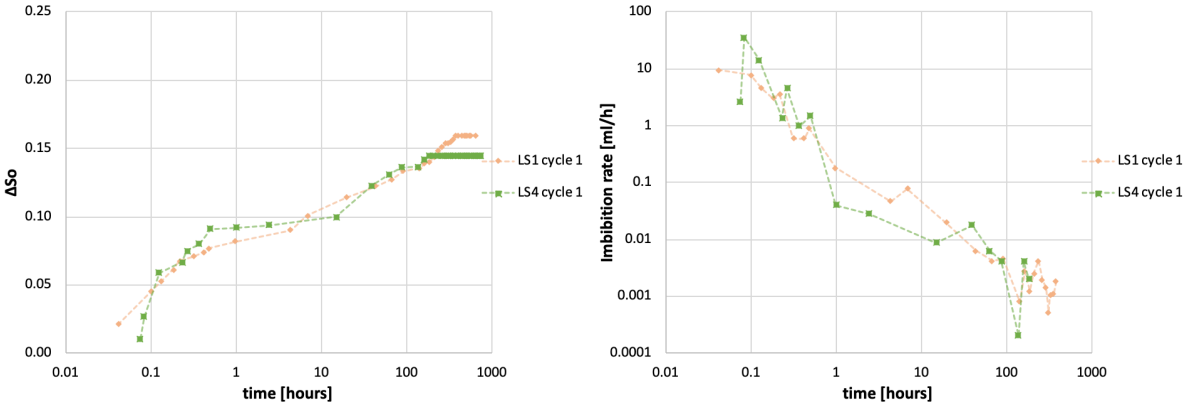

Figure 4.17: Increase in oil saturation (ΔS_o) as a function of time during spontaneous oil imbibition in LS1 and LS4 to the left, and imbibition rate as a function of time to the right.

4.3.2.4 Comparison of static and dynamic wettability alteration

Several important observations were made when statically and dynamically aged core plugs were subjected to repeated Amott-Harvey cycles under both whole and split conditions:

- Cores were aged by crude oil using a dynamic or static aging method. Amott-Harvey cycles were performed, that confirmed dynamically aged cores to be slightly oil-wet because oil was spontaneously imbibed while water was not during several Amott-Harvey cycles. Statically aged core plugs did not imbibe oil nor water, and were therefore considered neutrally wet.
- The aged core plugs were split longitudinally to expose the inner core volume to the imbibing fluid. An impact on oil spontaneous imbibition was recorded, where water was expelled from all open surfaces of the split, dynamically aged core plugs during spontaneous oil imbibition. In contrast, for statically aged split cores, water production was not observed from the core circumference, but water was expelled from the inner part of the core plugs. This suggests a more uniform wettability distribution in the dynamically aged core plugs than in the statically aged cores, which is in good agreement with previous publications, where a more pronounced wettability change and more uniform wettability was found by dynamic aging compared to static aging (Graue et al., 2002, Ferno et al., 2010, B Johannesen et al., 2019). Spontaneous imbibition with AFO boundary condition may be less reliable than previously expected to determine the wettability in statically aged cores, because oil only spontaneously imbibed when the inner part of the core volume was in direct contact with the imbibing fluid. AFO spontaneous imbibition in statically aged cores provided information about the

wettability, by not spontaneously imbibing either phase (neutral wettability), but the tendencies towards weakly oil-wet conditions in the core interior could not be captured.

- The final recovery and imbibition rate during spontaneous imbibition increased when exposing the inner part to oil using split cores, for both statically and dynamically aged cores. Water production during spontaneous oil imbibition increased by 12-15% when the dynamically aged cores were split, compared with 2-3% increased oil production during water imbibition when the water-wet baseline cores were split. A possible explanation for the greater increase in production in dynamically aged cores is slightly stronger oil-wet conditions in the core plug interior compared with the outer part of the core. The dynamically aged core plugs were continuously supplied with crude oil components active in the wettability process inside the core during the aging process, while the statically aged cores had a limited access to surface-active components in the interior during aging (only crude oil injected before submerging).

4.4 Wetting stability produced by dynamic aging

Dynamic aging was chosen for wettability alteration of the remaining core plugs in this thesis because of the more uniform wettability distribution obtained, as the results in section 4.3 suggested. In addition, the method is less time consuming than static aging. Results from four limestone core plugs, where brine constituted the aqueous phase and mineral oil (Decane) constituted the oil phase, are presented in this section. It was necessary to assess the wetting stability in dynamically aged core plugs using brine before the efficiency of polymers in wettability reversal could be assessed. Four core plugs (LS12, LS13, LS16, and LS19) were aged dynamically as described in section 3.5.1. "Twin" core plugs with approximately equal properties were aged under the same conditions to obtain optimum reproducibility. LS12 and LS16 had comparable properties, as did LS13 and LS19. After aging, five full Amott-Harvey cycles were performed to investigate the stability of the wettability alteration, i.e. whether the cores remained neutrally wet or slightly oil-wet after repeatedly being exposed to brine during imbibition and injection. Amott-Harvey indices and end-point relative permeabilities for water and oil were calculated for each cycle. The results are summarized in Table 4.4, where $k_{rw,or}$ is the end point relative permeability of water and $k_{ro,iw}$ is the end point relative permeability of oil. I_w is the water index, I_o is the oil index, and I_{AH} is the Amott-Harvey index of each core plug. The subscript describes which consecutive cycle the measurement describes.

Table 4.4: Water indices, oil indices, Amott-Harvey indices and end-point relative permeabilities during five Amott-Harvey cycles.

	LS12	LS13	LS16	LS19
$k_{rw,or1}$	0.27	0.29	0.30	0.40
$k_{ro,iw1}$	0.24	0.25	0.30	0.29
$I_{w,1}$	0	0	0	0
$I_{o,1}$	0.04	0.01	0.02	0.02
$I_{AH,1}$	-0.04	-0.01	-0.02	-0.02
$k_{rw,or2}$	0.31	0.27	0.31	0.27
$k_{ro,iw2}$	0.27	0.32	0.34	0.38
$I_{w,2}$	0	0	0	0
$I_{o,2}$	0.01	0	0.01	0.01
$I_{AH,2}$	-0.01	0	-0.01	-0.01
$k_{rw,or3}$	0.30	0.27	0.30	0.28
$k_{ro,iw3}$	0.25	0.33	0.32	0.39
$I_{w,3}$	0	0	0	0
$I_{o,3}$	0	0	0	0
$I_{AH,3}$	0	0	0	0
$k_{rw,or4}$	0.30	0.27	0.31	0.28
$k_{ro,iw4}$	0.26	0.28	0.31	0.38
$I_{w,4}$	0.01	0	0.03	0
$I_{o,4}$	0	0	0	0
$I_{AH,4}$	0.01	0	0.03	0
$k_{rw,or5}$	0.18	0.24	0.27	0.24
$k_{ro,iw5}$	0.35	0.37	0.41	0.37
$I_{w,5}$	0.01	0.02	0.01	0.03
$I_{o,5}$	0	0	0	0
$I_{AH,5}$	0.01	0.02	0.01	0.03

First Amott-Harvey cycle

No water spontaneously imbibed in cores LS12, LS13, LS16 and LS19 in the first Amott-Harvey cycle, but between 0.1 and 0.3 ml of water were produced during spontaneous oil imbibition. Measured Amott-Harvey indices were between -0.01 and -0.04, indicating near neutral wet, or slightly oil wet, conditions. It is important to keep in mind that the systems are not homogeneous. It is therefore conceivable that the cores had mixed wet large wettability: crude oil displaced the water in the largest and intermediate pores in the cores during the aging process, changing the wettability towards oil-wet, while the smallest pores remained water-wet and fully water-saturated. This can explain no spontaneous imbibition (SI) of water, because the smallest pores were already filled with water and the intermediate and large pores were oil-wet. Figure 4.18 shows the increase in oil saturation as a function of time during spontaneous oil imbibition in cores LS12, LS13, LS16, and LS19 in the first two Amott-Harvey cycles. Figure 4.19 shows water saturation as a function of time. The measured Amott-Harvey indices and the SI curves for the first Amott-Harvey cycle are comparable to the results for dynamically aged cores LS2 and LS3 presented in section 4.3.

Second Amott-Harvey cycle

In the second Amott-Harvey cycle, the volumes of water produced during spontaneous oil imbibition decreased for all cores: 0.05 ml (LS12), 0 ml (LS13), 0.1 ml (LS16) and 0.1 ml (LS19) compared to the first cycle (0.3 ml for LS12, 0.1ml for LS13, 0.2 ml for LS16, and 0.2 ml for LS19). No spontaneous water imbibition was observed. Good reproducibility of Amott-Harvey indices were achieved after two full Amott-Harvey cycles for cores LS12, LS13, LS16, and LS19, with measured Amott-Harvey indices of $I_{AH,1}/I_{AH,2}$: -0.04/-0.01, -0.01/0, -0.02/-0.01, and -0.02/-0.01, respectively. Measured imbibition rates were low for both cycles, between 0.003 and 6 ml/h at the highest. It was also good reproducibility of Amott-Harvey indices in the two first Amott-Harvey cycles in the dynamically aged cores presented in section 4.3. Measured average wettabilities were near neutral wet, or weakly oil-wet, both for cores LS12, LS13, LS16 and LS19, and for the dynamically aged cores in section 4.3.

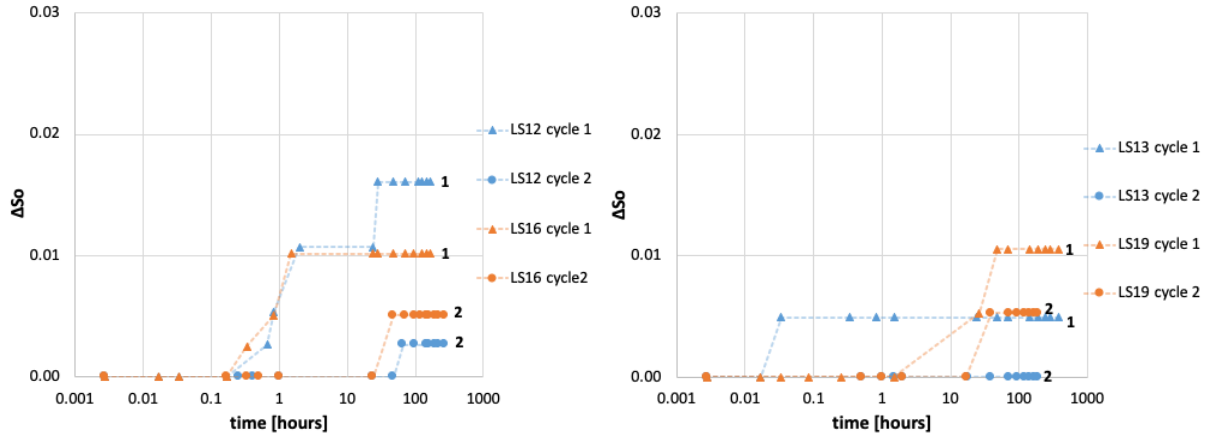

Figure 4.18: Increase in oil saturation (ΔS_o) as a function of time for cores LS12, LS13, LS16, and LS19 during spontaneous oil imbibition in the two first Amott-Harvey cycles. The cores are presented in two pairs, which were aged simultaneously.

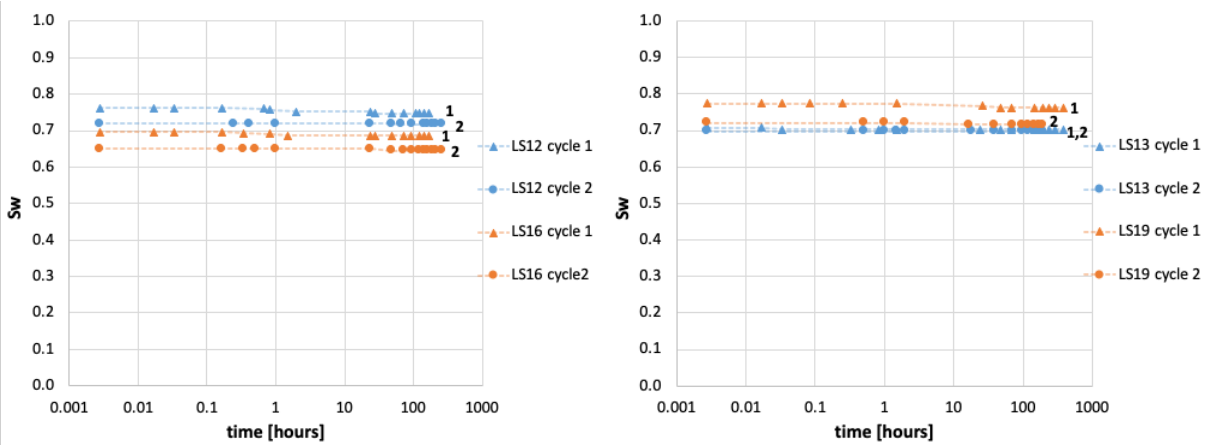

Figure 4.19: Water saturation as a function of time for cores LS12, LS13, LS16, and LS19 during spontaneous oil imbibition in the two first cycles Amott-Harvey cycles. The cores are presented in two pairs, which were aged simultaneously.

Third Amott-Harvey cycle

No spontaneous oil imbibition was recorded during the third Amott-Harvey cycle, neither was spontaneous water imbibition. Measured Amott-Harvey indices were 0 for all cores, corresponding to neutral wet conditions. This indicates a small change in wetting preference, because none of the cores spontaneously imbibed oil anymore.

Fourth Amott-Harvey cycle

Spontaneous water imbibition was recorded for the first time in cores LS12 and LS16 in the fourth Amott-Harvey cycle. 0.1 ml (LS12) and 0.3 ml (LS16) of oil production was recorded during spontaneous water imbibition, while no oil imbibed spontaneously. Measured Amott-Harvey indices were 0.01 in LS12 and 0.03 in LS16, corresponding to near neutral wet

conditions, although SI of water suggests weakly water-wet conditions. Cores LS13 and LS19 imbibed neither oil nor water, thus the measured Amott-Harvey indices were 0 for both cores, equal to the previous cycle.

Fifth Amott-Harvey cycle

Water imbibed spontaneously in cores LS13 and LS19 for the first time in the fifth Amott-Harvey cycle, with oil production of 0.2 ml in LS13 and 0.3 ml in LS19. Spontaneous oil imbibition was not recorded, and measured Amott-Harvey indices were 0.02 (LS13) and 0.03 (LS19). In cores LS12 and LS16, oil production of 0.1 ml was recorded in both cores during spontaneous water imbibition, while no oil spontaneously imbibed. Both cores exhibited an Amott-Harvey index of 0.01. The measured Amott-Harvey indices in the fifth Amott-Harvey cycle correspond to nearly neutral, or weakly water-wet, wetting conditions for all four core plugs. The fact that the four cores spontaneously imbibed oil in the first Amott-Harvey cycle and spontaneously imbibed water in the fifth cycle, indicates a change in wettability towards weakly water-wet after completion of five Amott-Harvey cycles. Figure 4.20 shows increase in water saturation as a function of time during spontaneous water imbibition in the fourth and fifth Amott-Harvey cycle, and Figure 4.21 shows water saturation as a function of time.

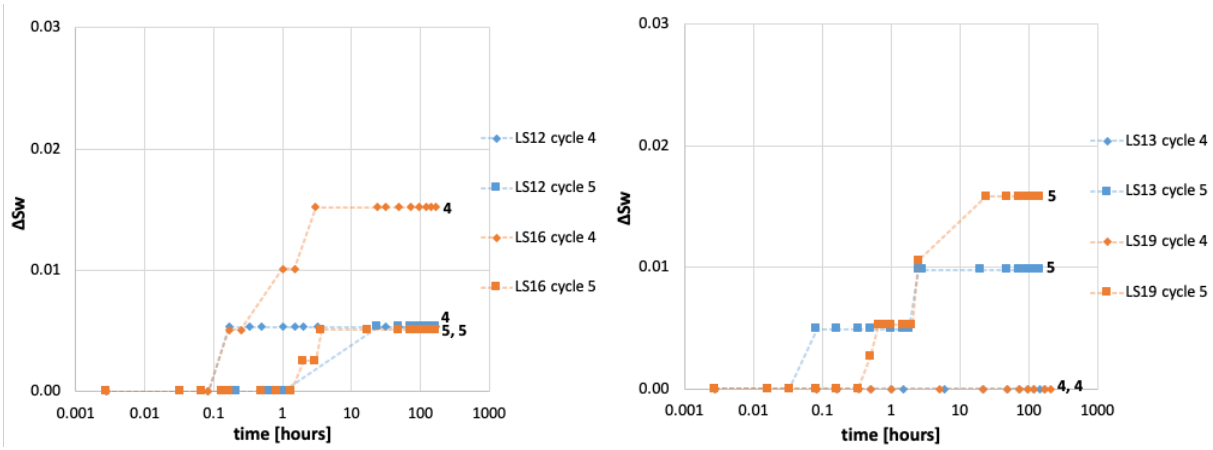

Figure 4.20: Increase in water saturation as a function of time in cores LS12, LS13, LS16, and LS19 during spontaneous water imbibition in fourth and fifth Amott-Harvey cycle. The cores are presented in two pairs, which were aged simultaneously.

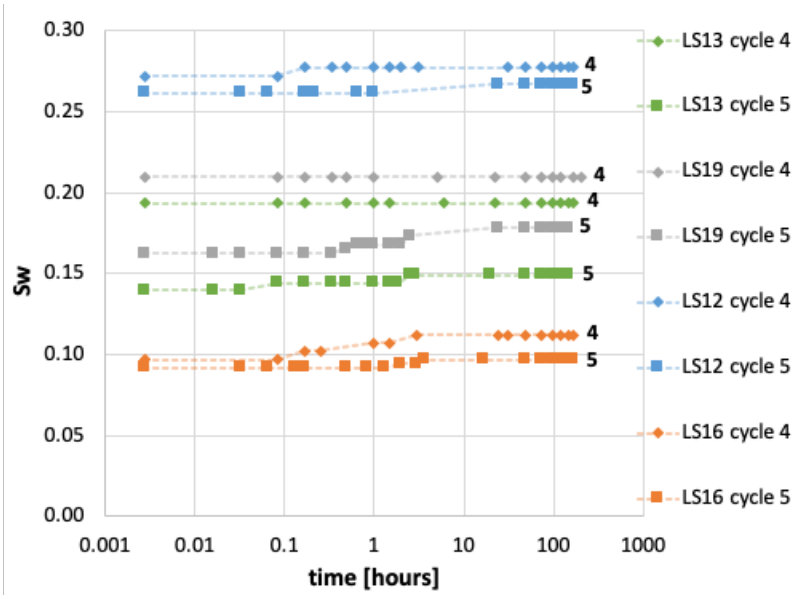

Figure 4.21: Water saturation as a function of time in cores LS12, LS13, LS16, and LS19 during spontaneous water imbibition in fourth and fifth Amott-Harvey cycle.

Amott-Harvey indices for each Amott-Harvey cycle are plotted for all cores in Figure 4.22. The Amott-Harvey indices changed from slightly negative values between -0.02 and -0.04 towards slightly positive values between 0.01 and 0.03 for all cores after completion of five Amott-Harvey cycles, corresponding to nearly neutral wet conditions. The change from SI of oil to SI of water in all cores indicates a change in wettability from weakly oil-wet towards weakly water-wet. The highest positive Amott-Harvey index measured during five Amott-Harvey cycles was 0.03 in cores LS16 and LS19. An overall increase of 0.05 in the Amott-Harvey index was obtained.

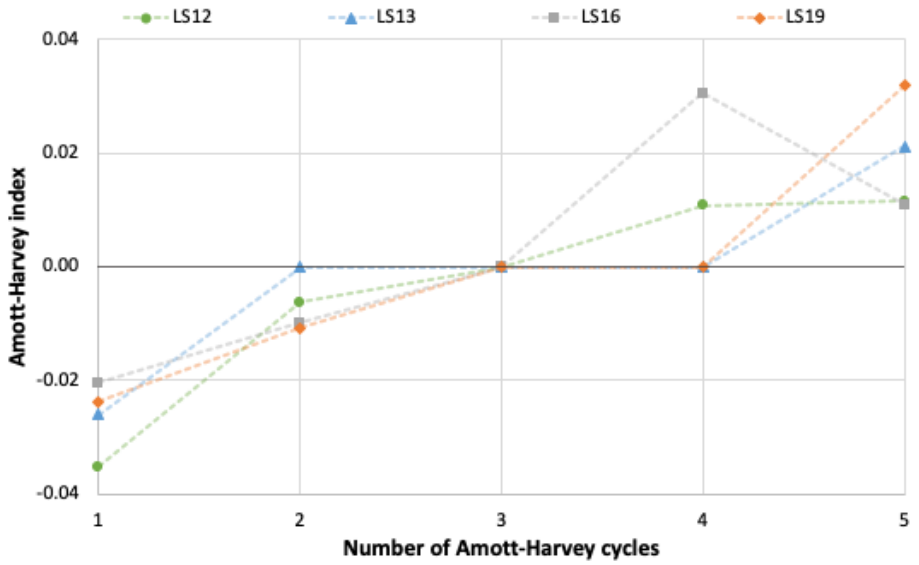

Figure 4.22: Amott-Harvey indices for each Amott-Harvey cycle for cores LS12, LS13, LS16 and LS19.

End-point relative permeability

End point relative permeabilities for oil ($k_{ro,iw}$) and water ($k_{rw,or}$) were calculated after each forced injection of water and oil. Figure 4.23 shows end-point relative permeabilities of water and oil during five Amott-Harvey cycles. Figure 4.24 shows end-point relative permeabilities of water and oil as a function of water saturation for one core (LS12) during five Amott-Harvey cycles. The end-point relative permeabilities of water ranged between 0.27-0.31 during the four first Amott-Harvey cycles in cores LS12, LS13, and LS16, while $k_{ro,iw}$ ranged between 0.24-0.34. According to Craig´s rules of thumb (described in section 2.3.3) this indicates near neutral wet conditions because $k_{rw,or}$ and $k_{ro,iw}$ are approximately the same.

The end-point relative permeability of water decreased to 0.18 (LS12), 0.24 (LS13), and 0.27 (LS16) in the fifth Amott-Harvey cycle, while $k_{ro,iw}$ increased to 0.35 (LS12), 0.37 (LS13), and 0.41 (LS16). Craig´s rules of thumb suggest a change in wettability towards water-wet conditions. In core LS19, $k_{rw,or}$ was measured to be 0.40 in the first Amott-Harvey cycle, and between 0.24-0.27 in the next four Amott-Harvey cycles. $k_{ro,iw}$ was measured to be 0.29 in the first cycle, and between 0.37 and 0.39 in the four next cycles. This indicates tendencies towards oil-wet conditions in the first cycle, because $k_{rw,or}$ was higher than $k_{ro,iw}$, and tendencies towards water-wet conditions in further cycles.

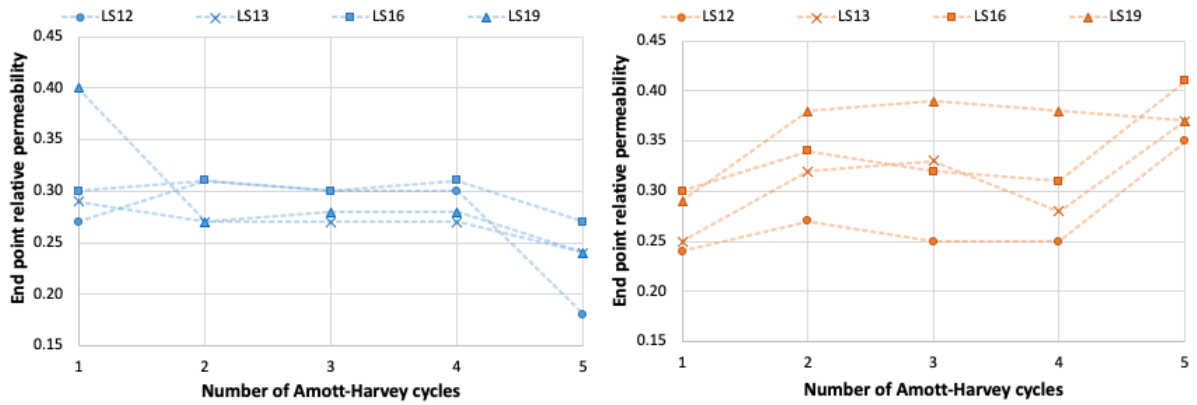

Figure 4.23: End-point relative permeabilities of water for each Amott-Harvey cycle to the left, and end-point relative permeability of oil for each Amott-Harvey cycle to the right.

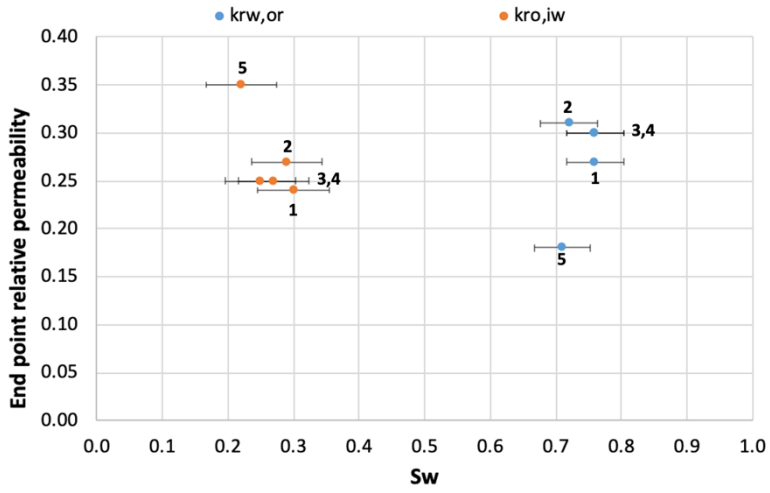

Figure 4.24: End-point relative permeabilities of water (krw,or) and oil (kro,iw) as a function of water saturation during five Amott-Harvey cycles for core LS12. The numbers (1-5) describes the consecutive cycle. Uncertainty bars for water saturations are included.

Figure 4.25 shows end-point relative permeabilities as a function of water saturation for LS12, LS13, LS16, and LS19 during five Amott-Harvey cycles. krw is the end-point relative permeability of water, kro is the end-point relative permeability of oil, and the numbers 1-5 describe the consecutive cycle. Spread in water saturations and decreasing end-point water saturations for each Amott-Harvey cycle can be seen in the figure. The uncertainties in saturations after completion of five Amott-Harvey cycles were calculated to be $\pm$5% (uncertainties for each cycle are presented in Appendix E). By taking the uncertainty into account, a total decrease in water saturation was 0.08$\pm$0.05 (LS12), 0.16$\pm$0.05 (LS13), 0.15$\pm$0.05 (LS16) and 0.14$\pm$0.05 (LS16) after completion of five full Amott-Harvey cycles. Because of the uncertainties in the saturations, the spread in water saturations might not be as large as it appears in Figure 4.25.

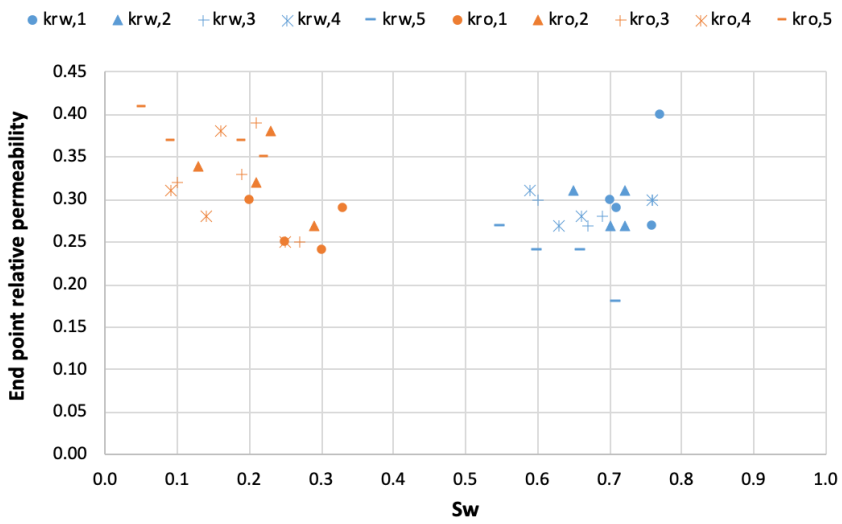

Figure 4.25: End-point relative permeability of water (krw) and oil (kro) as a function of water saturation for cores LS12, LS13, LS16 and LS19. The numbers (1-5) describe the consecutive cycle.

Important observations

Several important observations were made after completion of five Amott-Harvey cycles with brine/oil in four dynamically aged core plugs:

- The reproducibility of Amott-Harvey indices for all cores were good during the two first Amott-Harvey cycles. All cores spontaneously imbibed oil in the first cycle, and all cores expect LS13 spontaneously imbibed oil in the second cycle. In the third cycle, neither water nor oil imbibed spontaneously into the core plugs. Ferno et al. (2007) tested the stability of dynamic aging on two different limestone core plugs that were aged for 6 and 10 days by performing three subsequent Amott-Harvey cycles. Like the aged cores in this work, no spontaneous imbibition of water was observed during three Amott-Harvey cycles. They observed that the Amott-Harvey index was reproducible.
- In this work, minor spontaneous imbibition of water was recorded during the fourth and fifth Amott-Harvey cycles. The change from spontaneously imbibing oil to spontaneously imbibing water, and the change in Amott-Harvey indices from slightly negative values (between -0.01 and -0.04) to slightly positive values (between 0.01 and 0.03), suggests a change in wettability from weakly oil-wet to weakly water-wet, although the wettability did not revert back to strongly water-wet conditions by brine.

4.5 Wettability alteration by polymers

4.5.1 Fluid analysis

Results from dynamic viscosity measurements of glycerol and polymer solutions are presented in this section. Dynamic viscosity of seven different 5000ppm polymer solutions and four different glycerol solutions were measured. In addition, viscosities of effluent samples from core injection were measured. Viscosity was measured from low to high spindle RPM, and back to low spindle RPM for all fluid samples.

4.5.1.1 Polymer viscosity measurement

To study the efficiency of polymers in wettability reversal, seven different 5000ppm polymer solutions were made, following the procedure described in section 3.1.1. The viscosity measurements were performed with RPM´s of 2, 4, 5, and 12 for all solutions. The spindle RPM was first increased, then decreased back to initial RPM. Viscosity of HPAM1 and HPAM2 were also measured with an RPM of 20. None of the fluid samples had been in contact with a core plug. Viscosity as a function of shear stress is shown in Figure 4.26 for the seven different polymer solutions. All polymer solutions showed non-Newtonian shear-thinning behavior. In addition, HPAM2, HPAM3, HPAM4, HPAM5, and HPAM6 showed some tendency of hysteresis at viscosities measured at low shear stress. HPAM1 and HPAM7 showed no tendency of hysteresis.

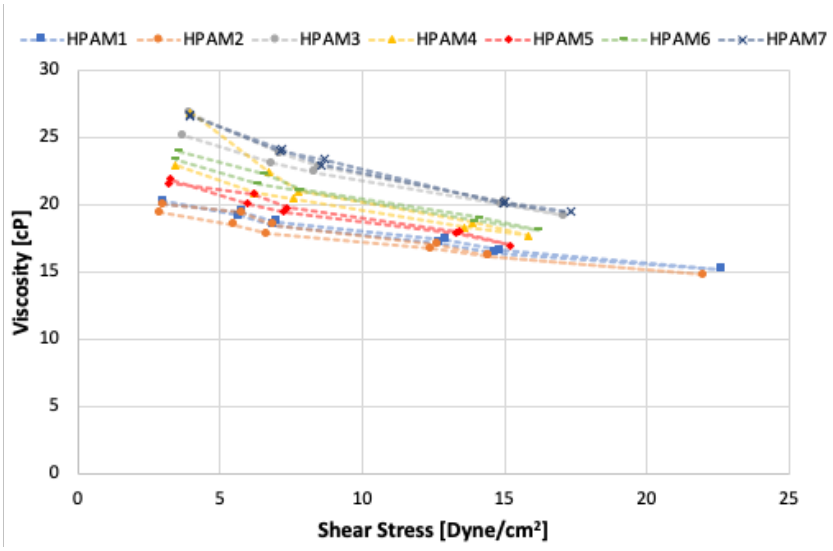

Figure 4.26: Viscosity as a function of shear stress for seven different 5000ppm polymer solutions.

One viscosity value had to be chosen for use in scaling of spontaneous imbibition because the viscosity of the polymer solutions varies with shear stress. In Figure 4.27 the highest value (21.6 cP), the lowest value (17.0 cP) and the average value (19.6 cP) of the measured viscosity for polymer solution HPAM6 are used in the scaling equation. The three different spontaneous imbibition curves are similar within a small range, which is an acceptable uncertainty for spontaneous imbibition at weakly oil-wet conditions. The average value of the viscosity was therefore used for scaling of spontaneous polymer imbibition and for end-point relative permeability calculations.

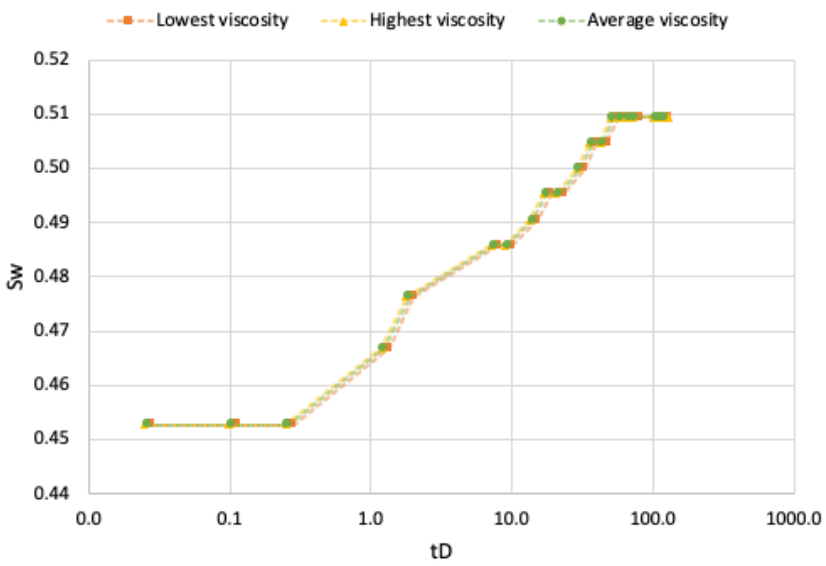

Figure 4.27: Spontaneous imbibition curves for LS11 (during fifth Amott-Harvey cycle) using three different viscosity values in the scaling equation.

4.5.1.2 Glycerol viscosity measurements

Viscosity of four different glycerol solutions were measured. One solution contained 61wt% glycerol and three solutions contained 69wt% of glycerol mixed with Ekofisk brine. These concentrations were chosen to produce a variation of viscosities in the same range as the polymer solutions. Viscosity as a function of shear rate is shown in Figure 4.28. A shear-thinning tendency was observed for some of the glycerol solutions initially but may be related to improper mixing of the solution and was not observed when the rate was reduced back towards initial RPM. For glycerol, the viscosity measured with the highest RPM (lowest uncertainty) was used for scaling of spontaneous imbibition and in end-point relative permeability calculations.

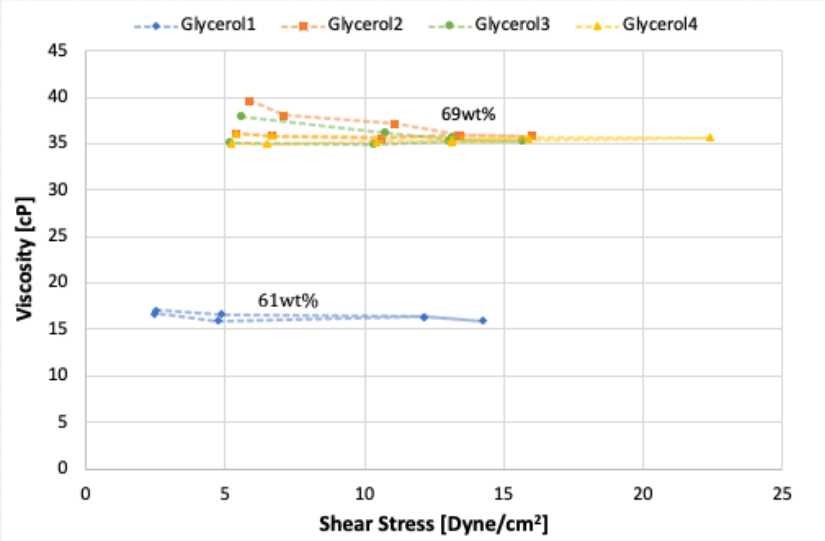

Figure 4.28: Viscosity as a function of shear stress for four different glycerol solutions.

4.5.2 Wettability alteration by polymer/oil and glycerol/oil

This section presents subsequent Amott-Harvey cycles performed on four dynamically aged limestone core plugs ($LS11_{polymer}$, $LS14_{polymer}$, $LS17_{glycerol}$, and $LS18_{glycerol}$), to assess the efficiency of polymers in wettability reversal. Glycerol was used as the aqueous phase in two core plugs, because it had the same viscosity and brine content as polymer, but without the presence of surface-active components that could potentially impact wettability. Glycerol was used as the aqueous phase in cores $LS17_{glycerol}$ and $LS18_{glycerol}$, and polymer was used in $LS11_{polymer}$ and $LS14_{polymer}$. Cores $LS11_{polymer}$ and $LS17_{glycerol}$ had high permeabilities (45.9-52.6mD), while $LS14_{polymer}$ and $LS18_{glycerol}$ had lower permeabilities (21.5-23.6mD). The core plugs with equal core properties were aged under the same conditions to obtain optimum reproducibility, and five subsequent Amott-Harvey cycles were performed. Water constituted the aqueous phase for all cores in the first cycle, while polymer and glycerol constituted the aqueous phase in four cycles. Mineral oil constituted the oil phase in all five cycles. Measured Amott-Harvey indices and spontaneous oil and water imbibition curves were used to determine wettability and wettability alterations. End-point relative permeabilities were measured after each injection. The results are summarized in Table 4.5. I_w is the water index, I_o is the oil index, I_{AH} is the Amott-Harvey index, $k_{rw,or}$ is the end-point relative permeability of the aqueous phase, and $k_{ro,iw}$ is the end-point relative permeability of oil. The subscript describes which consecutive cycle the measurement describes.

Table 4.5: Water indices, oil indices, Amott-Harvey indices and end-point relative permeabilities for water and oil for Amott-Harvey cycles with different aqueous fluids.

Core	LS11	LS14	LS17	LS18	LS12
Aqueous phase	Ekofisk brine	Ekofisk brine	Ekofisk brine	Ekofisk brine	Ekofisk brine
$k_{rw,or1}$	0.35	0.38	0.32	0.40	0.27
$k_{ro,iw1}$	0.40	0.34	0.39	0.29	0.24
$I_{w,1}$	0	0	0	0	0
$I_{o,1}$	0.06	0.03	0.08	0.08	0.04
$I_{AH,1}$	-0.06	-0.03	-0.08	-0.08	-0.04
Aqueous phase	Polymer	Polymer	Glycerol	Glycerol	Ekofisk brine
$k_{rw,or2}$	0.16	0.23	0.59	0.61	0.31
$k_{ro,iw2}$	0.13	0.12	0.16	0.12	0.27
$I_{w,2}$	0	0	0	0	0
$I_{o,2}$	0	0	0	0.05	0.01
$I_{AH,2}$	0	0	0	-0.05	-0.01
Aqueous phase	Polymer	Polymer/ brine	Glycerol	Glycerol/ brine	Ekofisk brine
$k_{rw,or3}$	0.13	0.01	0.36	0.29	0.30
$k_{ro,iw3}$	0.10	0.10	0.11	0.22	0.25
$I_{w,3}$	0.09	0.18	0.04	0	0
$I_{o,3}$	0	0	0	0	0
$I_{AH,3}$	0.09	0.18	0.04	0	0
Aqueous phase	Polymer	Polymer/ brine	Glycerol	Glycerol/ brine	Ekofisk brine
$k_{rw,or4}$	0.12	0.02	0.42	0.35	0.30
$k_{ro,iw4}$	0.09	0.11	0.10	0.27	0.26
$I_{w,4}$	0.27	0.16	0.11	0.01	0.01
$I_{o,4}$	0	0	0	0	0
$I_{AH,4}$	0.27	0.16	0.11	0.01	0.01
Aqueous phase	Polymer	Polymer/ brine	Glycerol	Glycerol/ brine	Ekofisk brine
$k_{rw,or4}$	0.11	0.02	0.46	0.28	0.18
$k_{ro,iw4}$	0.12	0.12	0.18	0.37	0.35
$I_{w,4}$	0.27	0.18	0.09	0	0.01
$I_{o,4}$	0	0	0	0	0
$I_{AH,4}$	0.27	0.18	0.09	0	0.01

First Amott-Harvey cycle

No water spontaneously imbibed into cores $LS11_{polymer}$, $LS14_{polymer}$, $LS17_{glycerol}$ and $LS18_{glycerol}$ in the first Amott-Harvey cycle where brine constituted the aqueous phase, while oil imbibition occurred spontaneously. Between 0.2-0.8 ml of water production was recorded during spontaneous oil imbibition, with measured Amott-Harvey indices between -0.03 and -0.08, corresponding to near neutral wet, or weakly oil-wet, conditions. The results are in accordance with the results for dynamically aged cores presented in section 4.3 and 4.4: no spontaneous water imbibition in the first Amott-Harvey cycle, and measured Amott-Harvey indices in the same range. Figure 4.29 shows saturation development as a function of dimensionless time during the first cycle of spontaneous oil imbibition in cores $LS11_{polymer}$, $LS14_{polymer}$, $LS17_{glycerol}$, and $LS18_{glycerol}$.

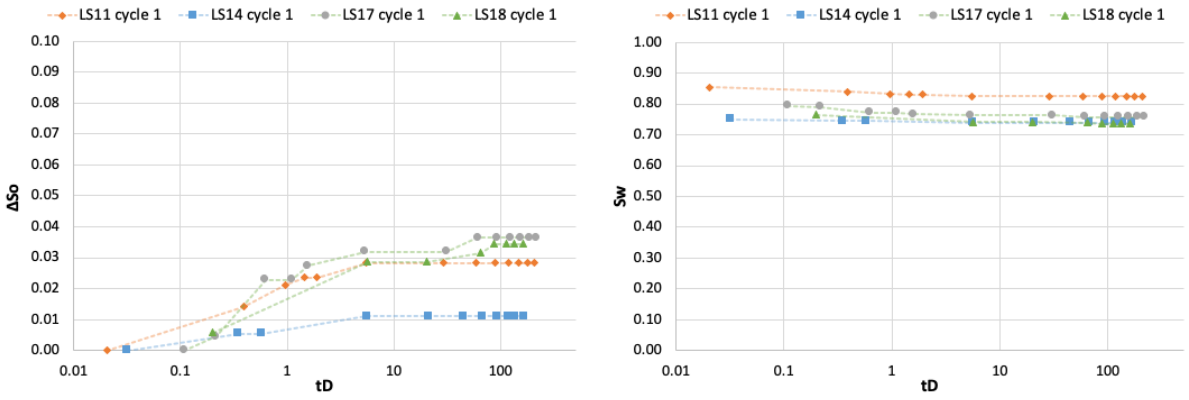

Figure 4.29: Increase in oil saturation (ΔS_o) as a function of dimensionless time during first cycle of spontaneous oil imbibition in $LS11_{polymer}$, $LS14_{polymer}$, $LS17_{glycerol}$, and $LS18_{glycerol}$ to the left, and water saturation as a function of dimensionless time to the right. The curves are scaled for viscosity according to equation (2.4).

Second Amott-Harvey cycle

Two cores, $LS11_{polymer}$ and $LS14_{polymer}$, were placed in Amott cells filled with polymer, and the remaining two cores, $LS17_{glycerol}$ and $LS18_{glycerol}$, were placed in Amott cells filled with glycerol. No polymer spontaneously imbibed in cores $LS11_{polymer}$ and $LS14_{polymer}$, and spontaneous imbibition of glycerol was not recorded in $LS17_{glycerol}$ nor $LS18_{glycerol}$. This was expected based on the results in section 4.4, where no SI of aqueous phase was observed during the second Amott-Harvey cycle in oil/brine systems. Polymer/glycerol was therefore injected into the cores to displace the oil. At least 1.5 pore volumes were injected in each direction, at low flow rates between 5-20 ml/h, until residual oil saturation (S_{or}) was reached. At S_{or}, the cores were placed in Amott cells filled with oil. Spontaneous oil imbibition was not recorded

in the cores saturated by polymer, thus the measured Amott-Harvey indices were 0 for both $LS11_{polymer}$ and $LS14_{polymer}$. Spontaneous oil imbibition was recorded in $LS18_{glycerol}$, while no spontaneous oil imbibition was recorded in $LS17_{glycerol}$. The measured $I_{AH,2}$ were 0 ($LS17_{glycerol}$) and -0.05 ($LS18_{glycerol}$), compared to -0.08 for both cores in previous Amott-Harvey cycle. In brine/oil systems (section 4.4), three out of four aged core plugs spontaneously imbibed oil in the second Amott-Harvey cycle. None of the cores saturated with polymer imbibed oil, which can indicate a change in wetting preference in the cores. It is conceivable that the injected polymer displaced the oil from the large and intermediate oil-wet pores and a "water-wet" polymer layer adsorbed along the pore walls. Oil injection was performed to bring the saturation back towards the irreducible water saturation.

Third Amott-Harvey cycle

Figure 4.30 shows saturation development as a function of dimensionless time in cores $LS11_{polymer}$, $LS14_{polymer}$, $LS17_{glycerol}$ and $LS18_{glycerol}$ during the third cycle of SI of aqueous phase. SI of polymer was recorded in $LS11_{polymer}$ and $LS14_{polymer}$ in the third Amott-Harvey cycle, with oil production of 0.6ml in $LS11_{polymer}$ and 0.8ml in $LS14_{polymer}$. In glycerol/oil systems, oil production of 0.3 ml was recorded during spontaneous glycerol imbibition in core $LS17_{glycerol}$, while no spontaneous glycerol imbibition was recorded in $LS18_{glycerol}$. Polymer/glycerol was injected into the cores to displace the oil, like in the second Amott-Harvey cycle. In $LS14_{polymer}$ and $LS18_{glycerol}$, brine was injected directly after polymer/glycerol injection to remove the polymer/glycerol from the pore network before spontaneous oil imbibition. It was expected that the glycerol in core $LS18_{glycerol}$ was diluted, or completely removed, during the brine injection. In core $LS14_{polymer}$, some of the polymer was expected to remain in the pore network as an adsorbed polymer layer along the pore walls. Brine injections were performed to assess whether wettability changes were influenced by the adsorbed polymer, and to assess any changes in the end-point relative permeabilities. The influence of brine injection on wettability changes and end-point relative permeabilities will be further assessed in the fourth and fifth cycles.

Spontaneous oil imbibition was not recorded in any of the cores, thus Amott-Harvey indices of 0.09 ($LS11_{polymer}$) and 0.18 ($LS14_{polymer}$) were measured for the polymer/oil systems, compared to Amott-Harvey indices of 0.04 ($LS17_{glycerol}$) and 0 ($LS18_{glycerol}$) for glycerol/oil. The measured I_{AH} correspond to nearly neutral wetting conditions, although SI of aqueous phases (polymer and glycerol) in some cores suggests alterations towards weakly water-wet conditions.

In brine/oil systems (section 4.4), no spontaneous water imbibition was recorded before the fourth or fifth Amott-Harvey cycles. This means that SI of aqueous phase occurred earlier in $LS11_{polymer}$, $LS14_{polymer}$ and $LS17_{glycerol}$, i.e. wettability alteration was quicker with polymer in the aqueous phase. Between 0.1-0.3 ml of oil were produced during spontaneous water imbibition in the fourth and fifth Amott-Harvey cycles in the brine/oil systems in section 4.4. Larger volumes, between 0.6-0.8 ml, of oil were recorded during SI of aqueous phase (polymer) in cores $LS11_{polymer}$ and $LS14_{polymer}$ in the third Amott-Harvey cycle. In brine/oil systems, spontaneous oil imbibition was not recorded after completion of one full Amott-Harvey cycle in one core, and after two cycles in three cores. In glycerol/oil systems spontaneous oil imbibition also stopped after completion of one-two full Amott-Harvey cycles, while no spontaneous oil imbibition was recorded in the polymer/oil systems after polymer was introduced to the cores (after completion of one Amott-Harvey cycle). The SI of polymer in the polymer/oil systems in the third Amott-Harvey cycle supports the theory of an adsorbed "water-wet" polymer layer along the pore walls. Oil was injected into the cores to bring the saturations back towards irreducible water saturation.

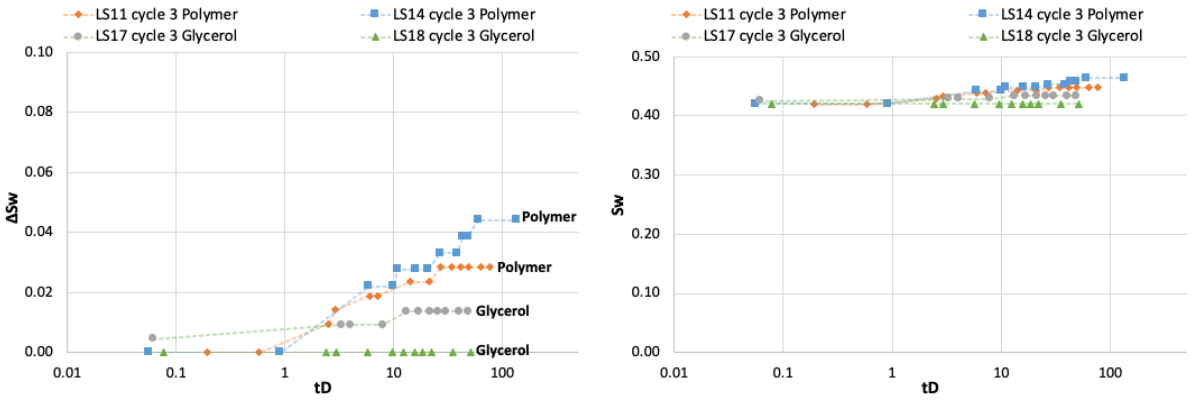

Figure 4.30: Increase in water saturation (ΔS_w) as a function of dimensionless time during third cycle of spontaneous imbibition of aqueous phase in cores $LS11_{polymer}$, $LS14_{polymer}$, $LS17_{glycerol}$, and $LS18_{glycerol}$ to the left, and water saturation as a function of dimensionless time to the right. The curves are scaled for viscosity according to equation (2.4).

Fourth Amott-Harvey cycle

In the beginning of the fourth Amott-Harvey cycle, $LS11_{polymer}$ was saturated by oil/polymer, $LS14_{polymer}$ was saturated by oil/brine/adsorbed polymer, $LS17_{glycerol}$ was saturated by oil/glycerol, and $LS18_{glycerol}$ was saturated by oil/brine. Oil production during spontaneous polymer imbibition increased for $LS11_{polymer}$ in the fourth Amott-Harvey cycle: producing 1.2 ml compared to 0.6 ml in previous cycle. $LS14_{polymer}$ produced 0.7 ml of oil during spontaneous

polymer imbibition, comparable to previous cycle. Oil production in $LS17_{glycerol}$ also increased during SI of aqueous phase (glycerol) in the fourth Amott-Harvey cycle: producing 0.8 ml compared to 0.3 ml in previous cycle. Glycerol imbibed spontaneously in $LS18_{glycerol}$ for the first time, with measured oil production of 0.1ml.

The cores were flooded with polymer/glycerol until residual oil saturation, then $LS14_{polymer}$ and $LS18_{glycerol}$ were flooded with brine to remove polymer/glycerol from the cores. Spontaneous oil imbibition was not recorded in any of the four cores, thus measured Amott-Harvey indices were 0.27 ($LS11_{polymer}$) and 0.16 ($LS14_{polymer}$) for polymer/oil systems, which correspond to weakly water-wet conditions. The measured I_{AH} did not increase between the third and fourth Amott-Harvey cycle in core $LS14_{polymer}$ where brine was injected after polymer injection, while I_{AH} increased for $LS11_{polymer}$, where brine was not injected. This suggests that the injected brine removed parts of the polymer in the core and prevented adsorption of additional polymer along the pore walls.

Amott-Harvey indices of 0.11 ($LS17_{glycerol}$) and 0.01 ($LS18_{glycerol}$) were measured for glycerol/oil systems, corresponding to near neutral wet, or weakly water-wet, conditions. Figure 4.31 shows saturation development as a function of dimensionless time during the fourth cycle of spontaneous imbibition of aqueous phase in cores $LS11_{polymer}$, $LS14_{polymer}$, $LS17_{glycerol}$, and $LS18_{glycerol}$. In brine/oil systems (section 4.4), two out of four cores started to imbibe water during the fourth Amott-Harvey cycle, with Amott-Harvey indices of 0.01 and 0.03. Here, the cores with polymer in the aqueous phase obtained higher Amott-Harvey indices (0.16 and 0.27) in the fourth Amott-Harvey cycle, i.e. the wettability changed both quicker and towards stronger water-wet conditions with polymer in the aqueous phase. The cores were flooded with oil back towards irreducible water saturation.

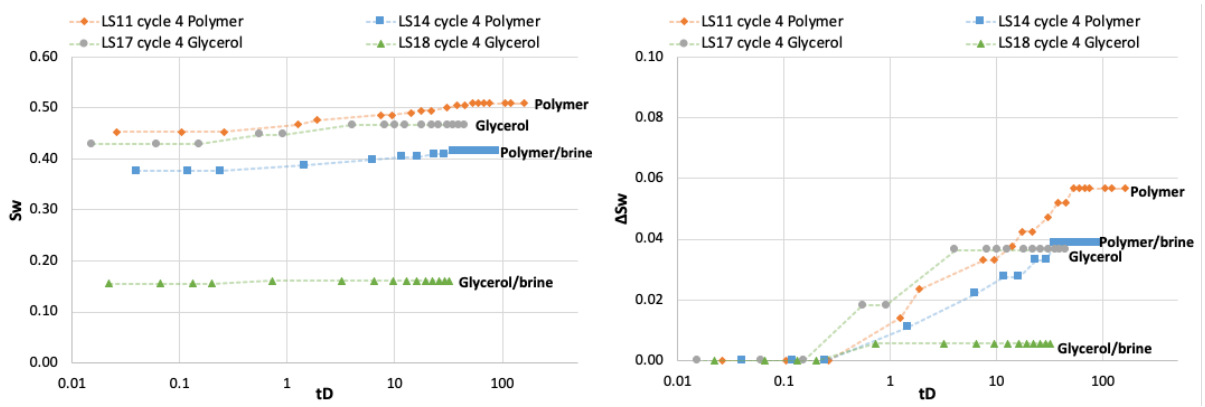

Figure 4.31: Increase in water saturation (ΔS_w) as a function of dimensionless time during the fourth cycle of spontaneous imbibition of aqueous phase in cores $LS11_{polymer}$, $LS14_{polymer}$, $LS17_{glycerol}$, and $LS18_{glycerol}$ to the left, and water saturation as a function of dimensionless time to the right. Brine injection was performed after polymer/glycerol injection in previous cycle in cores marked with polymer/brine or glycerol/brine. The curves are scaled for viscosity according to equation (2.4).

Fifth Amott-Harvey cycle

The cores consisted of oil/polymer ($LS11_{polymer}$), oil/brine/adsorbed polymer ($LS14_{polymer}$), oil/glycerol ($LS17_{glycerol}$), and oil/brine ($LS18_{glycerol}$) in the beginning of the fifth Amott-Harvey cycle. Oil production during spontaneous polymer imbibition in both core $LS11_{polymer}$ and $LS14_{polymer}$ was comparable to previous cycle, which indicates no further change in wettability. Oil production during spontaneous glycerol imbibition in cores $LS17_{glycerol}$ and $LS18_{glycerol}$ were also comparable to previous cycle.

Polymer/glycerol was injected into the cores until residual oil saturation. Brine was injected into cores $LS14_{polymer}$ and $LS18_{glycerol}$ to remove polymer/glycerol from the cores. The four cores were thereafter put in Amott cells filled with oil. Spontaneous oil imbibition was not recorded in any of the four cores, thus measured Amott-Harvey indices were 0.27 ($LS11_{polymer}$) and 0.18 ($LS14_{polymer}$) in the polymer/oil systems, both comparable to previous cycle, i.e. no further change in wettability. The Amott-Harvey indices in the polymer/oil systems correspond to weakly water-wet conditions. Measured I_{AH} for the glycerol/oil systems were also comparable to previous cycle: 0.09 in $LS17_{glycerol}$ and 0 in $LS18_{glycerol}$, corresponding to near neutral wet, or weakly water-wet conditions. Figure 4.32 shows development in saturation as a function of dimensionless time during the fifth cycle of spontaneous imbibition of aqueous phase in cores $LS11_{polymer}$, $LS14_{polymer}$, $LS17_{glycerol}$, and $LS18_{glycerol}$.

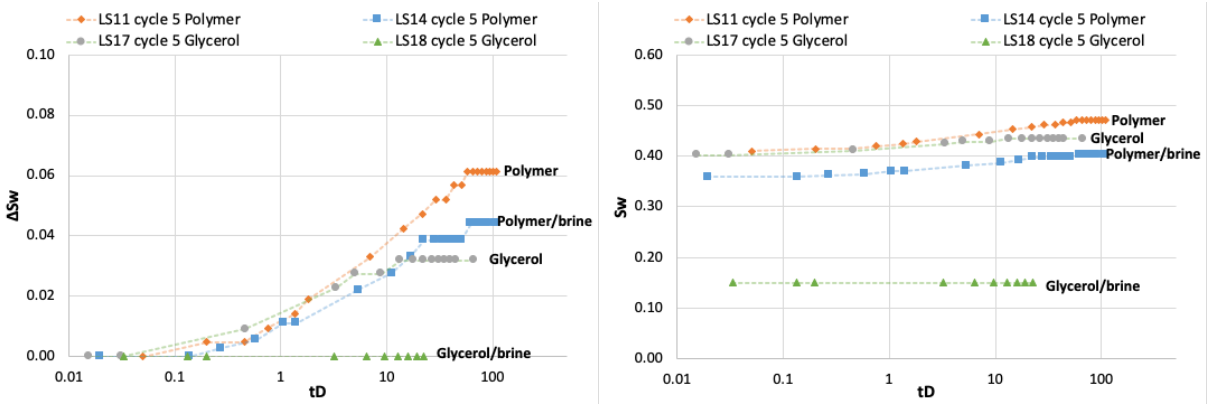

Figure 4.32: Increase in water saturation (ΔS_w) as a function of dimensionless time during the fifth cycle of spontaneous imbibition of aqueous phase in cores $LS11_{polymer}$, $LS14_{polymer}$, $LS17_{glycerol}$, and $LS18_{glycerol}$ to the left, and water saturation as a function of dimensionless time to the right. Brine injection was performed after polymer/glycerol injection in previous cycle in cores marked with polymer/brine or glycerol/brine. The curves are scaled for viscosity according to equation (2.4).

4.5.2.1 Comparison of polymer/oil systems, glycerol/oil systems and brine/oil systems

Increase in water saturation as a function of dimensionless time, for all five Amott-Harvey cycles in cores $LS11_{polymer}$, $LS14_{polymer}$, $LS17_{glycerol}$, and $LS18_{glycerol}$, is shown in Figure 4.33, and water saturation as a function of dimensionless time for all five Amott-Harvey cycles is shown in Figure 4.34. As can be seen in Figure 4.34, the water saturation in core $LS18_{glycerol}$, where brine was injected after glycerol injection, was ~20% lower than the water saturation in core $LS17_{glycerol}$ where brine was not injected. A decrease in water saturation in the same order as in $LS18_{glycerol}$ was not observed in $LS14_{polymer}$, where brine was injected after polymer injection. This supports the theory of glycerol being diluted by injected brine, leading to higher volumes of water being displaced during oil injection (thereby lower water saturation). Presumably the polymer adsorbed along the pore walls and was therefore not completely removed from the core during brine injection in $LS14_{polymer}$.

In $LS11_{polymer}$, the volume of polymer imbibed increased for each performed Amott-Harvey cycle, and the core wettability gradually changed from preferentially oil-wet (SI of oil) to weakly water-wet (SI of aqueous phase and no SI of oil). In $LS14_{polymer}$, polymer was displaced by brine before oil imbibition in Amott-Harvey cycles three, four, and five. The volumes of polymer imbibed did not increase in $LS14_{polymer}$ after the third Amott-Harvey cycle. This suggests that the injected brine displaced parts of the polymer and prevented adsorption of additional polymer in the core. Adsorption of a "water-wet" polymer layer along the pore walls is a likely reason for the change in wettability in the polymer/oil systems. All cores, except

$LS18_{glycerol}$, obtained higher Amott-Harvey indices after five Amott-Harvey cycles compared to the Amott-Harvey indices measured in brine/oil systems (section 4.4).

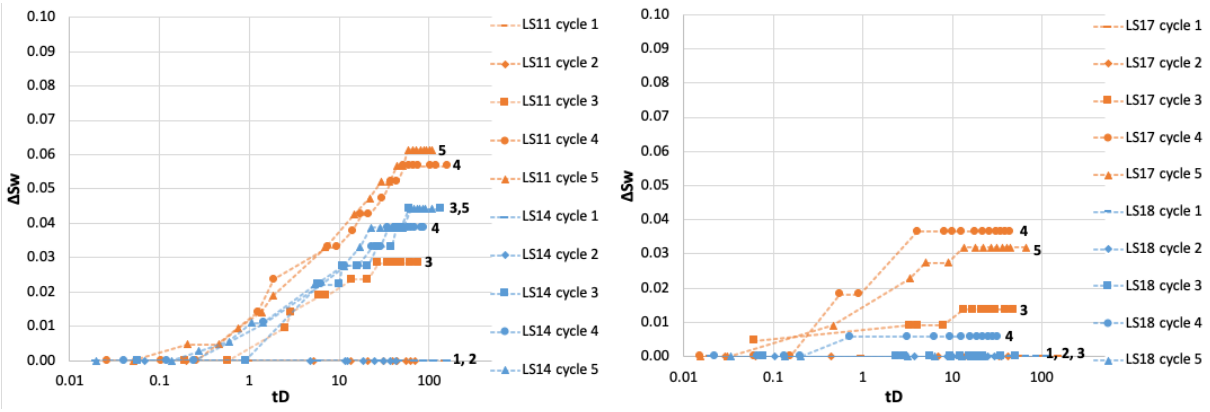

Figure 4.33: Increase in water saturation (ΔS_w) as a function of dimensionless time during five cycles of spontaneous imbibition of aqueous phase for $LS11_{polymer}$ and $LS14_{polymer}$ to the left, and increase in water saturation (ΔS_w) as a function of dimensionless time during five cycles of spontaneous imbibition of aqueous phase for $LS17_{glycerol}$ and $LS18_{glycerol}$ to the right. The curves are scaled for viscosity according to equation (2.4).

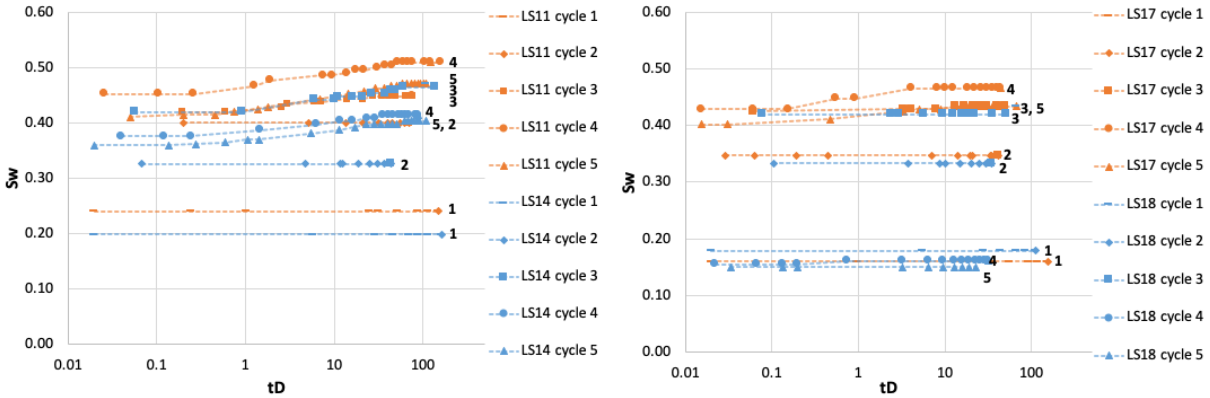

Figure 4.34: Water saturation as a function of dimensionless time during spontaneous imbibition of aqueous phase in $LS11_{polymer}$ and $LS14_{polymer}$ to the left, and water saturation as a function of dimensionless time for $LS17_{glycerol}$ and $LS18_{glycerol}$ to the right. The curves are scaled for viscosity according to equation (2.4).

One core with polymer in the aqueous phase and one core with brine in the aqueous phase was selected to compare the SI curves during five Amott-Harvey cycles. The core with polymer in the aqueous phase ($LS11_{polymer}$) is now called "Polymer" and the core with brine in the aqueous phase (LS12) is called "Brine". Saturation development as a function of dimensionless time is shown in Figure 4.35. Spontaneous imbibition of water was first observed in the fourth Amott-Harvey cycle in the brine core, while imbibition of aqueous phase (polymer) was observed for the first time already in the third cycle in the polymer core, i.e. the polymer changed the

wettability in the core quicker than brine. The volume of aqueous phase imbibed in the polymer core increased to the double from the third to the fourth Amott-Harvey cycle, and increased further in the fifth cycle. Increase in SI of brine was not observed between the fourth and fifth cycle. This means that not only did the polymer change the wettability in the core plug quicker than brine, polymer also changed the wettability towards stronger water-wet conditions.

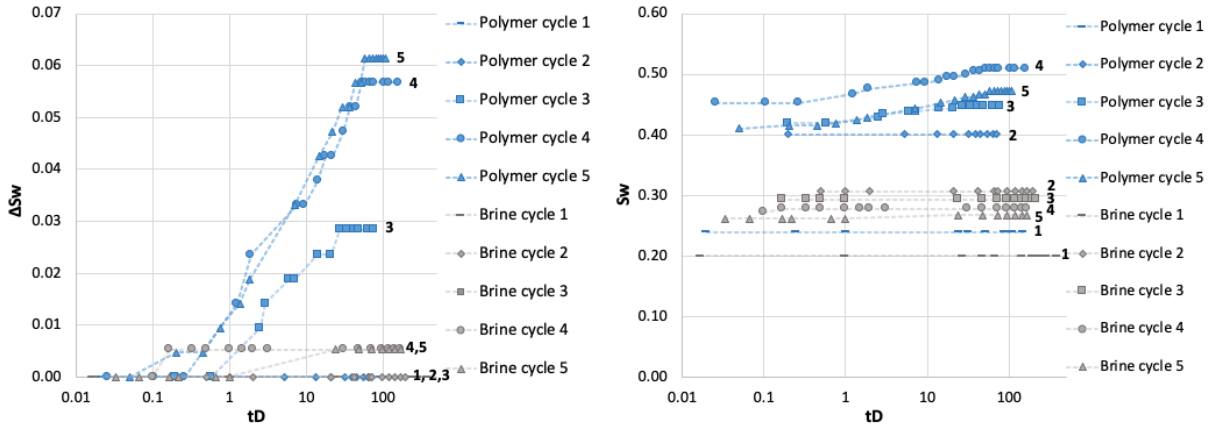

Figure 4.35: Increase in water saturation and water saturation as a function of dimensionless time during five Amott-Harvey cycles for one core with polymer in the aqueous phase and one core with brine in the aqueous phase. The curves are scaled for viscosity according to equation (2.4).

Figure 4.36 shows Amott-Harvey indices during five Amott-Harvey cycles for cores $LS11_{polymer}$, $LS14_{polymer}$, $LS17_{glycerol}$, and $LS18_{glycerol}$. The blue shaded area in the figure represents the Amott-Harvey indices for brine/oil systems (results from section 4.4). The highest increase in Amott-Harvey index was in the two cores saturated with polymer. It is conceivable that the polymer displaced the oil along the pore walls in the oil-wet pores and that a "water-wet" polymer layer adsorbed along the pore walls changed the wettability towards stronger water-wet conditions. The Amott-Harvey index did not increase after the third Amott-Harvey cycle in $LS14_{polymer}$ where brine was injected after polymer injection, while I_{AH} increased for core $LS11_{polymer}$ where brine was not injected, i.e. the brine injection prevented additional polymer to adsorb to the mineral surface.

<u>Important observations:</u>

When polymer constituted the aqueous phase, spontaneous imbibition started 1-2 cycles earlier compared to cores saturated with brine (section 4.4). Polymer altered the measured wettability from oil-wet to water-wet conditions quicker than brine, and towards stronger water-wet conditions. After completion of five Amott-Harvey cycles, polymer/oil systems obtained

Amott-Harvey indices of 0.18-0.27, compared to glycerol/oil systems (0-0.09) and brine/oil systems (0.01-0.03). This high increase in I_{AH} suggests that the presence of polymer in the pore space contribute to a wettability reversal from slightly oil-wet towards weakly water-wet conditions. This has also been reported in previous publications (Barreau et al., 1997, Elmkies et al., 2001, Juarez-Morejon et al., 2017), but without a baseline for comparison. The work in this thesis is the most thorough study on this topic so far.

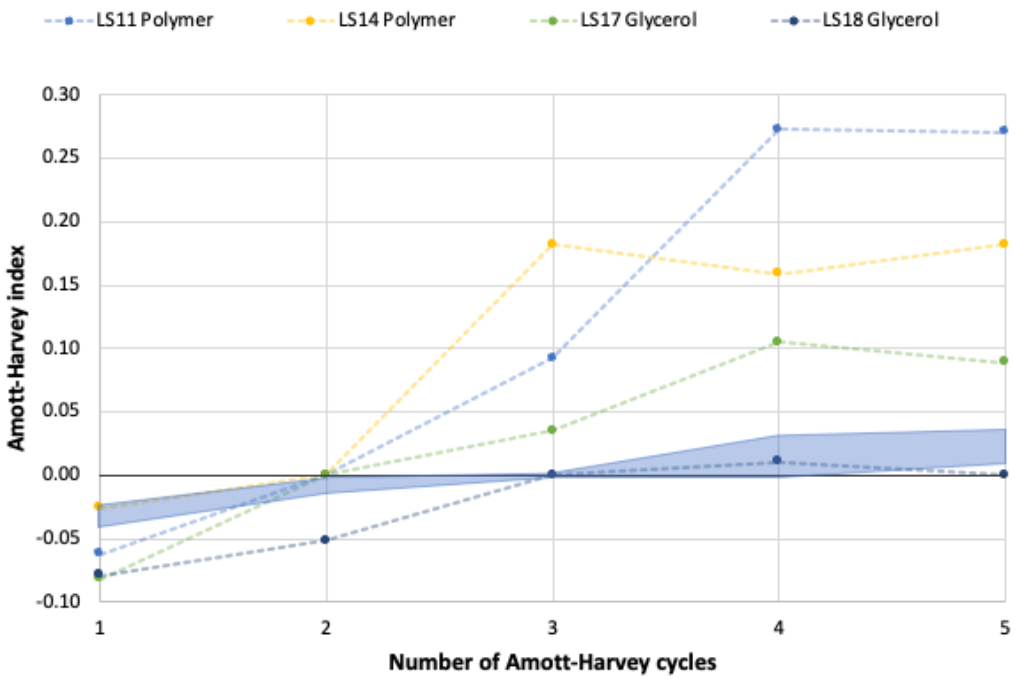

Figure 4.36: Amott-Harvey indices during five Amott-Harvey cycles for the polymer/oil systems ($LS11_{polymer}$ and $LS14_{polymer}$) and the glycerol/oil systems ($LS17_{glycerol}$ and $LS18_{glycerol}$). The blue shaded area represents the change in Amott-Harvey indices for the cores where brine constituted the aqueous phase during five cycles.

4.5.2.2 End-point relative permeability and disproportionate permeability reduction

End-point relative permeabilities were measured after each forced injection to investigate disproportionate permeability reduction (DPR) effects in the cores saturated with polymer. The end-point relative permeabilities for each Amott-Harvey cycle are listed in Table 4.5. End-point relative permeabilities of water and oil as function of water saturation for cores $LS11_{polymer}$, $LS14_{polymer}$, $LS17_{glycerol}$, and $LS18_{glycerol}$ when the cores were saturated with brine/oil are shown in Figure 4.37. The end-point relative permeabilities of water ($k_{rw,or}$) ranged from 0.32-0.40 when brine constituted the aqueous phase. The end-point relative permeabilities of oil ($k_{ro,iw}$) were in the same range, from 0.29-0.40, which indicates near neutral wet conditions according

to Craig´s rules of thumb (described in section 2.3.3). The end-point relative permeability values were in the same range as for the dynamically aged cores in section 4.4.

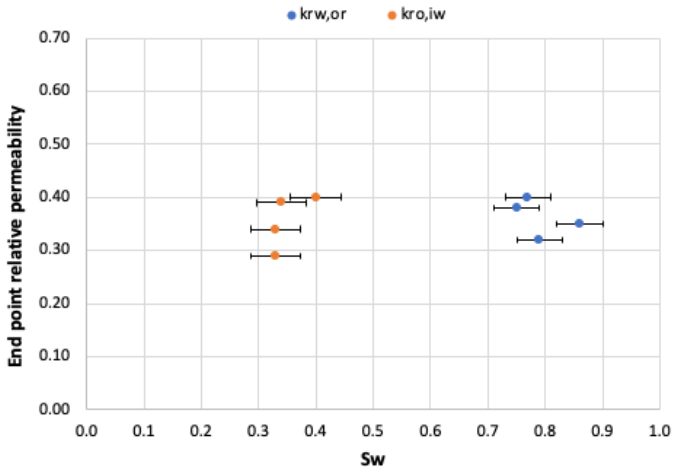

Figure 4.37: End-point relative permeabilities of water (krw,or) and oil (kro,iw) as a function of water saturation for LS11$_{polymer}$, LS14$_{polymer}$, LS17$_{glycerol}$, and LS18$_{glycerol}$ when the cores were saturated with brine/oil. Error bars for the water saturations are included.

End-point relative permeabilities of aqueous phase and oil as a function of water saturation when the cores were saturated with polymer/oil and glycerol/oil are shown in Figure 4.38 and Figure 4.39 shows end-point relative permeabilities of water and oil as a function of water saturation when the cores were saturated with adsorbed polymer/brine/oil and glycerol/brine/oil. In polymer/oil saturated cores LS11$_{polymer}$ and LS14$_{polymer}$, $k_{rw,or}$ decreased to values between 0.06-0.23. When brine was injected to displace polymer in LS14$_{polymer}$, $k_{rw,or}$ decreased further to values between 0.01-0.02, which is 38 times lower than $k_{rw,or}$ with only brine/oil in the system. This suggests that the brine did not displace all the polymer inside the core. The polymer presumably adsorbed along the pore walls as a "water-wet" polymer layer, restricting the water flow. The end-point relative permeability of oil also decreased, to values between 0.09-0.13, when the cores were saturated with polymer/oil. $k_{ro,iw}$ was not impacted by brine injection to displace polymer in core LS14$_{polymer}$. This suggests the consistent decrease in $k_{ro,iw}$ in both cores was caused by the adsorption of polymer inside the cores. Polymer clusters larger than 5μm were removed from the polymer solutions, using a 5μm filter, before use. It is conceivable that smaller polymer clusters accumulated in small and intermediate pores and narrow pore throats, blocking parts of the pore network. The blocking of pores may have forced the oil to flow through the smallest pores in the core that previously were assumed to be fully water saturated. The similar $k_{ro,iw}$ achieved in polymer/oil and adsorbed

polymer/brine/oil systems indicates that viscosity contrast between polymer and oil did not cause the decrease in $k_{ro,iw}$, but blocking of pores by polymer can be a viable explanation. Water flowing through a "water-wet" polymer layer adsorbed along the pore walls and in smaller pores (now shared with oil), and oil flowing in the middle of the large and intermediate pores and in the smallest pores can explain the larger decrease in $k_{rw,iw}$ compared to $k_{ro,iw}$.

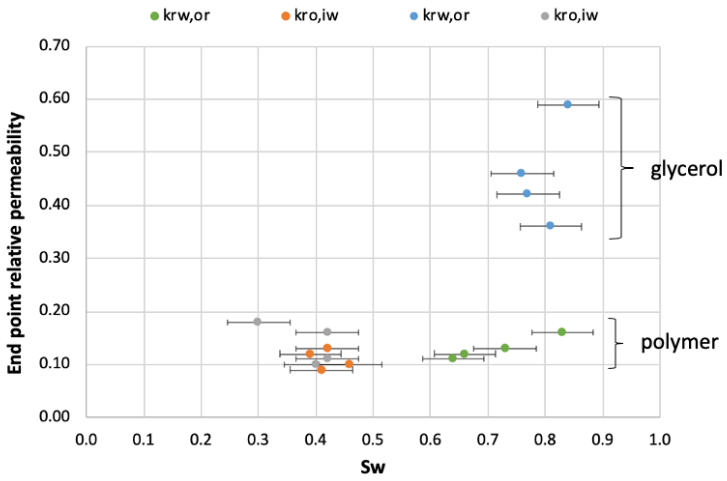

Figure 4.38: End-point relative permeabilities aqueous phase (krw,or) and oil (kro,iw) as a function of water saturation in cores saturated with polymer/oil and glycerol/oil. Error bars for the water saturations are included.

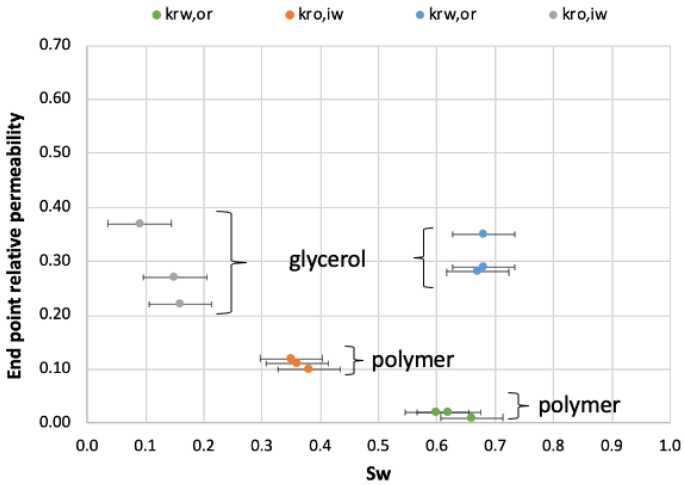

Figure 4.39:End-point relative permeabilities aqueous phase (krw,or) and oil (kro,iw) in the cores saturated with adsorbed polymer/brine/oil and glycerol/brine/oil as a function of water saturation. Error bars for the water saturations are included.

When glycerol/oil saturated cores LS17$_{glycerol}$ and LS18$_{glycerol}$, $k_{rw,or}$ was measured to values between 0.36-0.61, which was somewhat higher than previously measured values for brine/oil systems. The mobility ratio between aqueous phase and oil (M_{wo}) decreased from between 0.7-

1.2 with brine/oil to between 0.05-0.08 with glycerol/oil, i.e. the aqueous phase displaced the oil more easily when the viscosity was increased. The end-point relative permeability of oil decreased when the cores were saturated with glycerol/oil. The injection of brine to displace glycerol in core $LS18_{glycerol}$, however, increased $k_{ro,iw}$ back towards values similar to brine/oil systems. The mobility ratio between oil and aqueous phase (M_{ow}) increased from between 0.9 and 1.5 with brine/oil in the system to between 6.5-20 with glycerol/oil, and decreased back to initial values (brine/oil only) when brine was injected to remove the glycerol. Hence, the viscosity contrasts between glycerol and oil caused the decrease in $k_{ro,iw}$. When the glycerol was diluted by brine before oil injection, the aqueous phase was more easily displaced by the injected oil, leading to an increase in relative permeability.

Figure 4.40 shows the effects of brine injection after polymer and glycerol injection on end-point relative permeabilities of aqueous phase (krw,or) and oil (kro,iw) in polymer/oil systems and glycerol/oil systems. The figure shows a clear decrease in $k_{rw,or}$ both in polymer/oil systems and glycerol/oil systems when brine was injected after polymer and glycerol injection. Brine injection had no effect on $k_{ro,iw}$ in the polymer/oil systems, while decreasing water saturations and increasing $k_{ro,iw}$ can be seen for the glycerol/oil systems.

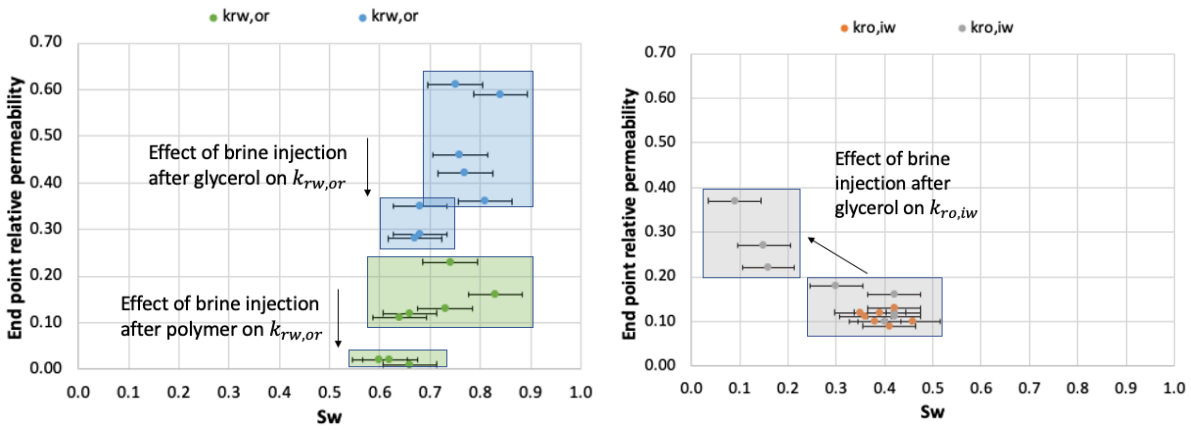

Figure 4.40: Effect of brine injection after polymer and glycerol injection on end-point relative permeabilities of aqueous phase (krw,or) and oil (kro,iw) in polymer/oil systems and glycerol/oil systems.

The uncertainties in saturations after completion of five Amott-Harvey cycles were calculated to be ±6% (ref. Appendix E). The irreducible water saturation in $LS18_{glycerol}$ decreased by 26-33% (from S_{iw}=0.42 to values between 0.09-0.16) when brine was injected after glycerol. This decrease in water saturation, which are 21-28% higher than the uncertainty, suggests that the

dilution of the glycerol inside the core made it easier to displace the aqueous phase by oil. This decrease in irreducible water saturation also explains the increase in $k_{ro,iw}$. The irreducible water saturation in core $LS14_{polymer}$ decreased by 4-7%, which are within the calculated saturation uncertainty.

Important observations

Several important observations were made when end-point relative permeabilities of cores saturated with polymer/oil, adsorbed polymer/brine/oil, glycerol/oil, and glycerol/brine/oil were compared:

- $k_{rw,or}$ decreased when polymer was introduced to the porous rock. Similarly, $k_{ro,iw}$ also decreased after polymer was introduced to the system. It is convenient that the injected polymer displaced the oil along the pore walls in the large and intermediate oil-wet pores and adsorbed along the pore walls as a "water-wet" polymer layer. Adsorption of thick polymer layers during polymer injection was reported by Grattoni et al. (2004) who studied the role of adsorption of polymer in micro-scale glass flow models. In addition, polymer clusters may have accumulated in small and intermediate pores and narrow pore throats, blocking parts of the pore network. The blocking of pores may have forced the oil to flow through the smallest pores in the core that previously were assumed to be fully water saturated. This can explain both the decrease in $k_{rw,or}$ and $k_{ro,iw}$.
- Disproportionate permeability reduction, where $k_{rw,or}$ is reduced more than $k_{ro,iw}$, was only observed when brine was injected after polymer injection in core $LS14_{polymer}$. Presumably, all the polymer was not displaced by the injected brine but adsorbed along the pore walls and restricted the water flow. In addition, it is likely that the polymer blocked parts of the pore network as described above. The water presumably flowed along the adsorbed, "water-wet", polymer layer and in the smaller pores (now shared with oil), while the oil flowed in the middle of the large and intermediate pores and in the smaller pores, which can explain the larger decrease in $k_{rw,or}$ than $k_{ro,iw}$.
- $k_{rw,or}$ increased when the cores were saturated with glycerol/oil compared to when the cores were saturated with brine/oil. The mobility ratio between aqueous phase and oil decreased from 0.70 with brine/oil to between 0.05-0.08 with glycerol/oil, i.e. the aqueous phase displaced the oil more easily when the viscosity was increased.

- $k_{ro,iw}$ decreased to similar values after injection of polymer and glycerol ($k_{ro,iw}$=0.12-0.16). Brine was injected to displace the viscous polymer/glycerol saturation, but $k_{ro,iw}$ did not change for the core saturated with polymer/oil ($LS14_{polymer}$). For the core saturated with glycerol/oil ($LS18_{glycerol}$), $k_{ro,iw}$ increased for each injection cycle, from 0.12-0.37. Similarly, the irreducible water saturation in $LS18_{glycerol}$ decreased by 26-33$\pm$5%. This large decrease in saturation was not expected. The increase in $k_{ro,iw}$, and simultaneous decrease in S_{iw} suggests that the glycerol inside the core was diluted by the injected brine, which made it easier to displace the aqueous phase during oil injection. Increase in $k_{ro,iw}$ and decrease in S_{iw} was not observed in $LS14_{polymer}$ when brine was injected, i.e. the decrease in $k_{ro,iw}$ in the cores containing polymer was not cause by viscosity contrasts between aqueous phase and oil, but by adsorption of a polymer layer along the pore walls and blocking of narrow pores and pore throats.

4.5.3 Water-wet baseline with polymer/oil and glycerol/oil

Polymer and glycerol were injected into three water-wet core plugs ($LS20_{polymer}$, $LS21_{polymer}$, and $LS22_{glycerol}$) to further investigate the separate effects on end-point relative permeabilities, without considering wettability alterations. The porosities were in range 21.8-25.6% and the permeabilities were in range 18.7-32.6mD. Brine constituted the aqueous phase in all three cores during two Amott-Harvey cycles. The aqueous phase was thereafter changed to polymer in $LS20_{polymer}$ and $LS21_{polymer}$, and glycerol in $LS22_{glycerol}$. In the fourth cycle, brine was injected directly after polymer injection in core $LS21_{polymer}$ to assess the effect on end-point relative permeabilities to water and oil. In $LS21_{polymer}$ and $LS22_{glycerol}$ only brine was injected to displace brine/adsorbed polymer and glycerol in the fifth cycle, and the effects on $k_{rw,or}$ and $k_{ro,iw}$ were assessed. An overview of aqueous fluid used and end-point relative permeabilities for each cycle are given in Table 4.6.

Table 4.6: Type of aqueous fluid, end-point water saturations and end-point relative permeabilities for water-wet baseline cores.

Core	LS20	LS21	LS22
Aqueous phase	Ekofisk brine	Ekofisk brine	Ekofisk brine
$k_{rw,or1}$	0.12	0.15	0.13
$k_{ro,iw1}$	0.51	0.55	0.46
Aqueous phase	Ekofisk brine	Ekofisk brine	Ekofisk brine
$k_{rw,or2}$	-	-	-
$k_{ro,iw2}$	-	-	-
Aqueous phase	Polymer	Polymer	Glycerol
$k_{rw,or3}$	0.08	0.15	0.58
$k_{ro,iw3}$	0.10	0.07	0.15
Aqueous phase	Polymer	Polymer/brine	Glycerol
$k_{rw,or4}$	0.12	0.01	0.25
$k_{ro,iw4}$	0.11	0.15	0.18
Aqueous phase	-	Ekofisk brine	Ekofisk brine
$k_{rw,or5}$	-	0.01	0.12
$k_{ro,iw5}$	-	0.17	0.49

Figure 4.41 shows end-point relative permeabilities of water and oil as a function of water saturation when brine/oil saturated the cores. $k_{ro,iw}$ ranged between 0.46-0.55 when the cores were saturated with brine/oil, and $k_{rw,or}$ ranged between 0.12-0.15. These values comply with Craig´s rules of thumb (described in section 2.3.3) for water-wet conditions, because the end-point relative permeabilities of water is less than 0.3 and the end-point relative permeabilities of oil is higher than for water.

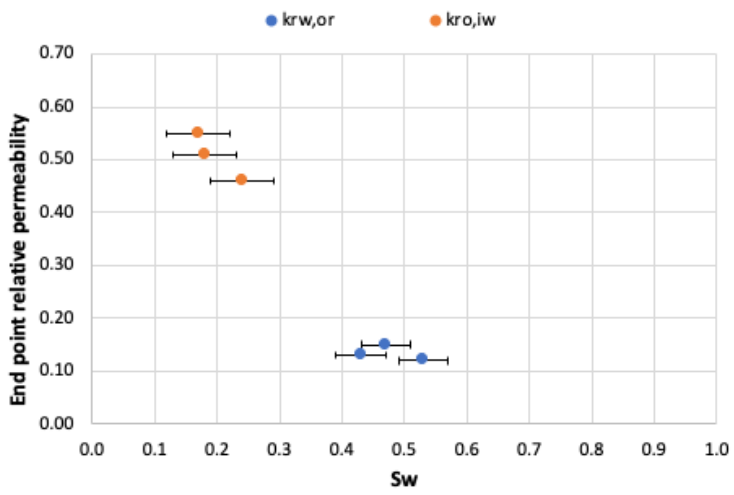

Figure 4.41: End-point relative permeabilities of water (krw,or) and oil (kro,iw) as a function of water saturation when brine/oil saturated the cores. Uncertainty bars for the saturations are included.

Figure 4.42 shows end-point relative permeabilities aqueous phase and oil as a function of water saturation when the cores were saturated with polymer/oil and glycerol/oil, and Figure 4.43 shows end-point relative permeabilities of aqueous phase and oil as a function of water saturation when the cores were saturated with adsorbed polymer/brine/oil and brine/glycerol/oil. In $LS20_{polymer}$ and $LS21_{polymer}$, saturated by polymer/oil, $k_{ro,iw}$ decreased to values between 0.07-0.11 (4-8 times lower than brine/oil systems), while $k_{rw,or}$ remained unchanged (values between 0.08-0.15). When brine was injected in core $LS21_{polymer}$ to displace the polymer from the pore network, $k_{rw,or}$ decreased to 0.01: 15 times lower than with brine/oil and polymer/oil. Adsorption of polymer on the mineral surface restricted both the water and oil flow. It is conceivable that accumulation of polymer clusters blocked small and intermediate pores, and that a polymer layer adsorbed along the pore walls in the core as described for the oil-wet cores, leading to a decrease in both $k_{rw,or}$ and $k_{ro,iw}$. This larger decrease in $k_{rw,or}$ than $k_{ro,iw}$, referred to as disproportionate permeability reduction (described in section 2.6.2), was also seen in the oil-wet core ($LS14_{polymer}$) when the system was saturated by brine/polymer/oil, but to a higher extent (38 times lower value). The end-point relative permeability of aqueous phase and oil remained constant when only brine/oil was injected in the last cycle.

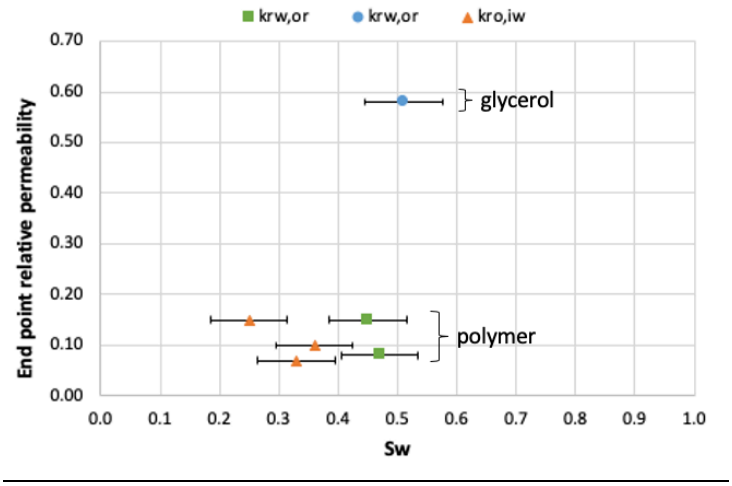

Figure 4.42: End-point relative permeabilities aqueous phase(krw,or) and oil (kro,iw) as a function of water saturation for cores saturated with polymer/oil and glycerol/oil. Uncertainty bars for the saturations are included.

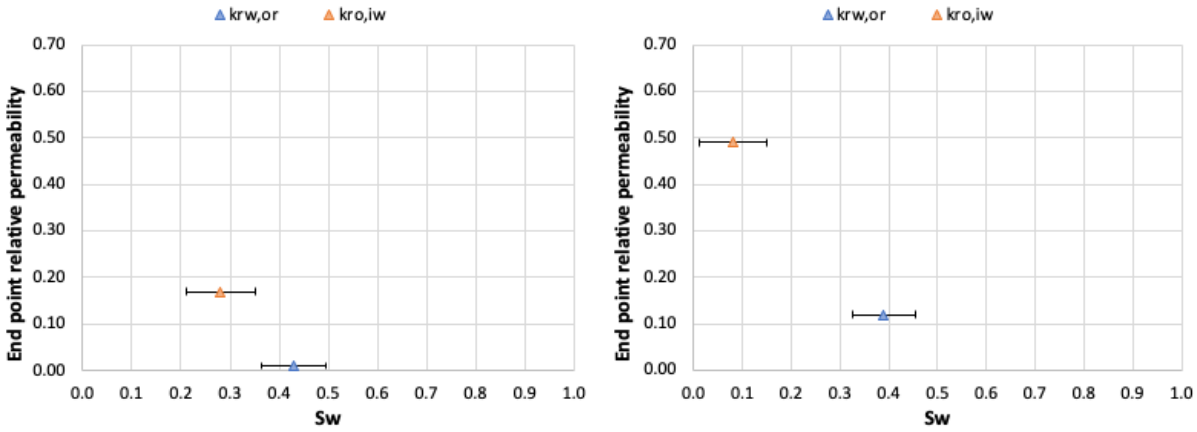

Figure 4.43: End-point relative permeabilities of oil (kro,iw) and water (krw,or) as a function of water saturation when adsorbed polymer/brine/oil saturated core $LS21_{polymer}$ to the left, and glycerol/brine/oil saturated core $LS22_{glycerol}$ to the right. Uncertainty bars for the saturations are included.

As in the oil-wet cores, $k_{rw,or}$ in core $LS22_{glycerol}$ increased (from 0.13 to 0.58) when glycerol/oil saturated the core compared to brine/oil. M_{wo} was reduced from 0.69 to values between 0.02-0.1, i.e. the aqueous phase displaced the oil more easily when the viscosity was increased. End-point relative permeability of oil decreased by a factor of 3, from 0.46-0.15, when the core was saturated with glycerol/oil. M_{ow} increased from 1.5 to values between 9 and 40, which explains the decrease in $k_{ro,iw}$. The end-point relative permeability of oil increased to the initial value (brine/oil only) when brine was injected in core $LS22_{glycerol}$, i.e. the viscosity contrasts between glycerol and oil caused the decrease in $k_{ro,iw}$.

Figure 4.44 shows effects of brine injection on $k_{rw,or}$ and $k_{ro,iw}$ in polymer/oil systems and glycerol/oil systems. $k_{rw,or}$ decreased for both the polymer/oil system and the glycerol/oil system when brine was injected to remove polymer/glycerol from the systems. Brine injection showed no effect on $k_{ro,iw}$ in the polymer/oil system, while $k_{ro,iw}$ increased to initial value (brine/oil only) when brine was injected into the glycerol/oil system. This indicates that the fluid flow, both aqueous phase and oil phase, behaved different when polymer adsorbed to the mineral surface of the rock. The decrease in $k_{ro,iw}$ when polymer was present in the system was not only caused by the viscosity contrasts between aqueous phase and oil, but by the adsorption of polymer along the pore walls and blocking of pores by polymer.

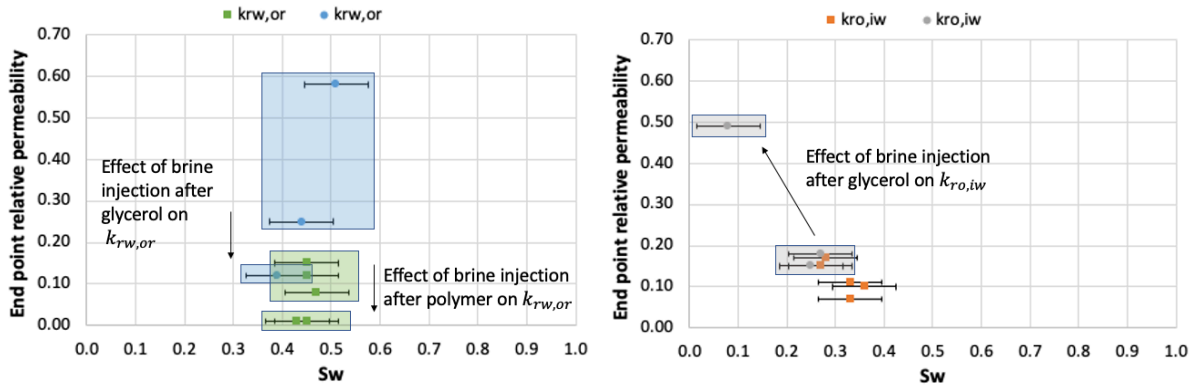

Figure 4.44: Effect of brine injection on end-point relative permeabilities of aqueous phase (krw,or) and oil (kro,iw) in polymer/oil systems and glycerol/oil systems.

Important observations

- $k_{rw,or}$ decreased when the oil-wet cores were saturated with polymer/oil compared to brine/oil. In water-wet cores $k_{rw,or}$ was not influenced by polymer injection. This suggests that a "water-wet" layer of polymer adsorbed along the pore walls, which altered the initial wettability in oil-wet cores towards water-wet. The aqueous phase was therefore transported along the water-wet polymer layer during injection instead of passing through the middle of the pores (oil-wet conditions), leading to a decrease in $k_{rw,or}$.
- Brine injection performed after polymer injection in water-wet core $LS21_{polymer}$ and oil-wet core $LS14_{polymer}$ prevented additional polymer adsorption in the core and additional changes in wettability. Disproportionate permeability reduction, where $k_{rw,or}$ is more reduced than $k_{ro,iw}$, was only observed when brine was injected after polymer.

Presumably, the decrease in $k_{rw,or}$ was caused by blocking of narrow pores and pore throats by polymer, and adsorption of polymer layers on the pore walls.

- Disproportionate permeability reduction was more pronounced in oil-wet cores, i.e. the decrease in $k_{rw,or}$ was higher. This is in accordance with previous publications which reported strongest DPR effect in intermediate wet, or oil-wet, cores (Seright et al., 2004, Liang et al., 1995, Nilsson et al., 1998).
- $k_{rw,or}$ increased in cores saturated with glycerol/oil compared to brine/oil. $k_{rw,or}$ decreased back towards the initial value (brine/oil only) when brine was injected to displace glycerol. In the oil-wet cores, M_{wo} decreased from between 0.7-1.2 with brine/oil to between 0.05-0.08 with glycerol/oil. In water-wet cores, M_{wo} decreased from 0.20 to 0.02 with glycerol/oil in the system, i.e. the aqueous phase displaced the oil more easily when the viscosity was increased.
- $k_{ro,iw}$ decreased for all cores after injection of polymer/glycerol, to values of 0.12-0.16 for oil-wet cores and 0.07-0.15 for water-wet cores. When brine was injected to displace polymer/glycerol, $k_{ro,iw}$ did not change for polymer/oil systems regardless of wettability ($LS14_{polymer}$ and $LS21_{polymer}$). For glycerol/oil systems ($LS18_{glycerol}$ and $LS22_{glycerol}$), $k_{ro,iw}$ increased when brine was injected. M_{ow} increased from 5 to values between 10-30 in the water-wet core when glycerol/oil saturated the core, and from values between 0.9-1.5 to values in range 6.5-20 in the oil-wet cores. M_{ow} decreased back to initial value (brine/oil only) when brine was injected after glycerol injection. This suggests that the initial decrease in $k_{ro,iw}$ when glycerol was introduced to the system was caused by viscosity contrasts between glycerol and oil.
- In polymer/oil systems the decrease in $k_{ro,iw}$ was not caused by viscosity contrasts between polymer and oil, because the brine injection showed no effect on $k_{ro,iw}$. Presumably the decrease in $k_{ro,iw}$ was caused by adsorption of a "water-wet" polymer layer along the pore walls in the large and intermediate pores, and blocking of small and intermediate pores in the pore volume, forcing the oil to flow through the smallest, water saturated pores.

4.6 In-situ PET-imaging

A quantitative analysis of the flooding experiments in core LS27, performed in the PET-scanner at Haukeland University hospital, will be presented in this section. The core plug was aged dynamically as described in section 3.5.1, and two subsequent Amott-Harvey cycles were performed before imaging. No spontaneous water imbibition was recorded during the two Amott-Harvey cycles, but oil imbibed spontaneously into the core. The measured Amott-Harvey indices were $I_{AH,1}$ =-0.21 and $I_{AH,2}$ =-0.06 (Table 4.7), corresponding to weakly oil-wet conditions. The core plug was brought to the Haukeland University hospital for flooding experiments in the PET-scanner as described in section 3.9.3. 3D-images from different time steps of the injections were used to qualitative describe the displacement fronts, and are presented together with production data and pressure graphs. Six consecutive injections were performed in following order: radioactive brine injection, oil injection, radioactive polymer injection, oil injection, radioactive brine injection and oil injection. Overview of injected fluids, injection rates, water saturations before and after each injection, change in water saturation after each injection, and end-point relative permeabilities after each injection in the PET-scanner are listed in Table 4.8. Pressure logs from all the injections are presented in Appendix F.

Table 4.7: Overview of water saturations and Amott-Harvey indices in the two Amott-Harvey cycles performed before the experiment in the PET-scanner. S_{iw} is irreducible water saturation and S_w is residual oil saturation, where the subscript describes the consecutive cycle.

Core	S_{iw}	$S_{w,1}$	$S_{iw,1}$	$I_{w,1}$	$I_{o,1}$	$I_{AH,1}$	$S_{w,2}$	$S_{iw,2}$	$I_{w,2}$	$I_{o,2}$	$I_{AH,2}$
LS27	0.20	0.85	0.45	0	0.21	-0.21	0.81	0.37	0	0.06	-0.06

Table 4.8: Overview of injected fluids, injection rates, water saturations before and after injection, change in water saturation (ΔS_w) after each injection, and end-point relative permeabilities for the experiment in the PET-scanner.

Injected fluid	Injection rate [ml/h]	S_w before injection	S_w after injection	ΔS_w	$k_{rw,or}/k_{ro,iw}$
$Brine_1$	15, 30	0.36	0.79	0.42	0.21
Oil_1	30	0.79	0.38	-0.41	0.10
$Polymer_1$	10, 15	0.38	0.82	0.45	0.10
Oil_2	15, 20, 30	0.82	0.36	-0.46	0.04
$Brine_2$	10, 15	0.36	0.71	0.35	0.04
Oil_3	10, 15, 30	0.71	0.36	-0.35	0.04

Brine injection to displace oil

During the first brine injection a total increase in water saturation of 0.42 was reached. The saturation development is shown in Figure 4.45 as a function of time. Figure 4.46 shows 3D-images of the core plug at different time steps during the first radioactive brine injection. There is a stronger signal in one side of the core plug, meaning that the displacement front moved faster in that part of the core. Water break through occurred after ~0.40 PV injected, and two-phase production (transient period) was recorded for 30 minutes, until an additional 0.40 PV of brine was injected. The end-point relative permeability of water was calculated to be 0.21.

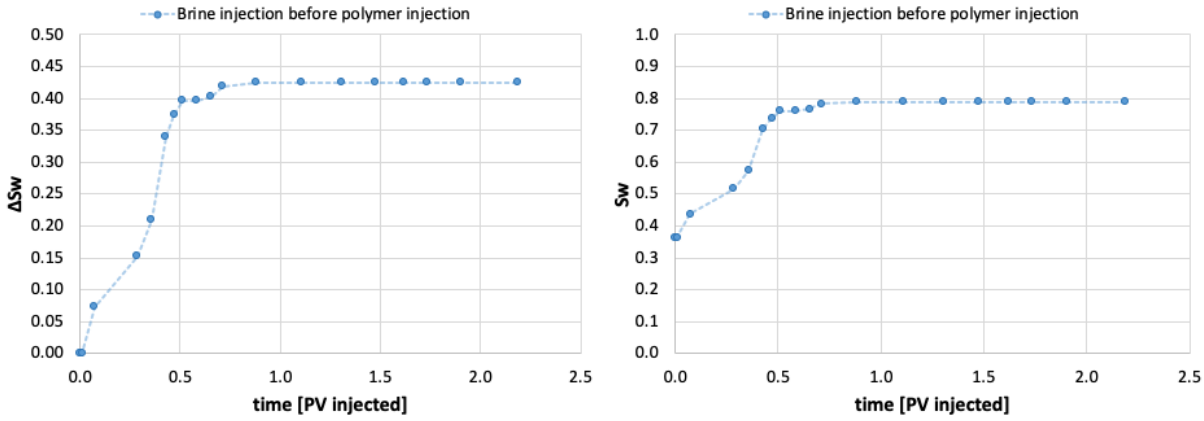

Figure 4.45: Increase in water saturation as a function of PV injected during the brine injection without polymer present in the core to the left, and water saturation as a function of PV injected to the right.

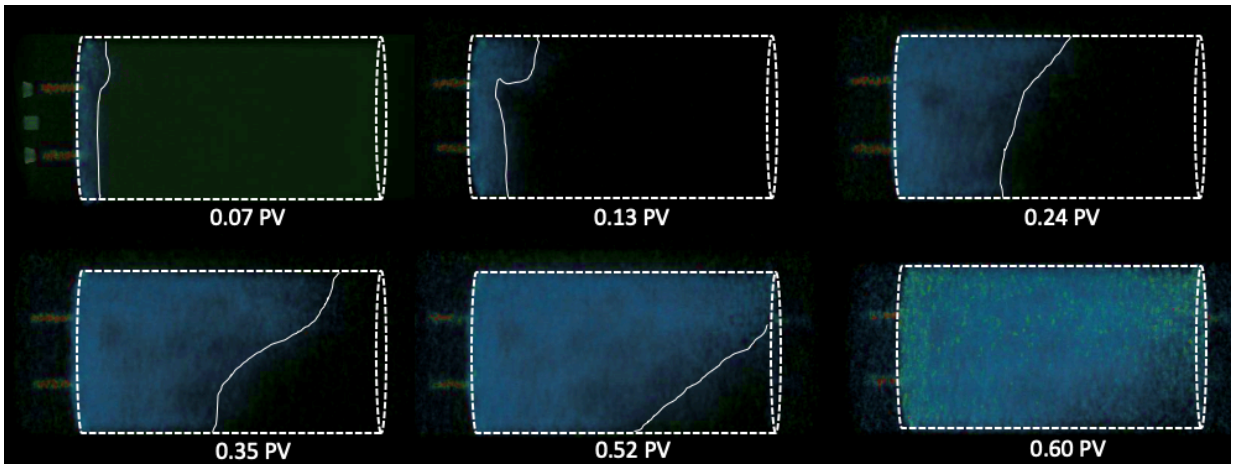

Figure 4.46: 3D-images at different time steps during the first radioactive brine injection in the PET-scanner.

Oil injection to displace brine

Oil injection was performed after the brine injection. A total decrease in water saturation of 0.41 was recorded. Figure 4.47 shows the saturation development as a function of time. Figure 4.48 shows 3D-images at different time steps during the first oil injection, where oil displaced the radioactive brine from the core. The displacement front appeared more uniform during the oil injection than during the brine injection. Oil break through occurred after ~0.37 PV injected, and two-phase production was recorded for 80 minutes, until an additional 2.2 PV was injected. A longer transient period during oil injection, with same injection rate as during the water injection, suggests that water displacement by oil was not significantly aided by capillary forces. Figure 4.49 shows differential pressure as a function of time during the brine and oil injections performed without polymer present in the core. The measured differential pressure during brine injection, with a flow rate of 30 ml/h, was between 1.4-1.9 bar, while the differential pressure was between 2.6-3.8 bar during oil injection using the same flow rate. End-point relative permeability of oil was calculated to be 0.10, 2.1 times lower than the end-point relative permeability of water. According to Craig´s rules of thumb this indicate neutral-wet wettability, because the end-point relative permeabilities of water and oil are in the same range, and the lower value for end-point relative permeability of oil suggests tendencies towards oil-wet. It is important to keep in mind that the system is not homogeneous, and it is conceivable that the core has mixed wettability. Oil flowing along the pore walls in the larger, oil-wet pores, and water flowing in the middle of the large pores and through the small, 100% water saturated, pores can explain the differences in differential pressure.

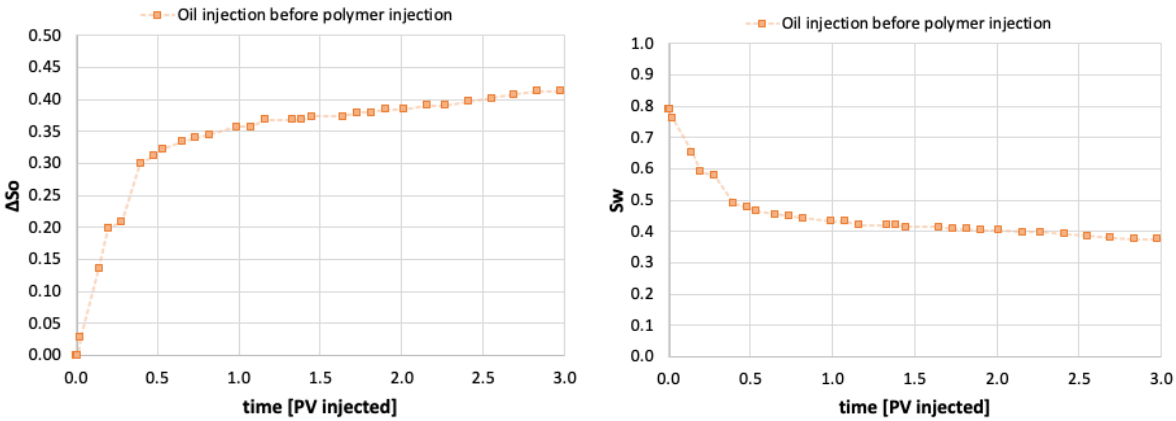

Figure 4.47: Increase in oil saturation as a function of PV injected during the oil injection without polymer present in the core to the left, and water saturation as a function of PV injected to the right.

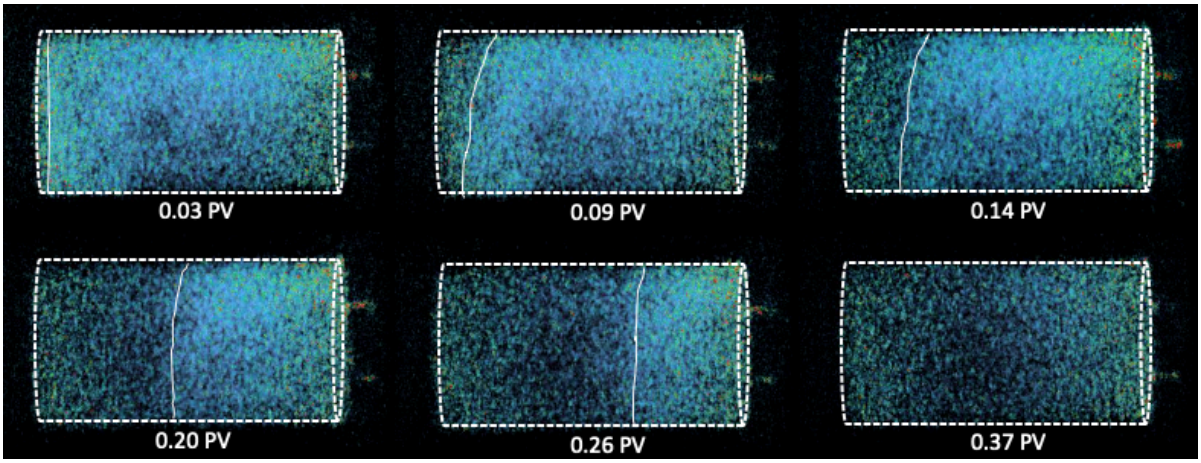

Figure 4.48: 3D-images at different time steps during the first oil injection in the PET-scanner, where oil displaces radioactive brine.

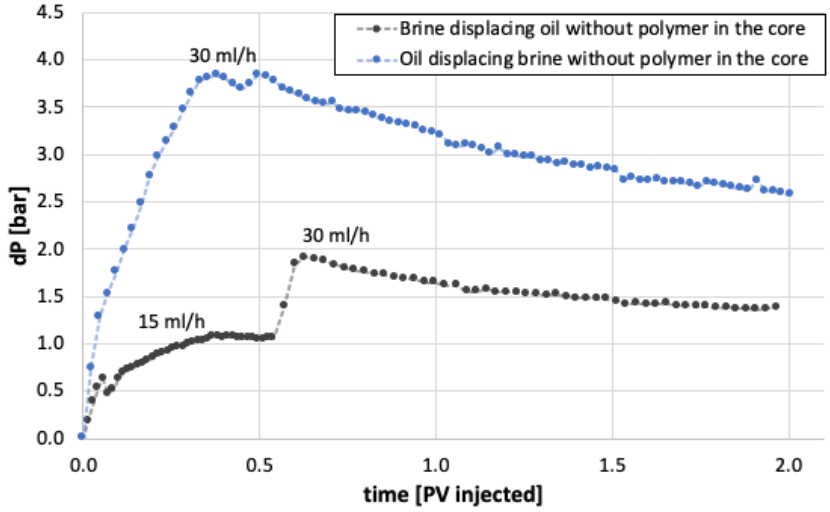

Figure 4.49: Differential pressure as a function of PV injected during the brine and oil injections performed before polymer injection. Injection rates are marked above the curves.

Polymer injection to displace oil

After brine and oil injections, a polymer solution with a viscosity of 9.1cP was injected into the core. The polymer solution was labelled by radioactive FDG and could be tracked by PET during injection. Figure 4.50 shows oil recovery and saturation development as a function of time during the polymer injection and the brine injection without polymer in the core. Oil recovery of 72% was recorded during the polymer injection, which was a 5% increase in oil recovery compared to the brine injection. The increase in oil recovery was caused by the improved mobility ratio between water and oil (M_{wo}) when polymer was used in the aqueous phase. M_{wo} was reduced from 1.7 during brine injection to 0.06 during polymer injection, which is a more favorable mobility ratio because the displacing fluid (polymer) is less mobile than the

displaced fluid (oil). Figure 4.51 shows differential pressure as a function of time during polymer injection. A differential pressure of 12.4 bar was measured with an injection rate of 15 ml/h. This increase in differential pressure compared to brine and oil injection was caused by the viscosity increase.

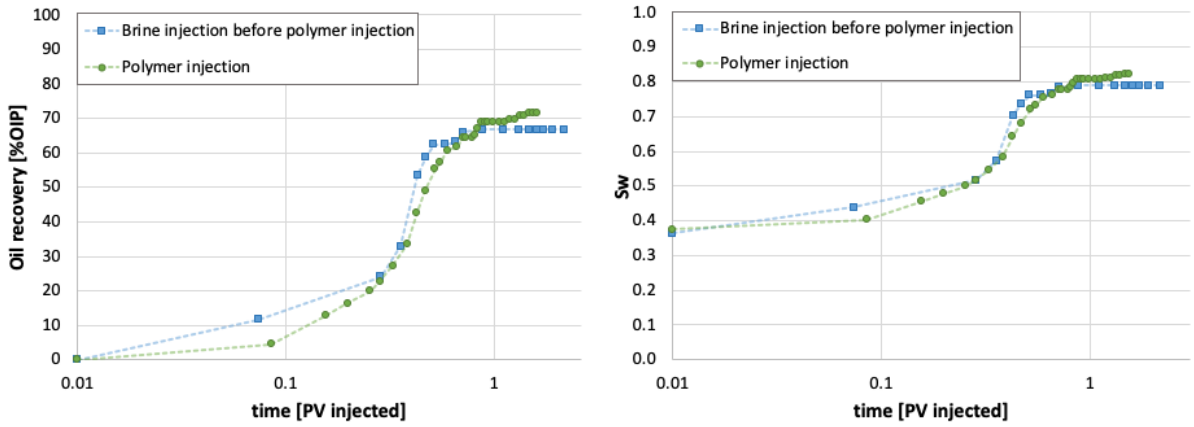

Figure 4.50: Oil recovery in percentage of oil in place (OIP) as a function of PV injected during the polymer injection and the brine injection before polymer injection to the left, and water saturation as a function of PV injected to the right.

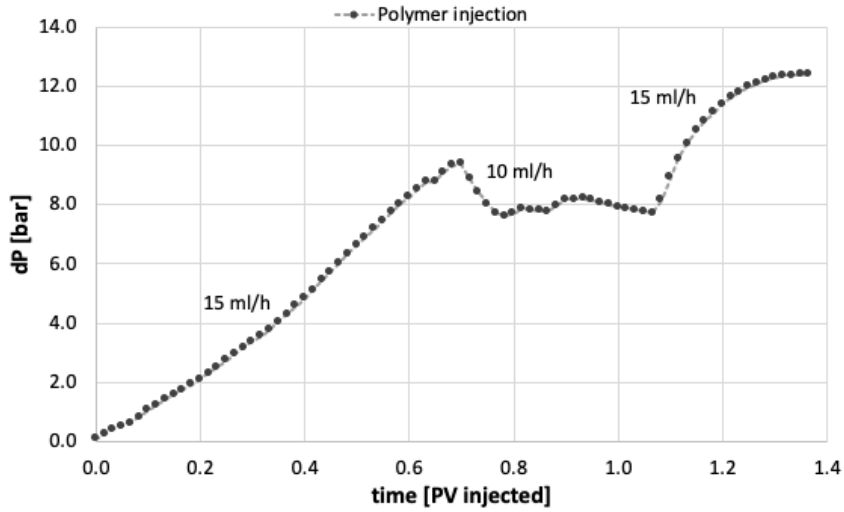

Figure 4.51: Differential pressure as a function of PV injected during the polymer injection. Injection rates are marked above the curve.

Figure 4.52 shows 3D-images of the core plug at different time steps during the radioactive polymer injection. As expected, a more uniform displacement front was obtained by polymer injection compared to brine injection. The water break through occurred after ~0.60 PV injected (compared to 0.40 PV injected during the first brine injection), i.e. polymer injection provides a more uniform displacement front, later water break through, and increase in oil

recovery. The transient period lasted for 15 minutes, until an additional of 0.30 PV of polymer was injected (0.10 PV less than during the brine injection due to the later break through). End-point relative permeability of polymer was calculated to be 0.10: 2.1 times lower than the end-point relative permeability of water during the first brine injection.

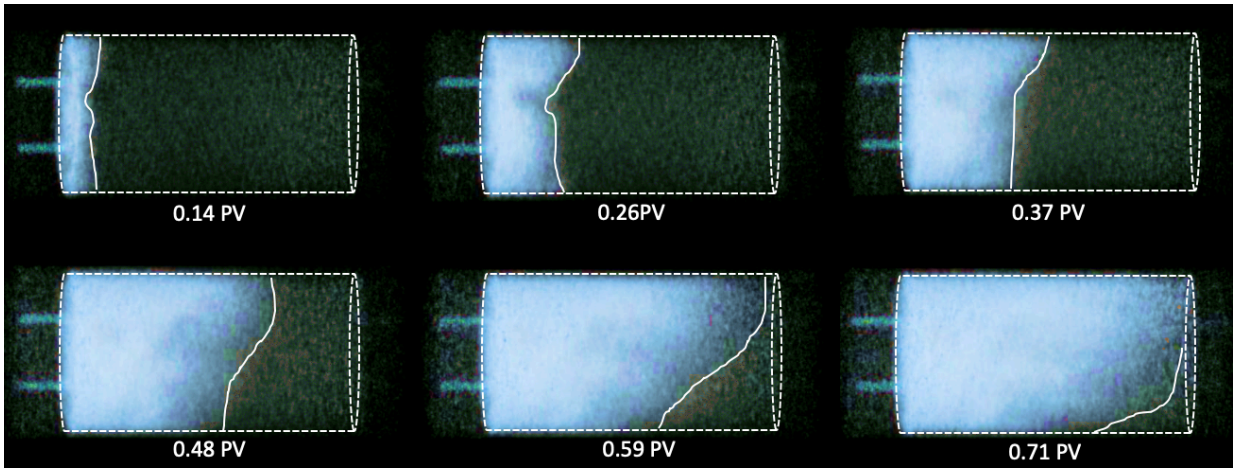

Figure 4.52: 3D-images at different time steps during the radioactive polymer injection in the PET-scanner.

Oil injection to displace polymer

A second oil injection was performed after the polymer injection. An overall decrease in water saturation of 0.46 was recorded, 5% more than during the first oil injection. This increase in volume of aqueous phase (polymer) displaced by injected oil can be explained by the higher water saturation reached during the polymer injection compared to the brine injection, which is the start saturation for the oil injection. Figure 4.53 shows the development in saturation as a function of time during the oil injections before and after polymer injection. Figure 4.54 shows 3D-images of the core plug at different time steps during the second oil injection, where oil displaced radioactive polymer from the core. The displacement front propagated faster in one side of the core plug, like observed in the first brine injection. Oil break through occurred after ~0.25 PV injected, 0.12 PV earlier than for the first oil injection. The transient period lasted for 66 minutes, until an additional 1.13 PV oil was injected. The increase in viscosity ratio between aqueous phase and oil increased from 1.2 to 10 when polymer was in the aqueous phase, which is a likely reason for the early break through.

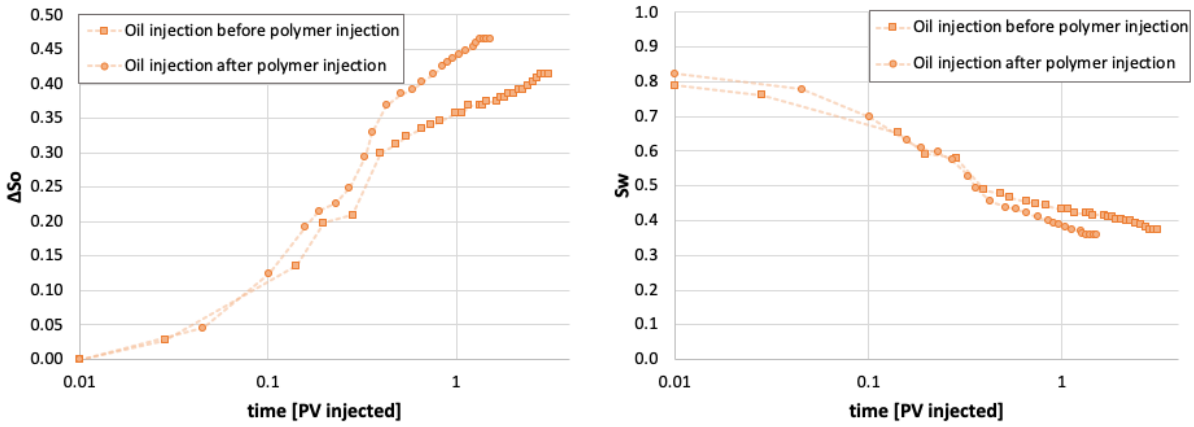

Figure 4.53: Increase in oil saturation as a function of PV injected during the oil injections before and after polymer injection the left, and water saturation as a function of PV injected to the right.

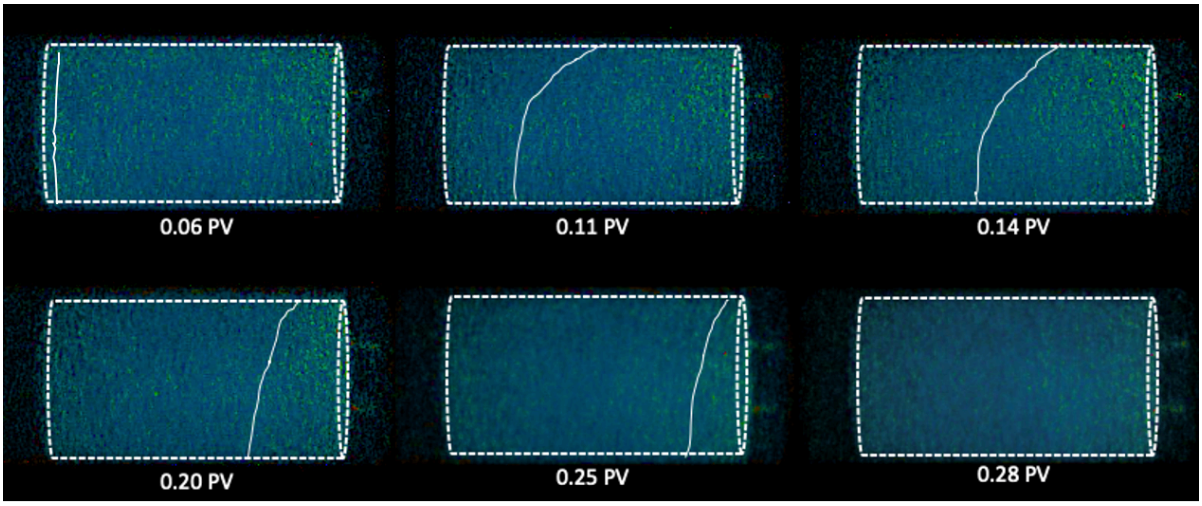

Figure 4.54: 3D-images of the core plug at different time steps during the second oil injection, where radioactive polymer was displaced by oil.

Differential pressure as a function of time during the oil injections before and after polymer injection is shown in Figure 4.55. The differential pressure increased during the oil injection when polymer saturated the core plug, compared to when brine saturated the core, which is natural because an aqueous fluid with higher viscosity (polymer) was displaced. The pressure decreased as polymer was produced, indicating less polymer in the core. Fluctuations in inlet and outlet pressure were also observed, suggesting that the pore volume available for fluid flow was not static: effluents visible in the clear production tubing stopped for a few seconds while both the inlet and outlet pressures increased. Movement of effluents in the production tubing was observed simultaneous to peaks in the measured pressure. The pressure swiftly decreased when production continued. This phenomenon was observed several times. Additional

production of polymer was also observed when the pump was started again after cylinder refill, and when the injection rate was increased. The pressure fluctuations may indicate that polymer blocked small pores and narrow pore throats in the core. The differential pressure increased, and the production "stopped", when the oil displaced trapped polymer from a narrow pore throat or a small pore. When the pressure peaked, the trapped polymer was presumably displaced out of the pore or pore throat, and the pressure swiftly decreased.

At the end of the oil injection, the differential pressure was between 6.6-7.5 bar using an injection rate of 30 ml/h, corresponding to 4.0-4.9 bar increase compared to oil the injection without polymer present in the core. This difference can not be explained only by viscosity contrasts between polymer and oil. It is conceivable that the injected polymer displaced the oil along the pore walls in the large and intermediate oil-wet pores and adsorbed to the pore walls as a "water-wet" polymer layer. Before use, the polymer solution was filtered using a 5μm filter. Thus, polymer clusters larger than 5μm was removed from the solution. Smaller polymer clusters could potentially block small and intermediate pores and narrow pore throats in the pore network, as the fluctuations in pressure indicated. Blocking of small and intermediate pores could force the oil to flow through the smallest pores in the core, that originally were assumed to be fully water saturated, which can explain the increase in differential pressure during oil injection. The end-point relative permeability of oil was calculated to be 0.04, 2.5 times lower than the end-point relative permeability of oil without polymer present in the core. The decrease in end-point relative permeability can also be explained by blocked pores in the pore network, which would decrease the absolute permeability of the core as well.

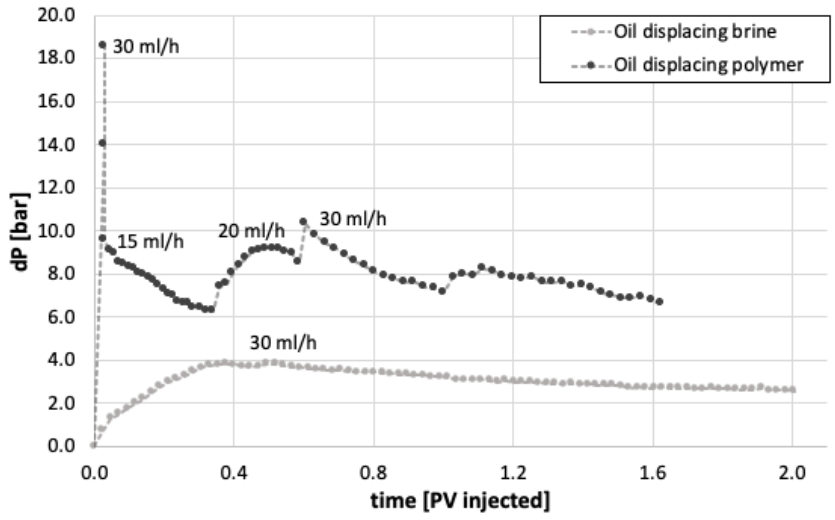

Figure 4.55: Differential pressure as a function of PV injected during the oil injections before and after polymer injection. Injection rates are marked above the curves.

Brine injection to displace oil with potential adsorbed polymer in the core

The oil recovery decreased from 72% (polymer injection) to 55% during the brine injection performed after polymer injection. The oil recovery also decreased compared to the brine injection without polymer in the core, i.e. there was an increase in trapped oil. Figure 4.56 shows the oil recovery and the saturation development as a function of time during the polymer injection and the brine injections before and after polymer injection. Highest oil recovery was recorded during the polymer injection, and the lowest recovery was recorded during the brine injection performed after the polymer injection. Figure 4.57 shows 3D-images of the core plug at different time steps during the second radioactive brine injection, performed after polymer injection. The signal is stronger in one side of the core, i.e. the displacement front moved faster in that part of the core. Similar was also observed during the first brine injection (performed before polymer injection), but water break through was recorded after ~0.25 PV injected, 0.15 PV earlier than during the brine injection without polymer present in the core.

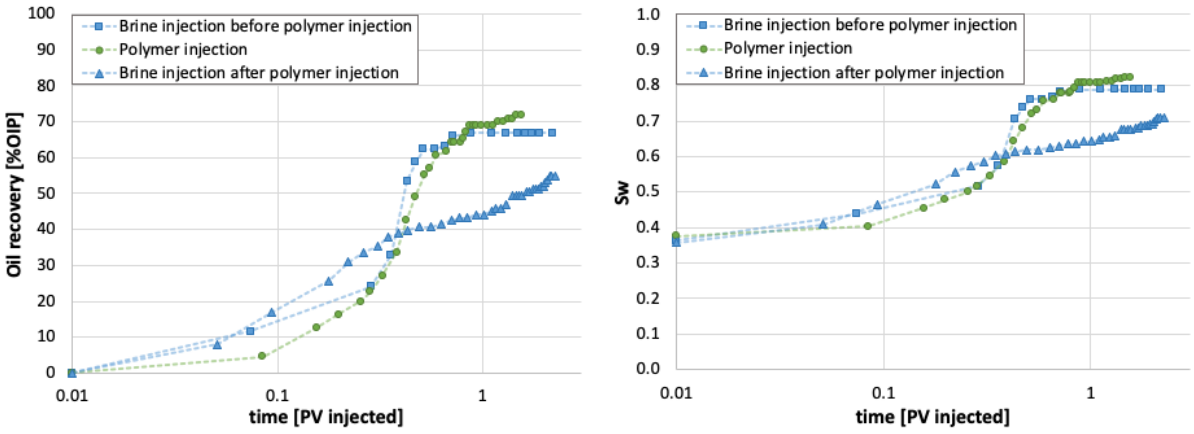

Figure 4.56: Oil recovery in percentage of oil in place (OIP) as a function of PV injected during the polymer injection and the brine injections performed before and after polymer injection to the left, and water saturation as a function of PV injected to the right.

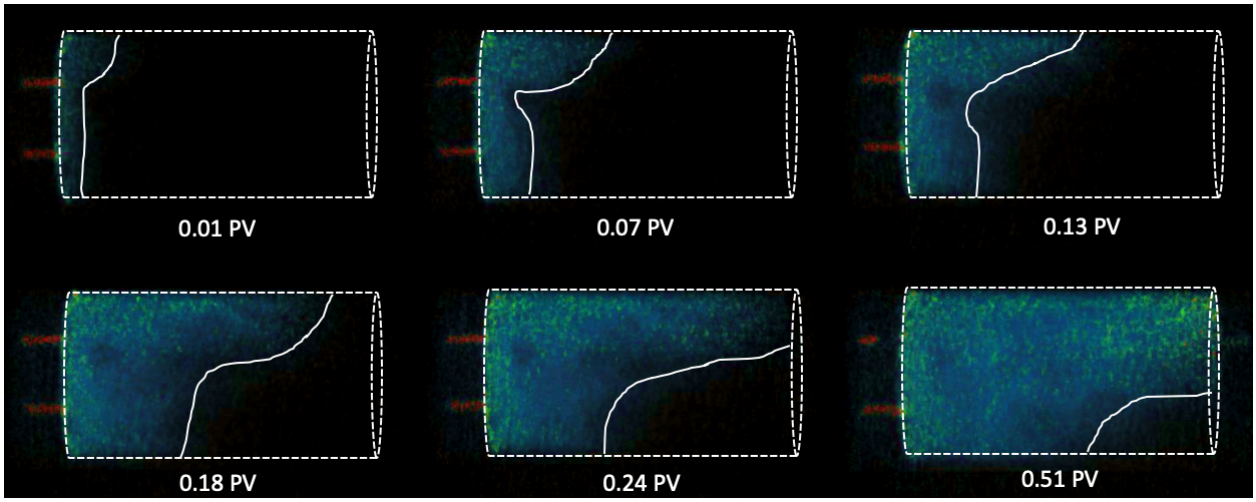

Figure 4.57: 3D-images of the core plug at different time steps during the second radioactive brine injection, performed after polymer injection.

Comparison of 3D-images at different time steps during the brine injections before and after polymer injection is shown in Figure 4.58. The displacement front propagated much faster during the brine injection after polymer injection than the brine injection before polymer injection, indicating that the pore volume available for water flooding decreased after polymer was injected into the core. This supports adsorption of polymer in the core plug, blocking pores and pore throats, leading to a decrease in available pore volume during flooding.

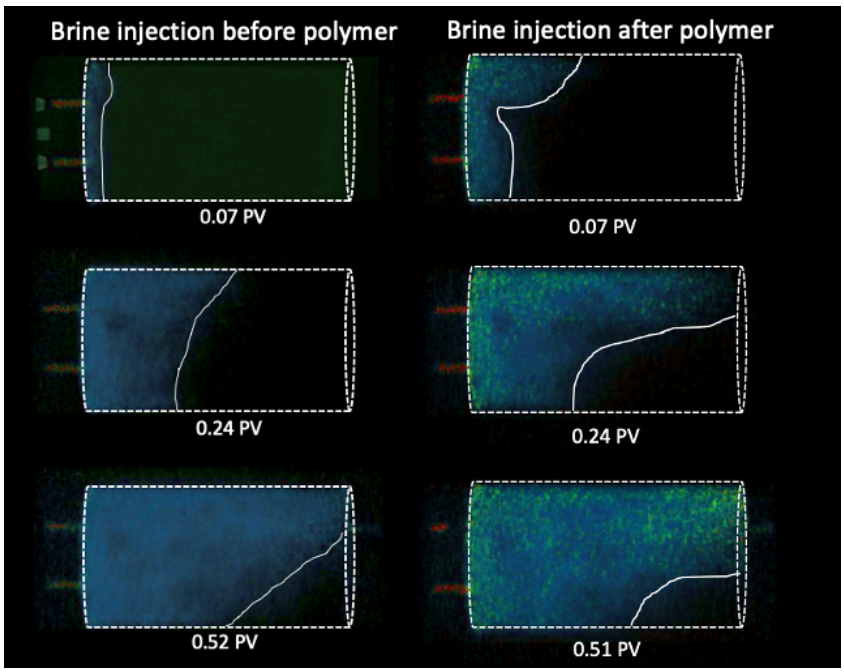

Figure 4.58: Comparison of 3D-images at different time steps during the brine injections performed before and after polymer injection.

Differential pressure as a function of time during the brine injections performed before and after polymer injection is shown in Figure 4.59. The pressure was decreasing as oil was produced. The differential pressure was stable during the brine injection without polymer in the pore volume, while during the brine injection performed after polymer injection, fluctuations in differential pressure can be seen. The fluctuations in pressure suggests that the pore volume available for fluid flow was not static. As suggested for the oil injection performed directly after the polymer injection, a possible explanation can be that the injected water (or oil) displaced polymer that were trapped in pores or pore throats, leading to an increase in pressure. When the polymer was displaced from the pore or pore throat the pressure swiftly decreased, and polymer was visible in the production tubing.

At the end of the brine injection performed after polymer injection, the measured differential pressure was 1.5-1.8 bar higher than the differential pressure at the end of the brine injection without polymer in the pore volume, even though the flow rate was three times lower. The end-point relative permeability of water was calculated to be 0.04, which is 5.3 times lower than the end-point relative permeability of water in the first brine injection. The end-point relative permeability of oil was 2.5 times lower during the oil injection when polymer/oil saturated the core compared to when brine/oil saturated the core. The increase in differential pressure during oil and water injections, and the decrease in end-point relative permeabilities of water and oil, suggest that the adsorption of polymer in the core plug restricted both the water and oil flow in the core. This was also seen in the PET-images: the front propagated faster during water and oil injections performed after polymer injection, indicating a smaller pore volume available for fluid flow. It is conceivable that the injected polymer solution displaced the oil from the pore walls in the large and intermediate oil-wet pores in the core and adsorbed to the pore walls as a "water-wet" polymer layer. In addition, polymer clusters may have accumulated in some of the smaller pores and pore throats in the core, leading to completely blocking of the pores. Blocking of small and intermediate pores could potentially force the oil to flow through the smallest pores in the core, which previously was assumed to be fully water saturated. The larger decrease in end-point relative permeability of water, and the higher differential pressure during brine injection than during oil injection, show that the water flow was more restricted than the oil flow. One explanation for this can be a change in wettability from oil-wet towards water-wet caused by the adsorbed polymer layer along the pore walls. Injected water presumably flowed through the adsorbed polymer layer along the pore walls and in the smallest pores (now shared with oil), while the oil flowed through the middle of the pores and in the smallest pores. The

larger decrease in end-point relative permeability of water is in agreement with the results in section 4.5, where the end-point relative permeability of water decreased more than the end-point relative permeability of oil after polymer was introduced to the core plug.

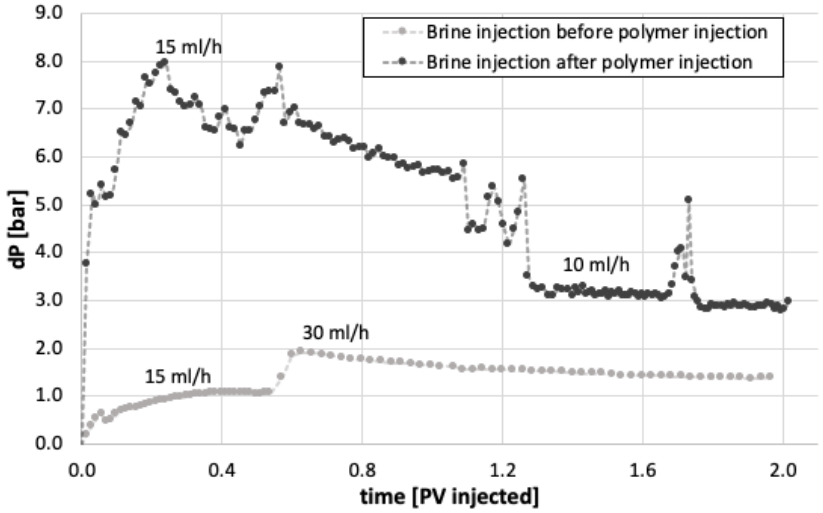

Figure 4.59: Differential pressure as a function of time during the brine injections performed before and after polymer injection. Injection rates are marked above the curves.

Oil injection to displace brine with potential adsorbed polymer in the core

During the third oil injection, a total decrease in water saturation of 0.35 was recoded, 11% less than during the oil injection performed directly after the polymer injection. The lower water saturation at oil injection initiation can partly explain this. PET-images from the oil and water injections after polymer injection suggested a decrease in pore volume available for fluid flow, which can also explain the decrease in recovery. Figure 4.60 shows the saturation development as a function of time during all three oil injections. Water recovery was highest when oil injection was performed directly after the polymer injection (second oil injection). Oil break through occurred after ~0.24 PV injected, similar to previous oil injection, and the transient period lasted until an additional of 0.49 PV of oil was injected (0.64 PV less than the second oil injection performed directly after polymer injection). Figure 4.61 shows 3D-images of the core plug at different time steps during the third oil injection, where radioactive brine, and possibly adsorbed polymer, were displaced by oil. Stronger signal can be seen in one side of the core, i.e. the displacement front propagated faster in one side of the core, as observed during previous oil and water injections.

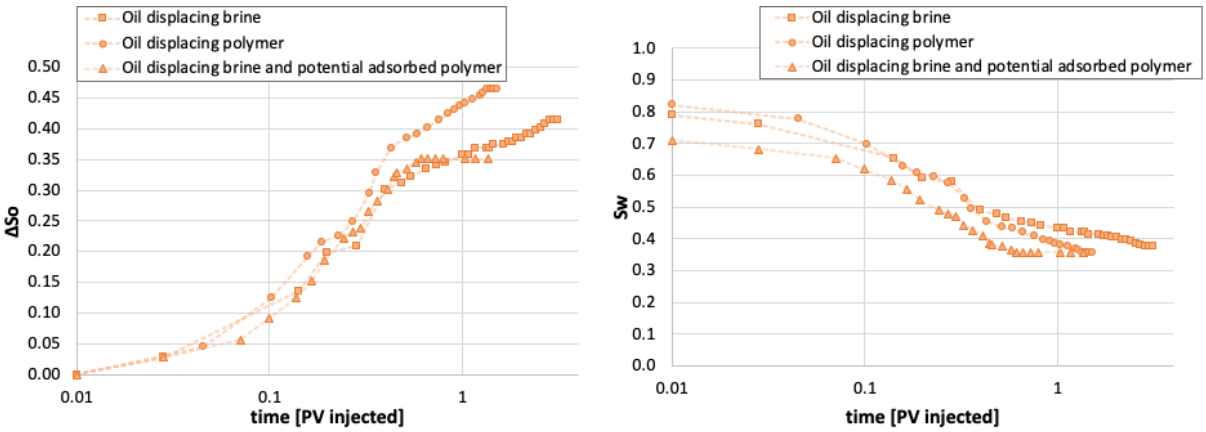

Figure 4.60: Increase in oil saturation as a function of PV injected during first, second and third oil injection to the left, and water saturation as a function of PV injected to the right. First oil injection was performed before polymer injection, while second and third oil injection were performed after polymer injection.

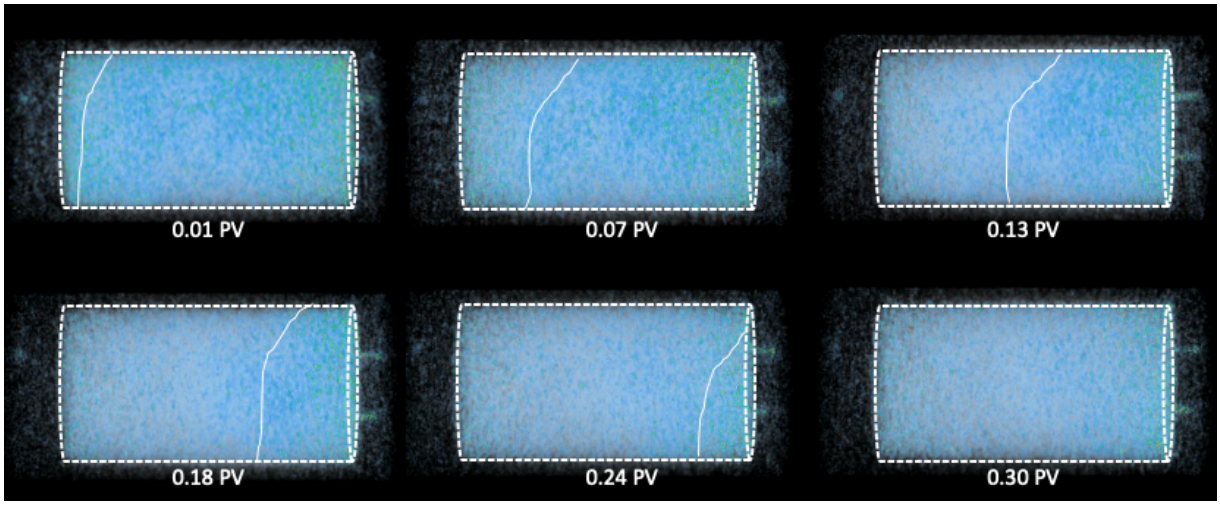

Figure 4.61: 3D-images of the core plug at different time steps during the third oil injection, where oil displaced radioactive brine.

Comparison of PET-images at different time steps when oil displaced brine (first oil injection), oil displaced polymer (second oil injection) and oil displaced brine and potential adsorbed polymer (third oil injection) is shown in Figure 4.62. The displacement front propagated much faster during the two oil injections performed after polymer injection. The viscosity ratios during the first and second oil injections were different due to the increased viscosity of aqueous phase, which can partly explain the faster propagation of the displacement front, but the viscosity ratios were equal in the first and third oil injections. This indicates that the pore volume available for fluid flow decreased as a result of the adsorption of polymer in the core.

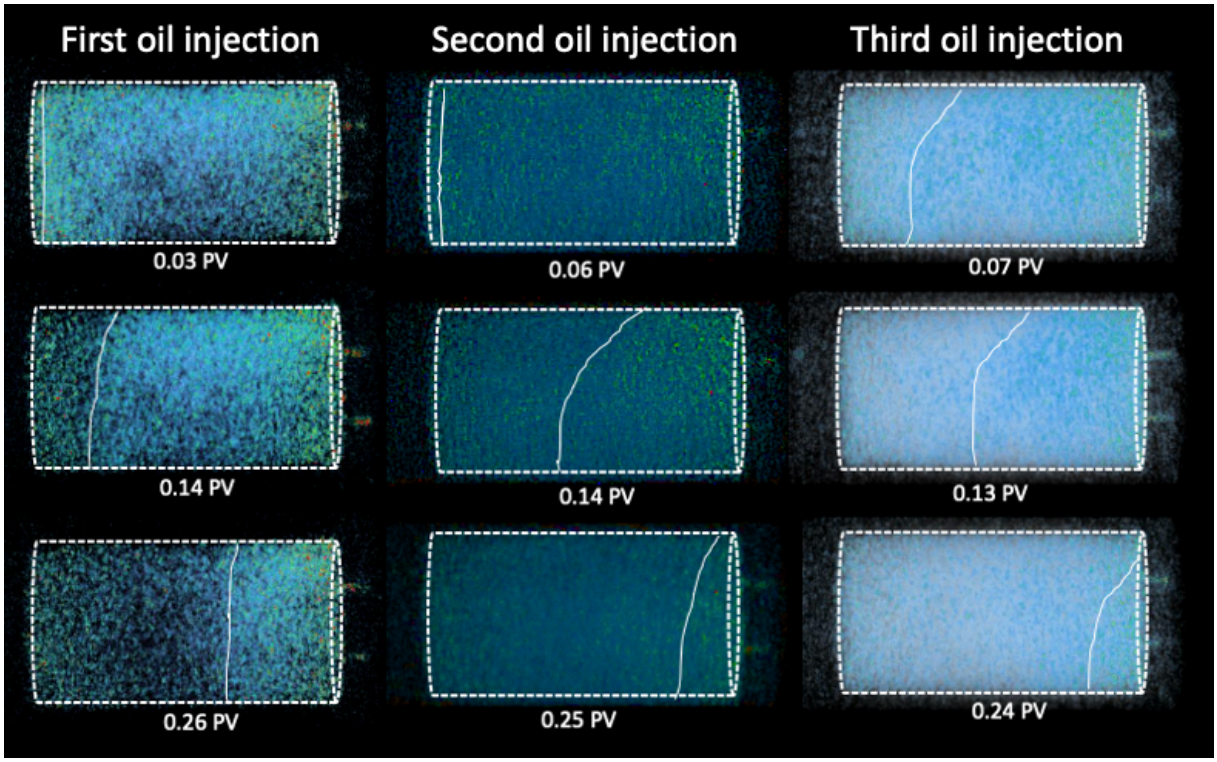

Figure 4.62: Comparison of 3D-images of the core plug at different time steps during the oil injection before polymer injection and the two oil injections after polymer injection.

Figure 4.63 shows differential pressure as a function of time when brine displaced oil and oil displaced brine with potential adsorbed polymer in the pore volume. The differential pressure was between 1.0-2.9 bar lower with the same flow rate when oil displaced brine compared to when brine displaced oil (both injections performed after polymer injection). This is opposite to the brine and oil injections without polymer present in pore volume, where the differential pressure was higher during oil injection than water injection for the same flow rate. The lower differential pressure during oil injection means that oil flowed more easily than water through the core plug after polymer injection. This may indicate that water flowed along the pore walls in the larger pores, due to a layer of "water-wet" adsorbed polymer, and through the smaller pores (now shared with oil), while oil flowed through the middle of the larger pores and in the smallest pores, due to blocking of small and intermediate pores by polymer, which would suggest a change in wettability towards water-wet conditions.

As observed in the second oil injection, effluents in the clear production tubing stopped for a few seconds while the pressure was increasing, and when the pressure peaked, either water or polymer was produced, and the pressure swiftly decreased. As previously suggested, an explanation for this can be that the oil displaced trapped polymer through narrow pore throats or small pores. Figure 4.64 shows differential pressure as a function of time when oil displaced

brine before polymer injection, oil displaced polymer and oil displaced brine after polymer injection. The differential pressures were higher at the same flow rates during the second and third oil injections, performed after polymer injection, compared to the oil injection performed before polymer injection. The differential pressure increase was 4.0-5.1 bar for the second and 3.2-3.6 bar for the third oil injection. This increase in differential pressure after polymer was injected into the core can be caused by blocking of pores by polymer, which forced the oil to flow through the smallest pores as previously suggested. The end-point relative permeability of oil was calculated to be 0.04, equal to the end-point relative permeability of water.

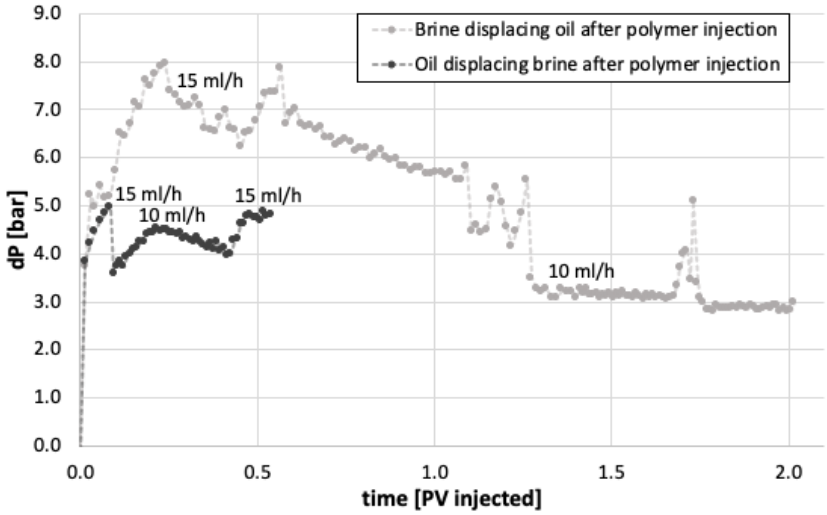

Figure 4.63: Differential pressure as a function of PV injected during oil displacement by brine and brine displacement by oil after polymer injection. Injection rates are marked above the curves.

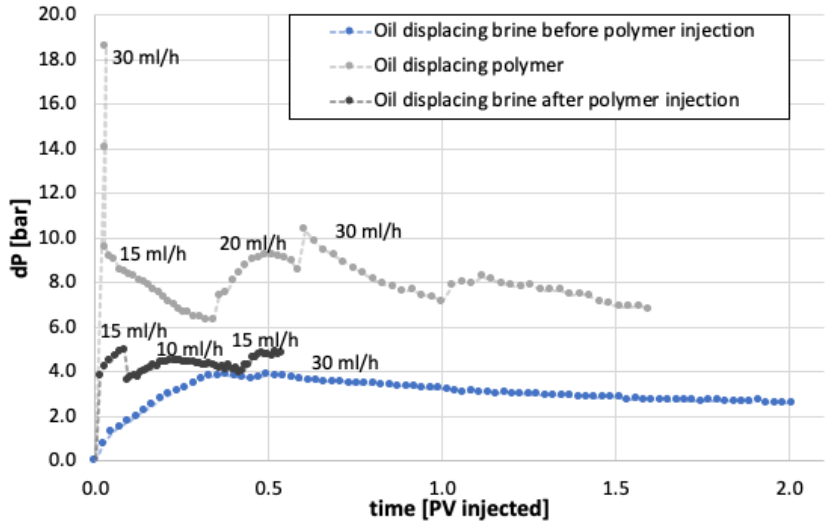

Figure 4.64: Differential pressure as a function of PV injected when oil displaced brine before polymer injection, oil displaced polymer and oil displaced brine after polymer injection. Injection rates are marked above the curves.

Important observations

Several observations were made during brine and oil injections before and after polymer injection, and during polymer injection:

1. Before polymer was introduced to the core plug, the differential pressure during brine injection was lower than during oil injection, and the transient period lasted for a longer period of time during oil injection than during brine injection. During the Amott-Harvey cycles performed before the PET-experiment, only oil imbibed spontaneously into the core plug. It is conceivable that the crude oil displaced the water in the large and intermediate pores in the core plug during aging, which altered the wettability in the large and intermediate pores to oil-wet, while the smallest pores remained water-wet and fully water saturated. This means that the core had mixed wet large wettability, i.e. the largest pores were oil-wet, while the smaller pores were water-wet.
2. Polymer injection provided a more uniform displacement front, with later break through, compared to oil and water injection, and an increase in oil recovey. This was expected because of the improvement of the mobility ratio (decrease from 1.7 to 0.06) by increasing the viscosity of the aqueous phase.
3. After polymer injection, the measured differential pressure was higher during water injection than during oil injection, opposite of before polymer was present in the core. This could indicate that the polymer displaced the oil from the pore walls of the oil-wet pores and adsorbed along the pore walls as a "water-wet" polymer layer. In addition, core transport properties changed after polymer was introduced to the core. Decrease in recovery and faster propagation of the displacement fronts during oil/brine and brine/oil displacements after polymer injection indicated a decrease in pore volume available for flooding. Blocking of small and intermediate pores and narrow pore throats can explain this. Injected water presumably flowed through the polymer layer and in the smallest pores, leading to increased pressure.
4. The end-point relative permeability of water decreased by a factor of 5.3 after polymer was introduced to the core, while the end-point relative permeability of oil decreased by a factor of 2.5. The adsorption of polymer restricted the water flow more than the oil flow. It is likely that polymer clusters accumulated in some of the pores and pore throats, leading to blocking of parts of the pore network. The blocking of small and intermediate pores may have forced the oil to flow through the smallest pores, which previously was assumed to be fully water-saturated. This can explain the decrease in $k_{ro,iw}$. The water

flowed presumably along the adsorbed, water-wet, polymer layer along the pore walls and in the smallest pores (now shared with oil), which can explain the larger decrease in $k_{rw,or}$. The larger decrease in $k_{rw,or}$ than $k_{ro,iw}$ is in good agreement with the results in section 4.5 where $k_{rw,or}$ also decreased more than $k_{ro,iw}$ after polymer injection. The results are also in agreement with previous publications (Nilsson et al., 1998, Liang et al., 1995, Zaitoun and Kohler, 1988, Al-Sharji et al., 1999, Willhite et al., 2002).

5 Conclusions and Future work

This section presents conclusions of the experimental work and suggestions for future work on this research topic.

5.1 Conclusions

- The heterogeneous nature of Edwards limestone core plugs was confirmed with CT, demonstrating a large range in pore and vug size distribution (27 – 300 μm). Pores smaller than the spatial resolution of the CT images were not captured.
- Nearly neutral or slightly oil-wet wettability preferences were obtained with both static and dynamic aging of Edwards limestone cores. The obtained wetting preference was stable for more than two full Amott-Harvey cycles, with small amounts of water imbibition observed after four cycles for dynamically aged cores. The wettability preference was more uniformly distributed using dynamic aging compared with static aging.
- Presence of polymer changed the wetting preference for oil-wet core plugs towards water-wet conditions quicker compared with using only brine: aqueous phase imbibition was observed in the third Amott-Harvey cycle for polymer/oil systems, compared with fourth or fifth cycle in brine/oil systems.
- For both water-wet and oil-wet cores the oil relative permeability was lower in polymer/oil systems compared with brine/oil systems. The oil relative permeability was not impacted by brine injection to remove polymer from the core in polymer/oil systems, while the oil relative permeability increased back to initial values (brine/oil only) in brine/oil systems with matched aqueous phase viscosity (glycerol added to brine). This was explained by an adsorbed polymer layer along the pore walls in large and intermediate pores, and blocking of small and intermediate pores in the pore volume.
- The water relative permeability was more reduced than the oil relative permeability, for both water-wet and oil-wet core plugs. The DPR effect was more pronounced in oil-wet cores, i.e. the decrease in $k_{rw,or}$ was higher.
- Three-dimensional PET-images showed that the displacement front was more uniform during polymer injection than water injection. Polymer injection also increased the oil recovery by 5% compared with water injection.
- The core transport properties changed after polymer was introduced to the core. The recovery decreased, and faster propagation of the displacement fronts during oil/brine and

brine/oil displacements could be seen in the PET-images. This indicates a decrease in pore volume available for flooding after polymer was injected into the core. Blocking of small and intermediate pores and narrow pore throats, and adsorption of polymer layers on the pore walls can explain this.

5.2 Future work

Some suggestions for future work within this subject are listed below:

- Finish the planned MRI-experiment: image the dynamically aged core plug LS26 during consecutive water and polymer injections. Perform static MRI-imaging and T_2 relaxation time measurements before and after each injection, in addition to dynamic measurements during both injections. Investigate the spatial wettability distribution in the core plug.
- Further analysis of the PET-images: investigate the flow pathways after polymer injection. Calculate relative permeability curves.
- Investigate the effect of polymer on wettability reversal in more homogeneous rock material, e.g. sandstone or chalk.
- Investigate the effect of polymer on fluid flow on pore scale in both water-wet and oil-wet systems.

APPENDIX

A. Porosity and permeability

Porosity is a key property in core analysis and is normally defined as the ratio of the void volume of the core plug to the total bulk volume of the core (Jenkins, 1966):

$$\phi_{tot} = \frac{V_p}{V_b} = \frac{V_b - V_m}{V_b} = 1 - \frac{V_m}{V_b} \tag{A.1}$$

where ϕ_{tot} is the total porosity of the core plug, V_p is the absolute pore volume of the core plug, V_b is the bulk volume of the core plug, and V_m is the matrix volume of the core plug.

Permeability is a measure of the ability of the porous medium to conduct flow and is dictated by the geometry of the pore network (Honarpour and Mahmood, 1988). Permeability can be subdivided into *absolute*, *effective* and *relative* permeability. The *absolute* permeability is a property of the porous medium, and is defined by Darcy's law when the pore space is 100% saturated with one fluid:

$$Q = \frac{KA}{\mu}\frac{dp}{dx} \tag{A.2}$$

where Q is the volumetric flow rate of a fluid with viscosity μ flowing through a porous medium with cross section area A. dp/dx is the differential pressure drop over a unit length of the porous medium.

When two or more immiscible fluids are present in the porous medium the permeability of each fluid at a given saturation is called *effective* permeability. The effective permeability k_{ie} of a fluid i is defined by a generalization of Darcy's law:

$$k_{ie} = Q_i \frac{\mu_i}{A}\frac{\Delta x}{\Delta p_i} \tag{A.3}$$

Craig (1971) described relative permeability as a "direct measure of the ability of the porous system to conduct one fluid when one or more fluids are present". These flow properties are the composite effect of pore geometry, wettability, fluid distribution, and saturation history. The

relative permeability (k_{ri}) is defined as the ratio of the effective permeability of a fluid to the absolute permeability of the rock (Honarpour and Mahmood, 1988):

$$k_{ri} = \frac{k_{ie}}{K} \tag{A.4}$$

B. Saturation

Core saturation describes the fraction of pore volume occupied by a certain fluid:

$$S_i = \frac{V_i}{V_p} \tag{B.1}$$

where V_i is the volume of a fluid *i* present in a core plug and V_p is the pore volume of the core plug.

The saturation of each fluid is a value between 0 and 1, thus the sum of all fluid saturations in the pore volume is 1. Water based (aqueous) fluids and oil saturates all core plugs in this work, and dynamic changes in fluid saturations are monitored by material balance. Material balance is based on the fact that one volume of injected fluid displaces another, equal volume of fluid from the pore space. When one immiscible fluid displaces another, the average core saturation may be calculated versus time by monitoring the produced effluents.

C. Capillary pressure

Capillary pressure (P_c) is defined as the molecular pressure difference between two immiscible fluids, e.g. water and oil, often generalized as:

$$P_c = P_o - P_w \tag{C.1}$$

where P_o and P_w is the pressure in the oil and the water phase, respectively.

Laplace complied a relation for capillary pressure of two immiscible fluids in a narrow cylindrical tube, with a curved interface in the form of meniscus between the two fluids as illustrated in Figure C.1. The pressure difference across the oil/water-interface is given by Laplace's equation:

$$P_c = \sigma_{ow}\left(\frac{1}{R_1} + \frac{1}{R_2}\right) \tag{C.2}$$

where R_1 and R_2 are the principal radii of the interface curvature and σ_{ow} is the interfacial tension between oil and water.

Using standard trigonometric rules, if $R_1 = R_2 = R$, the expression for the capillary pressure in a tube becomes:

$$P_c = \frac{2\sigma_{ow} \cdot cos\theta_{ow}}{r} \tag{C.3}$$

where θ_{ow} is the wetting angle and r is the radius of the capillary. The radius *r* can be compared to the radius of a pore throat, and equation(C.3) used to describe the capillary pressure of a bundle of tubes with varying pore throat radii, i.e. a simplified porous medium.

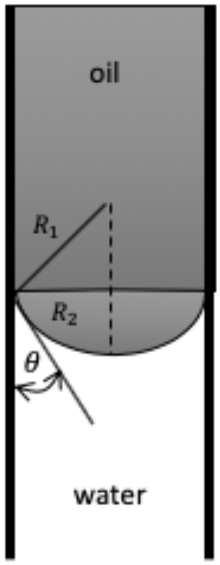

Figure C.1: Illustration of oil/water interface in capillary tube where water is the wetting phase and oil is the non-wetting phase.

Figure C.2 shows a capillary pressure curve for a more complex porous medium, e.g. a core plug, as a function of saturation. The curve is an example of capillary pressure behaviour in a water-wet system, where water coats the pore walls and saturates the smaller pores. During primary drainage in a water-wet core plug, the oil will first enter the pores with the lowest capillary pressure (i.e. the largest pores). Oil will then enter successively smaller pores, and the capillary pressure increases, until the irreducible water saturation (S_{wi}) is reached. This is the

initial condition to an oil reservoir. When water is injected, the pressure increases, and oil is produced until residual oil saturation is reached (S_{or}).

During imbibition, water will imbibe spontaneously into the smallest pores and displace the oil until $P_C = 0$. Additional displacement of oil is accomplished by water injection. The wettability of the core plug dictates the volume of water that will imbibe spontaneously into the core, by controlling the capillary pressure. For a strongly water-wet core (Figure C.2), water might imbibe spontaneously until the residual oil saturation (S_{or}) is reached, and oil will not be displaced during forced water injection.

Capillary pressure curves for imbibition and drainage differ due to a phenomenon called capillary hysteresis, i.e. capillary pressure is not only a function of saturation, but also the saturation history of the system. This is partly caused by the tortuosity of a porous system, e.g. caused by oil globules trapped in the centres of large pore bodies or stretching over several pores. Due to the heterogeneous nature of limestone core plugs used in this study, capillary trapping is expected.

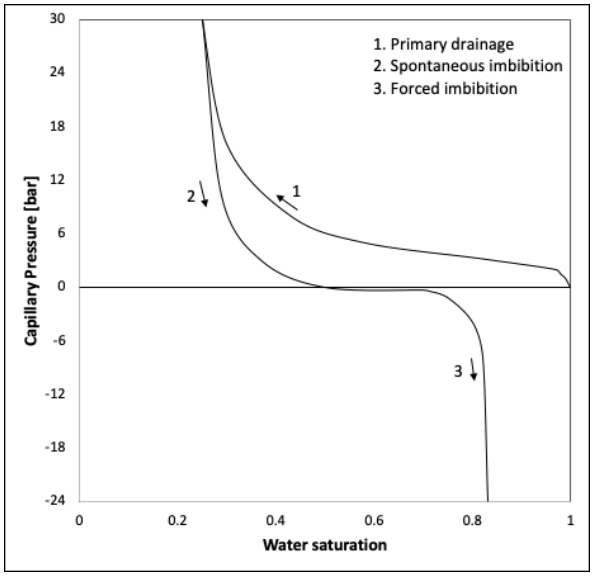

Figure C.2: Oil/water capillary pressure curves for a water-wet core.

D. Equations for calculation of shear stress and full-scale viscosity range

The following equation was used to calculate the shear stress the fluid sample was subjected to during viscosity measurements:

$$\tau = TK \cdot SMC \cdot SRC \cdot Torque\% \quad \text{(D.1)}$$

where Torque% is output from the viscometer, TK (Torque Constant), SMC (Spindle Multiplier Constant), and SRC (Shear Rate Constant) are constants relating to the viscometer and spindle size/type. Values can be found in the viscometer manual (Brookfield DV-II+Pro Viscometer Operating Instructions, Manual No. M03-165-F0612, page 76-78), and are listed below:

- TK = 0.09373
- SMC = 0.64
- SRC = 3.8

Full scale viscosity range for a given RPM setting may be calculated using the equation:

$$Full\ scale\ Viscosity\ Range = TK \cdot SMC \cdot \frac{10000}{RPM} \quad \text{(D.2)}$$

Viscosity measurement accuracy is 1% of the range.

E. Uncertainty Estimation

The variance formula (Ku, 1966) was used to estimate propagating error. The formula assumes that the variables ($s_x, s_y, s_z, \ldots$) are independent.

$$s_f = \sqrt{\left(\frac{\partial f}{\partial x}\right)^2 {s_x}^2 + \left(\frac{\partial f}{\partial y}\right)^2 {s_y}^2 + \left(\frac{\partial f}{\partial z}\right)^2 {s_z}^2 + \cdots} \quad \text{(E. 1)}$$

where s_f represents the standard deviation of the function f, s_x represents the standard deviation of x, s_y represents the standard deviation of y, and so forth.

Figure E.1: Instrumental uncertainties.

Instrument	Parameter	Uncertainty (±)
Weight	Mass	0.01 g
Caliper	Length	0.1 mm
ESI Pressure Transducer 0-10 barg	Pressure	0.10 % of scale
ESI Pressure Transducer 0-16 barg	Pressure	0.10 % of scale
Quizix Pump	Flow rate	0.10 % of rate
Measuring cylinder (25ml)	Volume	0.5 ml
Measuring cylinder (10ml)	Volume	0.2 ml
Graded imbibition tube	Volume	0.05 ml

Cyclic imbibition as performed in this work leads to increased uncertainty in saturation for each cycle. To reduce this uncertainty accurate measuring methods should be used. The saturation in two of the core plugs ended up very low after multiple Amott-Harvey cycles; particularly, saturations in LS13 and LS22 had to be adjusted because negative water saturation was measured in fifth cycle. 25 ml measuring cylinders (0.5 ml uncertainty) were used to monitor saturations during the first Amott-Harvey cycles. The measuring cylinders were replaced with imbibition cells for production measurements during further cycles to reduce the uncertainties. This yields inaccurate measurements of effluents, especially during water injections. The measured production of the first Amott-Harvey cycles in LS13 and LS22 were therefore calibrated to accurate production measured in further cycles. Total uncertainties after each completed Amott-Harvey cycle were calculated using equation (E. 1) for a selection of cores and are presented in Figure E.2.

Figure E.2: Calculated total uncertainties in saturation after drainage (drain.) and each completed Amott-Harvey cycle (1-5).

	LS11	LS12	LS13	LS14	LS16	LS17	LS18	LS19	LS20	LS21	LS22
Drain.	±0.02	±0.03	±0.03	±0.03	±0.03	±0.02	±0.03	±0.03	±0.03	±0.03	±0.03
1	±0.05	±0.04	±0.04	±0.05	±0.05	±0.05	±0.05	±0.04	±0.05	±0.05	±0.05
2	±0.05	±0.05	±0.05	±0.06	±0.05	±0.06	±0.06	±0.05	±0.07	±0.07	±0.06
3	±0.06	±0.05	±0.05	±0.06	±0.05	±0.06	±0.06	±0.05	±0.07	±0.07	±0.06
4	±0.06	±0.05	±0.05	±0.06	±0.05	±0.06	±0.06	±0.05	±0.07	±0.07	±0.07
5	±0.06	±0.05	±0.05	±0.06	±0.05	±0.06	±0.06	±0.05	-	±0.07	±0.07

F. Pressure logs from the PET-experiment

Pressure logs from the PET-experiment performed at Haukeland University hospital are presented. Figure F.1 shows the pressure log from the first brine injection, first oil injection and polymer injection. Figure F.2 shows the pressure log from the second oil injection, and Figure F.3 shows the pressure log from the second brine injection and the third oil injection. Inlet and outlet pressure are presented in the logs, and comments explaining pressure changes are added.

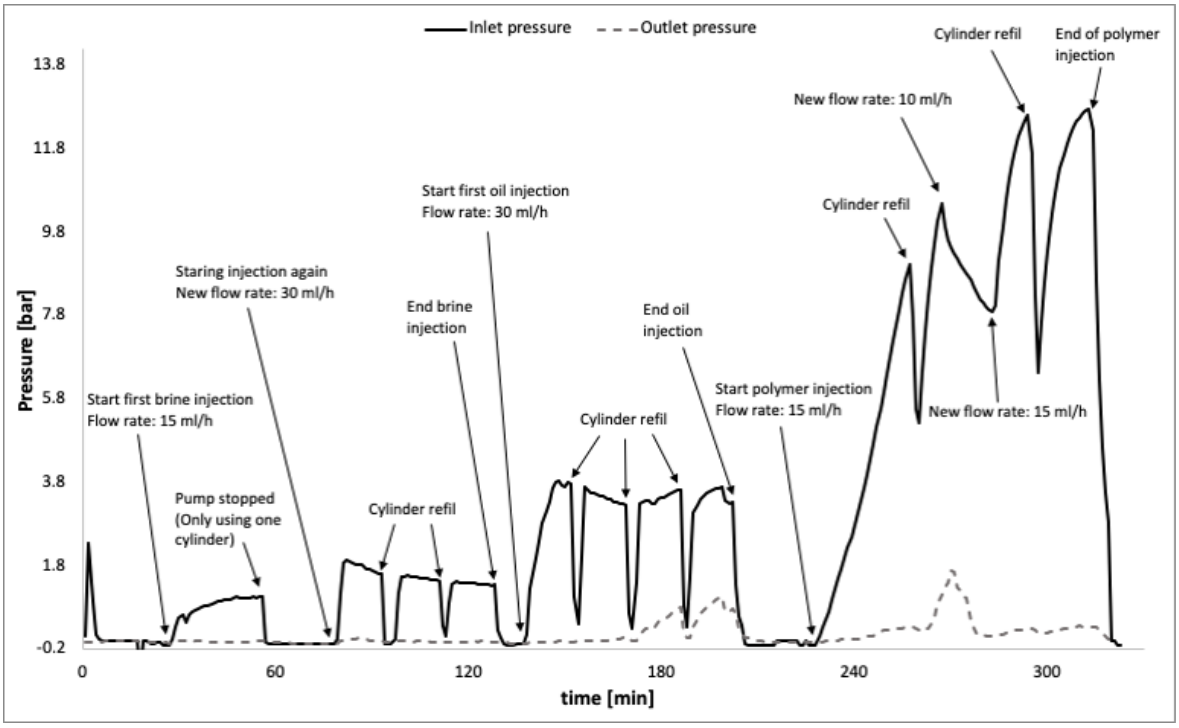

Figure F.1: Pressure log from first brine injection, first oil injection and polymer injection in the PET-scanner. Comments are added to explain pressure changes.

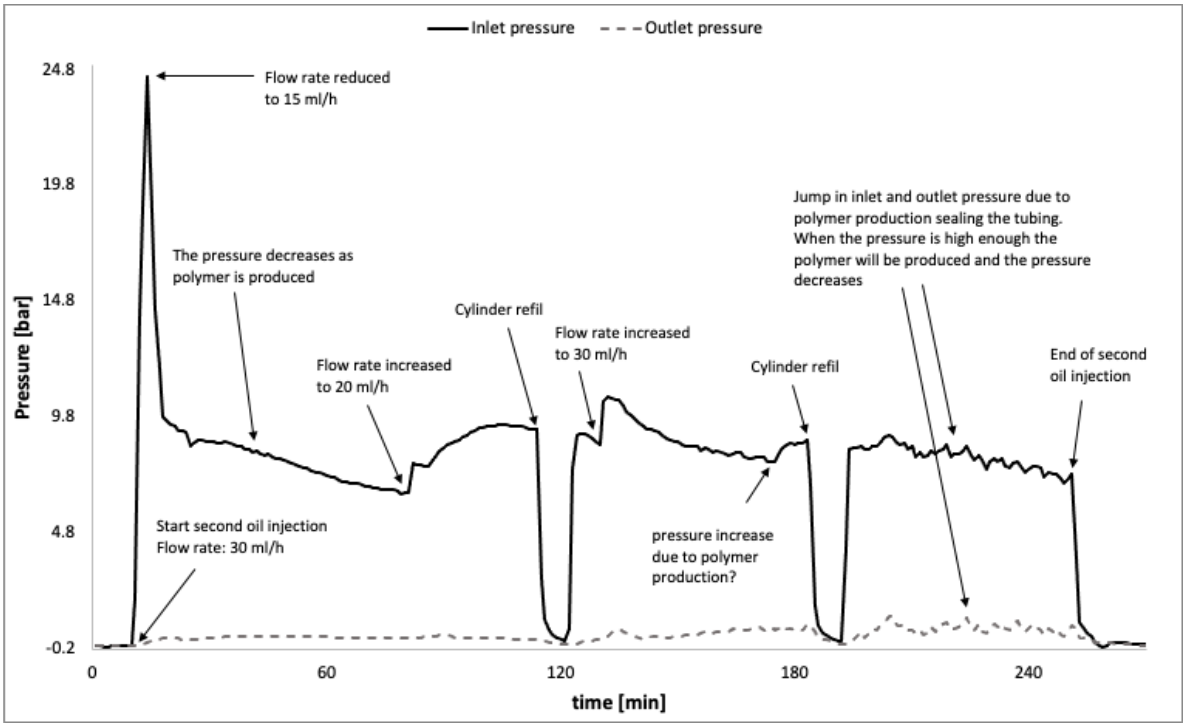

Figure F.2:Pressure log from second oil injection in the PET-scanner. Comments are added to explain pressure changes.

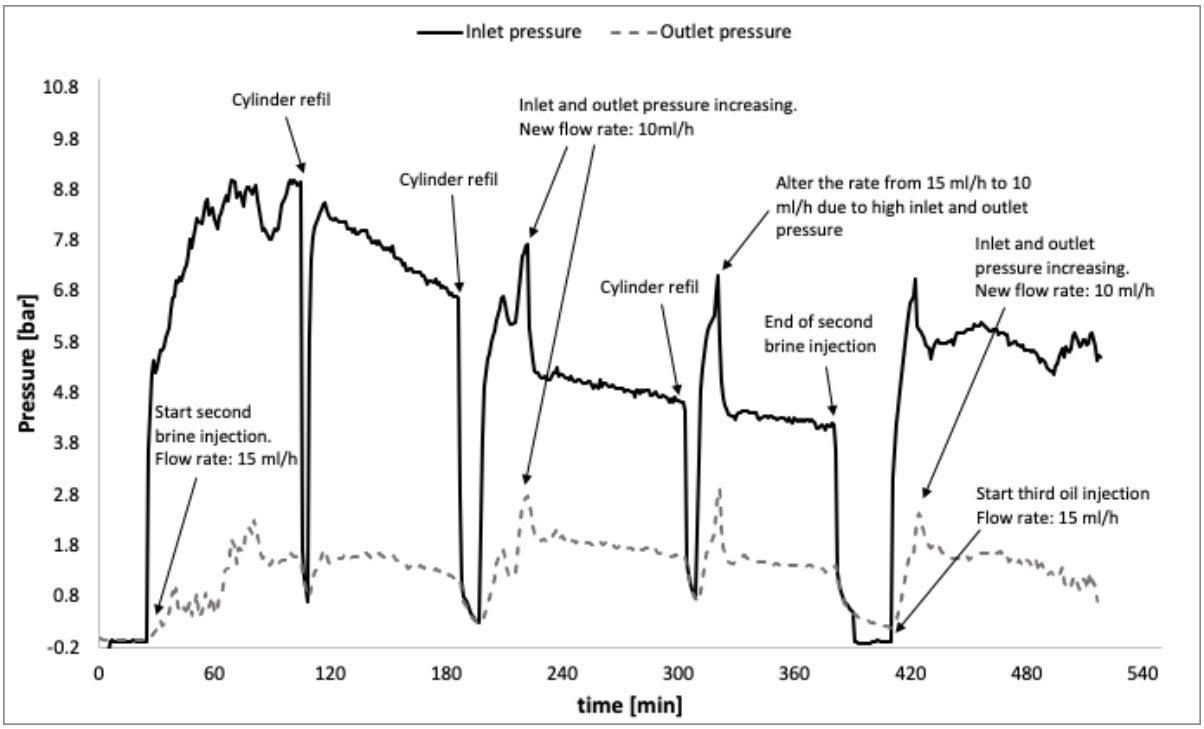

Figure F.3: Pressure log from second brine injection and part of the third oil injection in the PET-scanner. Comments are added to explain pressure changes.

Bibliography

ABDALLAH, W., BUCKLEY, J. S., CARNEGIE, A., EDWARDS, J., HEROLD, B., FORDHAM, E., GRAUE, A., HABASHY, T., SELEZNEV, N., SIGNER, C., HUSSAIN, H., MONTARON, B. & ZIAUDDIN, M. 2007. Fundamentals of wettability. *Oilfield Review,* 19**,** 44-61.

AKIN, S. & KOVSCEK, A. 2003. Computed tomography in petroleum engineering research. *Geological Society, London, Special Publications,* 215**,** 23-38.

AL-SHARJI, H. H., GRATTONI, C. A., DAWE, R. A. & ZIMMERMAN, R. W. 1999. Pore-Scale Study of the Flow of Oil and Water through Polymer Gels. *SPE Annual Technical Conference and Exhibition.* Houston, Texas: Society of Petroleum Engineers.

ALI, S. M. F. & THOMAS, S. 1996. The Promise And Problems of Enhanced Oil Recovery Methods. *Journal of Canadian Petroleum Technology,* 35**,** 7.

AMOTT, E. 1959. Observations Relating to the Wettability of Porous Rock. Society of Petroleum Engineers.

ANDERSON, W. 1986a. Wettability Literature Survey- Part 2: Wettability Measurement. *Journal of Petroleum Technology,* 38**,** 1246-1262.

ANDERSON, W. G. 1986b. Wettability Literature Survey- Part 1: Rock/Oil/Brine Interactions and the Effects of Core Handling on Wettability. *Journal of Petroleum Technology,* 38**,** 1125-1144.

ANDERSON, W. G. 1987. Wettability Literature Survey Part 5: The Effects of Wettability on Relative Permeability. *Journal of Petroleum Technology,* 39**,** 1453-1468.

B JOHANNESEN, E., STEINSBØ, M., HOWARD, J. & GRAUE, A. 2019. WETTABILITY CHARACTERIZATION BY NMR T 2 MEASUREMENTS IN CHALK.

BARREAU, P., BERTIN, H., LASSEUX, D., GLÉNAT, P. & ZAITOUN, A. 1997. Water Control in Producing Wells: Influence of an Adsorbed-Polymer Layer on Relative Permeabilities and Capillary Pressure. *SPE Reservoir Engineering,* 12**,** 234-239.

BERGOSH, J. L. & LORD, G. D. 1987. New Developments in the Analysis of Cores From Naturally Fractured Reservoirs. *SPE Annual Technical Conference and Exhibition.* Dallas, Texas: Society of Petroleum Engineers.

BJORLYKKE, K. 2010. Petroleum Geoscience : From Sedimentary Environments to Rock Physics. Berlin, Heidelberg: Springer Berlin Heidelberg.

BOBEK, J. E., MATTAX, C. C. & DENEKAS, M. O. 1958. Reservoir Rock Wettability - Its Significance and Evaluation. Society of Petroleum Engineers.

BRATTEKÅS, B., STEINSBØ, M., GRAUE, A., FERNØ, M. A., ESPEDAL, H. & SERIGHT, R. S. 2016. New Insight to Wormhole Formation in Polymer Gel During Water Chasefloods Using Positron Emission Tomography PET. *SPE Bergen One Day Seminar.* Grieghallen, Bergen, Norway: Society of Petroleum Engineers.

BUCKLEY, J. S., TAKAMURA, K. & MORROW, N. R. 1989. Influence of Electrical Surface Charges on the Wetting Properties of Crude Oils. *SPE Reservoir Engineering,* 4**,** 332-340.

CRAIG, F. F. 1971. *The reservoir engineering aspects of waterflooding,* New York, Henry L. Doherty Memorial Fund of AIME.

DONALDSON, E. C. 2008. *Wettability,* Houston, Tex, Gulf Publ. Co.

DUNN, K. J. 2002. *Nuclear magnetic resonance : petrophysical and logging applications,* Amsterdam, Pergamon.

ELMKIES, P., BERTIN, H., LASSEUX, D., MURRAY, M. & ZAITOUN, A. 2001. Further Investigations on Two-Phase Flow Property Modification by Polymers: Wettability Effects. *SPE International Symposium on Oilfield Chemistry.* Houston, Texas: Society of Petroleum Engineers.

FERNO, M. A., ERSLAND, G., HAUGEN, A., JOHANNESEN, E. B., GRAUE, A., STEVENS, J. & HOWARD, J. J. Impacts From Fractures On Oil Recovery Mechanisms In Carbonate Rocks At Oil-Wet And Water-Wet Conditions-Visualizing Fluid Flow Across Fractures With MRI. International Oil Conference and Exhibition in Mexico, 2007. Society of Petroleum Engineers.

FERNO, M. A., TORSVIK, M., HAUGLAND, S. & GRAUE, A. 2010. Dynamic Laboratory Wettability Alteration. *Energy Fuels,* 24**,** 3950-3958.

FERNØ, M., GAUTEPLASS, J., HAUGE, L. P., ABELL, G. E., ADAMSEN, T. & GRAUE, A. 2015. Combined positron emission tomography and computed tomography to visualize and quantify fluid flow in sedimentary rocks. *Water Resources Research,* 51**,** 7811-7819.

FERNØ, M., TORSVIK, M., HAUGLAND, S. & GRAUE, A. 2010. Dynamic laboratory wettability alteration. *Energy & Fuels,* 24**,** 3950-3958.

FERNØ, M. A., HAUGEN, Å., WICKRAMATHILAKA, S., HOWARD, J., GRAUE, A., MASON, G. & MORROW, N. R. 2013. Magnetic resonance imaging of the development of fronts during spontaneous imbibition. *Journal of Petroleum Science and Engineering,* 101**,** 1-11.

FISCHER, H. & MORROW, N. R. 2006. Scaling of oil recovery by spontaneous imbibition for wide variation in aqueous phase viscosity with glycerol as the viscosifying agent. *Journal of Petroleum Science and Engineering,* 52**,** 35-53.

FOSHEE, W. C., JENNINGS, R. R. & WEST, T. J. 1977. Preparation And Testing Of Partially Hydrolyzed Polyacrylamide Solutions. *Annual Technical Meeting.* Edmonton: Petroleum Society of Canada.

FRANSHAM, P. B. & JELEN, J. 1987. Displacement Of Heavy Oil Visualized By CAT Scan. *Journal of Canadian Petroleum Technology,* 26**,** 7.

GRATTONI, C., LUCKHAM, P., JING, X., NORMAN, L. & ZIMMERMAN, R. W. 2004. Polymers as relative permeability modifiers: adsorption and the dynamic formation of thick polyacrylamide layers. *Journal of petroleum science and engineering,* 45**,** 233-245.

GRAUE, A., ASPENES, E., BOGNØ, T., W MOE, R. & RAMSDAL, J. 2002. Alteration of wettability and wettability heterogeneity. *Journal of Petroleum Science and Engineering - J PET SCI ENGINEERING,* 33**,** 3-17.

GREEN, D. W. 1998. Enhanced oil recovery. *In:* WILLHITE, G. P. (ed.). Richardson, TX: Henry L. Doherty Memorial Fund of AIME, Society of Petroleum Engineers.

HEINDEL, T. J. 2011. A Review of X-Ray Flow Visualization With Applications to Multiphase Flows. Digital Repository @ Iowa State University.

HONARPOUR, M. & MAHMOOD, S. M. 1988. Relative-Permeability Measurements: An Overview. *Journal of Petroleum Technology,* 40**,** 963-966.

HOWARD, J. J. & KENYON, W. E. 1992. Determination of pore size distribution in sedimentary rocks by proton nuclear magnetic resonance. *Marine and petroleum geology,* 9**,** 139-145.

HUH, C., LANGE, E. A. & CANNELLA, W. J. 1990. Polymer Retention in Porous Media. *SPE/DOE Enhanced Oil Recovery Symposium.* Tulsa, Oklahoma: Society of Petroleum Engineers.

IEA 2019a. Global electricity demand by region in the Stated Policies Scenario, 2000-2040. IEA.

IEA 2019b. World Energy Balances 2019.

IEA 2019c. World Energy Outlook 2019.

JENKINS, R. J. 1966. Accuracy of porosity determinations. *The Log Analyst***,** 29-34.

JOHNS, R. A., STEUDE, J. S., CASTANIER, L. M. & ROBERTS, P. V. 1993. Nondestructive measurements of fracture aperture in crystalline rock cores using X ray computed tomography. *Journal of Geophysical Research: Solid Earth,* 98**,** 1889-1900.

JUAREZ-MOREJON, J., BERTIN, H., OMARI, A., HAMON, G., COTTIN, C., BOURDAROT, G. & MOREL, D. Spontaneous Imbibition as Indicator of Wettability Change During Polymer Flooding. IOR 2017-19th European Symposium on Improved Oil Recovery, 2017. European Association of Geoscientists & Engineers, 1-10.

KAMAT, P. V. 2007. Meeting the clean energy demand: nanostructure architectures for solar energy conversion. *The Journal of Physical Chemistry C,* 111**,** 2834-2860.

KARACAN, C. Ö. & OKANDAN, E. 1999. Heterogeneity Effects on the Storage and Production of Gas from Coal Seams. *SPE Annual Technical Conference and Exhibition.* Houston, Texas: Society of Petroleum Engineers.

KENYON, W. E., HOWARD, J. J., SEZGINER, A., STRALEY, C., MATTESON, A., HORKOWITZ, K. & EHRLICH, R. 1989. Pore-Size Distribution And NMR In Microporous Cherty Sandstones. *SPWLA 30th Annual Logging Symposium.* Denver, Colorado: Society of Petrophysicists and Well-Log Analysts.

KU, H. H. 1966. Notes on the use of propagation of error formulas. *Journal of Research of the National Bureau of Standards, Section C: Engineering and Instrumentation,* 70C**,** 263.

KYTE, J. R. & RAPOPORT, L. A. 1958. Linear Waterflood Behavior and End Effects in Water-Wet Porous Media. *Journal of Petroleum Technology,* 10**,** 47-50.

LAKE, L. W. 2014. *Fundamentals of enhanced oil recovery,* Richardson, Tex, Society of Petroleum Engineers.

LIANG, J.-T., SUN, H. & SERIGHT, R. S. 1995. Why Do Gels Reduce Water Permeability More Than Oil Permeability? *SPE Reservoir Engineering,* 10**,** 282-286.

LIU, L. & BUCKLEY, J. S. 1999. Alteration of wetting of mica surfaces. *Journal of Petroleum Science and Engineering,* 24**,** 75-83.

MA, S., ZHANG, X. & MORROW, N. R. 1999. Influence of Fluid Viscosity On Mass Transfer Between Rock Matrix And Fractures. *Journal of Canadian Petroleum Technology,* 38**,** 6.

MCCABE, W. L. 2005. *Unit operations of chemical engineering,* Boston, McGraw-Hill.

MELLOR, M. & HAWKES, I. 1971. Measurement of tensile strength by diametral compression of discs and annuli. *Engineering Geology,* 5**,** 173-225.

METZNER, A. B. & OTTO, R. E. 1957. Agitation of non-Newtonian fluids. *AIChE Journal,* 3**,** 3-10.

MIRZAEI-PAIAMAN, A. & MASIHI, M. 2013. Scaling Equations for Oil/Gas Recovery from Fractured Porous Media by Counter-Current Spontaneous Imbibition: From Development to Application. *Energy Fuels,* 27**,** 4662-4676.

MOHANTY, K. & JOHNSON, S. 1993. Interpretation of laboratory gasfloods with multidimensional compositional modeling. *SPE reservoir engineering,* 8**,** 59-66.

MONICK, J. A. 1968. Alcohols; their chemistry, properties and manufacture.

NGUYEN, T. Q., GREEN, D. W., WILLHITE, G. P. & MCCOOL, C. S. 2006. Effects of Gelant Composition and Pressure Gradients of Water and Oil on Disproportionate Permeability Reduction of Sandpacks Treated with Polyacrylamide-Chromium Acetate Gels. *SPE Journal,* 11**,** 145-157.

NILSSON, S., STAVLAND, A. & JONSBRATEN, H. C. 1998. Mechanistic Study of Disproportionate Permeability Reduction. *SPE/DOE Improved Oil Recovery Symposium.* Tulsa, Oklahoma: Society of Petroleum Engineers.

OPDAL, I. E. 2014. *Mobility Control by CO2-foam Injection for Integrated EOR.* The University of Bergen.

PETERS, E. J. & AFZAL, N. 1992. Characterization of heterogeneities in permeable media with computed tomography imaging. *Journal of Petroleum Science and Engineering,* 7**,** 283-296.

PETERS, E. J. & HARDHAM, W. D. 1990. Visualization of fluid displacements in porous media using computed tomography imaging. *Journal of petroleum Science and Engineering,* 4**,** 155-168.

RAPOPORT, L. A. & LEAS, W. J. 1953. Properties of Linear Waterfloods. *Journal of Petroleum Technology,* 5**,** 139-148.

REITE, S. I. S. 2019. *An Experimental Study of Polymer Spontaneous Imbibition in Sandstone.* Master, University of Bergen.

RISKEDAL, H. 2008. Wettability and rock characterization of heterogeneous limestone utilizing NMR. Bergen: H. Riskedal.

SAUNES, A. S. 2018. Establishing a homogeneous and stable sand pack to study parameters during spontaneous imbibition. The University of Bergen.

SERIGHT, R. S., PRODANOVIC, M. & LINDQUIST, W. B. 2004. X-Ray Computed Microtomography Studies of Disproportionate Permeability Reduction. *SPE/DOE Symposium on Improved Oil Recovery.* Tulsa, Oklahoma: Society of Petroleum Engineers.

SERIGHT, R. S., PRODANOVIC, M. & LINDQUIST, W. B. 2006. X-Ray Computed Microtomography Studies of Fluid Partitioning in Drainage and Imbibition Before and After Gel Placement: Disproportionate Permeability Reduction. *SPE Journal,* 11**,** 159-170.

SHENG, J. J., LEONHARDT, B. & AZRI, N. 2015. Status of Polymer-Flooding Technology. *Journal of Canadian Petroleum Technology,* 54**,** 116-126.

SKAUGE, A., SPILDO, K., HØILAND, L. & VIK, B. 2007. Theoretical and experimental evidence of different wettability classes. *Journal of Petroleum Science and Engineering,* 57**,** 321-333.

SKJELSVIK, E. B. 2018. *Synergy of Nanoparticles and Surfactants for CO2 Foam Enhanced Oil Recovery and CO2 Storage in Carbonates.* The University of Bergen.

SYDANSK, R. D., AL-DHAFEERI, A., XIONG, Y. & SERIGHT, R. 2004. Polymer gels formulated with a combination of high- and low-molecular-weight polymers provide improved performance for water-shutoff treatments of fractured production wells. *SPE Prod. Fac.,* 19**,** 229-236.

TAKAMURA, K., FISCHER, H. & MORROW, N. R. 2012. Physical properties of aqueous glycerol solutions. *Journal of Petroleum Science and Engineering,* 98**,** 50-60.

TIPURA, L. 2008. Wettability characterization by NMR T_2 measuments in Edwards Limestone. Bergen: L. Tipura.

VIKSUND, B., MORROW, N., MA, S., WANG, W. & GRAUE, A. Initial water saturation and oil recovery from chalk and sandstone by spontaneous imbibition. Proceedings, 1998 International Symposium of Society of Core Analysts, The Hague, 1998. Citeseer.

WENNBERG, A. C. & PETERSEN, K. 2017. Biodegradation of selected offshore chemicals.

WILLHITE, G. P., ZHU, H., NATARAJAN, D., MCCOOL, C. S. & GREEN, D. W. 2002. Mechanisms Causing Disproportionate Permeability Reduction in Porous Media Treated With Chromium Acetate/HPAM Gels. *SPE Journal,* 7**,** 100-108.

WITHJACK, E. M. 1988. Computed Tomography for Rock-Property Determination and Fluid-Flow Visualization. *SPE Formation Evaluation,* 3**,** 696-704.

WITHJACK, E. M., ORSHAM, S. K. & YANG, C. T. 1991. CT Determination of Heterogeneities and Miscible Displacement Characteristics. *SPE Formation Evaluation,* 6**,** 447-452.

ZAHASKY, C., KUROTORI, T., PINI, R. & BENSON, S. M. 2019. Positron emission tomography in water resources and subsurface energy resources engineering research. *Advances in water resources,* 127**,** 39-52.

ZAITOUN, A. & KOHLER, N. 1988. Two-Phase Flow Through Porous Media: Effect of an Adsorbed Polymer Layer. *SPE Annual Technical Conference and Exhibition.* Houston, Texas: Society of Petroleum Engineers.

ZHANG, X., MORROW, N. & MA, S. 1996. Experimental verification of a modified scaling group for spontaneous imbibition. *SPE Reserv. Eng.,* 11**,** 280-285.

ZOLOTUCHIN, A. B. 2000. *Introduction to petroleum reservoir engineering,* Kristiansand, Høyskoleforl.